Mapping oxygen in the awake mouse brain

Declan Lyons

Université Pierre et Marie Curie

Ecole Doctorale Cerveau Cognition Comportement (ED3C)

Cartographie de l'oxygénation cérébrale chez la souris éveillée

Mapping oxygen in the awake mouse brain

Présentée par

Declan LYONS

Thèse de doctorat de Neurosciences

Dirigée par Serge CHARPAK

Présentée et soutenue publiquement le 06 février 2015 à Paris

Devant un jury composé de :

Serge CHARPAK (Directeur de thèse)

Bruno WEBER (Rapporteur)

Gilles BONVENTO (Rapporteur)

Philippe FAURE (Président)

Résumé en français

Comprendre la relation entre l'activité cérébrale, le flux sanguin et le métabolisme énergétique impose de déterminer comment l'oxygène est délivré et consommé par les neurones *in vivo*. Suite à la synthèse récente du PtP-C343, une sonde bi-photonique phosphorescente sensible à l'oxygène, notre laboratoire a développé l'imagerie bi-photonique de phosphorescence en profondeur, pour mesurer la concentration en oxygène *in vivo*, avec une résolution micrométrique dans le cerveau de rongeurs anesthésiés (Parpaleix et al. 2013). Le laboratoire a quantifié, dans le bulbe olfactif de la souris, la pression partielle d'oxygène (Po_2) dans les vaisseaux et dans le tissu. Il a également fait l'observation que la valeur de la Po_2 à mi-distance entre deux érythrocytes d'un capillaire, peut être utilisée pour évaluer indirectement la Po_2 dans le tissu voisin. Mon projet de thèse a été de mettre au point une approche permettant de mesurer la Po_2 cérébrale chez l'animal éveillé non-stressé.

Dans un premier temps, j'ai développé une approche chirurgicale permettant d'observer en microscopie bi-photonique, le bulbe olfactif et le cortex somato-sensoriel de souris éveillées. J'ai ensuite mis au point une technique d'entrainement permettant à ces souris d'être maintenues en contention en l'absence de stress.

La première partie de mon travail, menée dans la couche glomérulaire, a permis de déterminer pour la première fois les paramètres vasculaires physiologiques de la micro-vascularisation, associés aux mesures de Po_2 vasculaires et tissulaires: une Po_2 érythrocytaire de 60.6 mm Hg et une Po_2 tissulaire de 23 mm Hg, un flux érythrocytaire moyen de 30.6 cellules/s et un hématocrite moyen de 34.6 %.

Dans un deuxième temps, j'ai reproduit ces mesures dans le cortex somato-sensoriel et observé des différences régionales, selon l'organisation en couches corticales. De manière générale, la Po_2 tissulaire moyenne est plus basse dans la couche I (14.7 mm Hg) que dans les deux couches sous-jacentes (couche II/III, 22.9 mm Hg; couche IV, 27.4 mm Hg). De même, des différences dans les relations dynamiques entre les Po_2 globulaire/tissulaire et les paramètres vasculaires, tels l'hématocrite et le flux érythrocytaire varient selon les couches corticales.

Enfin, j'ai comparé les valeurs des Po_2 tissulaire et vasculaire chez l'animal éveillé et anesthésié, et observé que l'anesthésie change dramatiquement l'état d'oxygénation cérébrale. Ceci démontre la nécessité de mesurer l'ensemble des paramètres vasculaires et métaboliques dans des conditions vraiment physiologiques. De cette manière, mes données permettront d'améliorer les modèles de diffusion de l'oxygène, ainsi que l'analyse quantitative du métabolisme cérébral et l'interprétation de la nature des signaux mesurés en imagerie cérébrale humaine.

Abstract

Understanding brain metabolism at rest and during periods of activity requires quantifying the amount of oxygen entering, being consumed in, and exiting selected volumes of neural tissue. Two-photon phosphorescence lifetime microscopy (2PLM) is a new technique that has been used for depth-resolved micron-scale measurements of the partial pressure of oxygen (Po_2) in the rodent brain. It has allowed mapping of Po_2 in depth in both the olfactory bulb and the cortex of anaesthetised mice. The spatiotemporal resolution of 2PLM Po_2 measurements has revealed that the portion of plasma in the vicinity of individual red blood cells (RBCs) has a higher oxygen content(Po_2RBC) than that which is at a distance from RBCs(Po_2InterRBC). Our laboratory has shown that Po_2 InterRBC is at equilibrium with Po_2 in the neuropil and can thus be used to non-invasively measure tissue Po_2 (Parpaleix et al., 2013). However, the relevance of all reported high-resolution Po_2 values has remained uncertain as measurements have only been performed during anaesthesia, which affects both neuronal activity and cerebral blood flow, two major parameters that affect brain vascular and tissue oxygenation.

My project aimed to map the physiological values of brain Po_2 at rest, in the awake, unstressed mouse. I have done so in two brain regions, the olfactory bulb glomerular layer and the somatosensory cortex. In the initial phase of this project, I implemented surgical techniques to allow for long-term optical access to the olfactory bulb or the somatosensory cortex, and also methods for training mice to allow for 2-photon imaging and 2PLM while minimising the stress induced by these procedures.

The first section of my research, conducted in the olfactory bulb glomerular layer, produced the first measurements of blood flow and Po_2 parameters in the cerebral microvasculature in physiological conditions. I determined mean Po2 levels of values of 60.6 mmHg for RBC Po_2, 23 mmHg for tissue Po_2, a mean capillary RBC flow rate of 30.6 cells/s and a mean capillary haematocrit level of 34.6%

In the second section of my work, I performed similar measurements in the somatosensory cortex and observed regional differences between the superficial cortical laminae. Measured from the capillaries, the mean local tissue Po_2 in Layer I (14.7 mmHg) is generally lower than in the two underlying layers (Layer II/III: 22.9 mmHg, Layer IV: 27.4 mmHg). Furthermore the relationships of RBC Po_2 and tissue Po_2 to the blood flow parameters differed between the cortical layers, and also in comparison to the olfactory bulb glomerular layer.

Finally, I compared the values of vascular and tissue Po2 between the awake and anaesthetised states, and observed that anaesthetics can dramatically change the state of cerebral oxygenation at the microvascular scale. This final finding emphasises the importance of measuring these values in the physiologically normal brain.

In this way, my research will help improve our understanding of cerebrovascular function and brain metabolism.

Foreword and Acknowledgements

I wish to offer my thanks to the École des Neurosciences, Paris Île-de-France, for the opportunity to live and study in Paris over the last number of years. Had it not been for the support offered by their graduate programme I sincerely doubt that I would have been able to embark on this tremendous experience. I would also like to thank La Fondation pour la Recherche Médicale for their support during the fourth year of my thesis studies.

Great thanks must go to Serge Charpak for welcoming me to his lab and for all his guidance over the course of my PhD studies.

I am very grateful to Dr. Gilles Bonvento, Dr. Phillipe Faure and Prof. Dr. Bruno Weber for accepting to serve on my thesis jury.

I wish to thank all the members, past and present, of the Charpak team and of the wider Laboratoire de Neurophysiologie et des Nouvelles Microscopies, with whom I have shared the past few years. I would especially like to thank Kiri Couchman and Alexandre Parpaleix, with whom I worked extensively, and Yannick Goulam Houssen, Mathieu Ducros, and Serguei Sasnouski for their technical advice and assistance. Moreover, I have to thank all those people, too numerous to name here, who have been there with smiles and kind words, concerned questions and precious advice, and jokes and laughs throughout all the ups and downs of the past few years.

I am grateful to my friends Brendan, Alex, Sean, and Emma for their various journeys to attend my thesis defence.

Thank you also to my family, who have always been there for me, each in their own way listening to me, advising me, encouraging and distracting me.

My deepest thanks go to Róisín-Ana Ní Chárthaigh, firstly, for proofreading this thesis and making sure that all my 'Po2's were 'Po_2's. But more than that, I will be forever grateful to you for your love. Your care and kindness and thoughtfulness and encouragement have brought me through all the trials on the way to here. I can never thank you enough.

I will give a proof of my zeal: one day, on tearing off some old bark, I saw two rare beetles and seized one in each hand; then I saw a third and new kind, which I could not bear to lose, so that I popped the one which I held in my right hand into my mouth. Alas it ejected some intensely acrid fluid, which burnt my tongue so that I was forced to spit the beetle out, which was lost, as well as the third one.

- Charles Darwin

I love deadlines.

I like the whooshing sound they make as they fly by.

- Douglas Adams

Table of Contents

Résumé en français ii

Abstract iv

Foreword and Acknowledgements v

PART 1: INTRODUCTION 1

Chapter 1: Oxygen, Metabolism and the Brain 2
Section 1 – Cellular metabolism, ATP turnover, and the role of oxygen in these processes 2
1.1 – Thermodynamics and the central role of ATP in the processes of life 2
1.2 – Cellular production of ATP 5
Section 2 – Oxygen in Physiology 10
2.1 – The physical and chemical properties of oxygen in biological systems 10
2.2 – The transport of oxygen from the atmosphere to the mitochondria 11
2.3 – Mechanisms of oxygen delivery from the microvasculature to the tissue 15
Section 3 – Metabolism, ATP turnover and Oxygen Consumption in the Brain 17

Chapter 2: Supply of Blood to the Brain, and our Model Systems. 20
Section 1 – Blood supply to the Brain 20
Section 2 – Our Model Systems 23
2.1 – The olfactory bulb 23
2.1.1 – Structure and basic functions 23
2.1.2 – Vascular supply and organisation of the olfactory bulb 25
2.2 – The somatosensory cortex 27
2.2.1 – Structure and basic functions 27
2.2.2 – Vascular supply and organisation of the Somatosensory Cortex 30

Chapter 3: Tools and Techniques for measuring Oxygen 33
Section 1 – Measurements of oxygen parameters other than Po_2 33
1.1 – Measurement techniques based on measurement of haemoglobin and So_2 33
1.2 – Positron Emission Tomography (PET) 34
Section 2 – Methods of Measuring Po_2 35
2.1 – Polarographic measurements of Po_2 35
2.2 – Electron Parametric Resonance (EPR) oximetry 36
2.3 – Mass spectrometry for measuring Po_2 38
2.4 – Optical methods for determining Po_2 38

Chapter 4: The Current Understanding of Oxygen in the Brain 48
Section 1 - What is known of Po_2 in the Brain? 48
1.1 – Po_2 in the human brain 48
1.2 – Po2 in the mammalian brain 48
1.2.1 – Po_2 in the brain vasculature 49
1.2.2 – Po_2 in brain neural tissue 53
1.2.3 – Relationship of tissue Po_2 to vascular Po_2 56
1.3 – The effect of inspired gases and anaesthetics on brain Po_2 57
Section 2 – Conclusion 57

PART 2: METHODS & PROCEDURES 59
Section 1 – Combined 2-photon Imaging and 2PLM for Simultaneous Po_2 Measurement, and RBC detection 60
Section 2 – Surgical Procedures 65
Section 3 – Training procedure 68
Section 4 – Procedure for recording of Po_2 and Blood flow Parameters in Awake Mice 71

PART 3: RESULTS 73
Section 1 – Oxygenation of the Olfactory Bulb Glomerular Layer 74
3.1.1 – Capillary and tissue Po_2 in the olfactory bulb glomerular layer 74
3.1.2 – Capillary RBC flow and haematocrit in the olfactory bulb glomerular layer 77
3.1.3 – The relationship between blood flow and Po_2 in the olfactory bulb glomerular layer 79
3.1.4 – The relationship between haematocrit and Po_2 in the olfactory bulb glomerular layer 80
3.1.5 – Capillary blood flow parameters in areas of low tissue Po_2 in the olfactory bulb glomerular layer 81
Section 2 – Oxygenation of the superficial layers of the somatosensory cortex 82
3.2.1 - Capillary and local tissue Po_2 in the somatosensory cortex 82
3.2.2 – Capillary RBC flow and haematocrit in the somatosensory cortex 84
3.2.3 – The relationship between capillary blood flow and Po_2 in the somatosensory cortex 86
3.2.4 – The relationship between capillary haematocrit and Po_2 in the somatosensory cortex 87
3.2.5 – Capillary blood flow parameters in areas of low tissue Po_2 in the somatosensory cortex 88
3.2.6 – Laminar variations in capillary Po_2 in the somatosensory cortex 89
3.2.7 – Laminar variations in capillary RBC flow and haematocrit in the somatosensory cortex 92
3.2.8 – Laminar variations in the relationship between capillary blood flow parameters and Po_2 in the somatosensory cortex 92
3.2.9 – Po_2 in penetrating arterioles and venules in the somatosensory cortex 97
Section 3 – The effect of isoflurane anaesthesia on capillary Po_2 and RBC flow rates in the brain 99
Section 4 – Summary 101

PART 4: DISCUSSION 102
Section 1 – The olfactory bulb glomerular layer 103
1.1 – Po_2 in the olfactory bulb GL 103
1.2 – RBC flow and haematocrit in the olfactory bulb GL 104
1.3 – Correlations of Po_2 with capillary haematocrit and RBC flow in the GL 105
1.4 – Low tissue Po_2 in the GL is linked to low capillary haematocrit 105
1.5 – Are there hypoxic regions in the GL? 105
1-6 – Why are capillary haematocrit levels low in the GL? 106
Section 2 – The cerebral cortex 108
2.1 – Capillary haematocrit in the awake cortex is higher than previous estimates from anaesthetised mice 108
2.2 – Cortical tissue Po_2 is correlated with both capillary haematocrit and RBC flow 109
2.3 - Tissue Po_2 is lower in layer I than in underlying layers 109
2.4 - The correlation of Po2 and blood flow parameters in layers II/III and IV 110
2.5 – Po_2RBC is independent of blood flow parameters in layer IV 112
2.6 – Penetrating arterioles and venules in the cortex 112
Section 3 – Comparison of Po_2 and RBC flow in the awake state and under isoflurane anaesthesia 113
Section 4 – Comparison of my data with previous measurements of P_{O2} in the awake brain 114
Section 5 - Comparison of my data with similar measurements made under anaesthesia 115
Section 6 – Appraisal of Sakadzic et al. (2014) "Large arteriolar component of oxygen delivery implies a safe margin of oxygen supply to cerebral tissue" 117
6.1 – Experimental animal preparation 117
6.2 – Measurement of near-RBC P_{O2} and its difference from P_{O2}RBC 118
6.3 – Change in 'P_{O2}RBC' with depth in the cortex 120
6.4 – Evidence for a large supply of oxygen to the cortical tissue from arterioles 120
6.5 – Conclusion 123
Section 7 – A perspective on the applicability of anaesthetised animal preparations in cerebrovascular research 124
Section 8 - Potential application of the present data to theoretical studies of oxygen dynamics 125
Section 9 - Remaining questions and future directions 126

PART 5: CONCLUSION 129

PART 6 : BIBLIOGRAPHY & APPENDICES 133

Bibliography 134

List of Figures.....144

Part 1: Introduction

Chapter 1: Oxygen, Metabolism and the Brain

Section 1 – Cellular metabolism, ATP turnover, and the role of oxygen in these processes

1.1 – Thermodynamics and the central role of ATP in the processes of life

Life can be defined as a temporary, but regenerative, area of order in a universe of ever-increasing disorder.

For any process to occur, the end result must involve an increase in the entropy of the universe. Overall increases in entropy are understood as decreases in the Gibb's energy associated with a particular process. The Gibb's energy is decreased in any overall process that can occur, and so it can be thought of as denoting the thermodynamic potential of a process to occur.

On all scales from macromolecules to whole individuals, the order implicit in the structure and organisation of organisms requires that the processes that establish and maintain this order be coupled to processes that increase disorder elsewhere.

This holds true for the biosphere as a whole (with overall increasing disorder generated by reactions in the sun or by the exothermic oxidation of inorganic molecules such as hydrogen sulphide in chemosynthesis), and within individual organisms down to the cellular and biomolecular level[1].

[1] Although the general principle discussed here is applicable to all life, for the purposes of this thesis the discussion will be limited to processes concerning eukaryotic heterotrophs, and more precisely to mammals.

Some such processes can be coupled directly, such that the entropy increase induced by one allows for the other to proceed in spite of its own thermodynamic unfavourability. An example of this type of direct coupling of processes can be seen when one considers the transport of glucose into enterocytes from the intestinal lumen. The sodium-glucose symporter proteins provide a mechanism for co-transport of sodium and glucose across the cell membrane. In this case, the increase in order (and decrease in entropy) associated with moving glucose against a concentration gradient is counterbalanced by the increased disorder induced by sodium moving along a concentration gradient, thus rendering the entire process a spontaneous, thermodynamically possible one.

Mechanisms that are available to allow other processes to occur however are not directly coupled, and require an intermediate process to allow for coupling.

If we once again consider the example of co-transport of sodium and glucose out of the intestinal lumen across the enterocyte apical membrane, one can ask how it is that a sodium concentration gradient exists across the cell membrane in the first place. In this case, the gradient is maintained by the operation of the Na^+-K^+ ATPase. This protein antiporter extrudes 3 Na^+ ions from the cell (while bringing 2 K^+ ions into the cell), with this process made thermodynamically possible by the increase in entropy associated with the hydrolysis of one molecule of adenosine triphosphate (ATP) into an adenosine diphosphate (ADP) and an inorganic phosphate (Pi).

In an aqueous solution at 37°C the ATP ⇌ ADP + Pi reaction will reach an equilibrium whereby almost all the ATP has been dissociated into ADP + Pi. In cells however, the concentration of ATP is typically 1-10 mM, which is ~3-10 times that of ADP, and thus this reaction is very far from equilibrium (a displacement of ~10^{10} fold). Thus, this reaction, the production of ADP+ Pi from ATP, is extremely

thermodynamically favourable. ATP hydrolysis is coupled mechanistically to many other processes in the organism, and in this way, ATP serves as an energy currency, allowing these thermodynamically unfavourable, order generating, processes to proceed. These processes and reactions include such essential biological functions as the synthesis of nucleic acids from nucleotides, synthesis of proteins from amino acids, transport across membranes (for example to generate, maintain and restore ion gradients and membrane potentials), and intracellular transport processes.

The maintenance of the ATP ⇌ ADP + Pi reaction far from equilibrium is central to the utility of ATP as a thermodynamic intermediate. This state is maintained by continuous production of ATP from ADP and Pi. The fact that progress of the reaction in this direction to produce ATP is itself thermodynamically unfavourable is circumvented by coupling this synthetic reaction to controlled catabolic consumption of complex molecules. This serves to increase the total entropy sufficiently to allow the overall process to progress.

In this way, the ordered structure and operation of eukaryotic heterotrophs is generated and maintained by linking these processes to the disordering of other complex structures, leading to a global increase in entropy. ATP's role in this overall process is to allow for coupling of spatially and temporally separated steps by acting as an intermediate store of thermodynamic potential (in this case Gibb's energy). The mechanisms that underlie synthesis of ATP in mammalian systems will be discussed in the following section.

1.2 – Cellular production of ATP

The total mass of ATP in the human body at any one time is approximately 100g. However, a resting adult human consumes approximately 40kg of ATP over the course of 24h, and indeed during strenuous exercise, the rate of ATP consumption can be as high as 0.5kg per minute (Berg et al., 2002) . Thus it is necessary that ATP is continually replenished, primarily achieved by synthesis from ADP and a P_i. In the following description, unless stated, the production of ATP is achieved in this way, with the consumption of 1 ATP and 1 P_i, resulting in the production of 1 ADP and 1 H_2O.

Generally, animal cells have two mechanisms in which ATP is produced by oxidation of energy substrates (primarily glucose but also fatty acids)[2]. The first, glycolysis, is a complex series of reactions, the end result of which is the splitting of a molecule of glucose to produce two pyruvate molecules, two NADH molecules and two ATP molecules. Pyruvate is readily interconverted with lactate, with the oxidation of an NADH molecule to NAD^+, or the reduction of NAD^+ to NADH for the production of lactate or pyruvate respectively.

The second way of making ATP in cells is via a linked set of processes, which utilise the pyruvate (either generated directly from glucose or indirectly from lactate) and fully oxidise it to CO_2, with the energy liberated being used to generate large quantities of ATP. In contrast to glycolysis, which takes place in the cytosol, these processes all take place in mitochondria.

[2] The brain metabolises only a very small amount of fatty acids, utilising almost exclusively glucose, as evidenced by its respiratory quotient of nearly 1 (0.97, with this number representing the ratio of CO_2 production to O_2 consumption by the brain, and indicating that carbohydrates are the primary energy substrate) (Clarke and Sokoloff, 1999) . For this reason I will only discuss metabolism of glucose as an energy substrate.

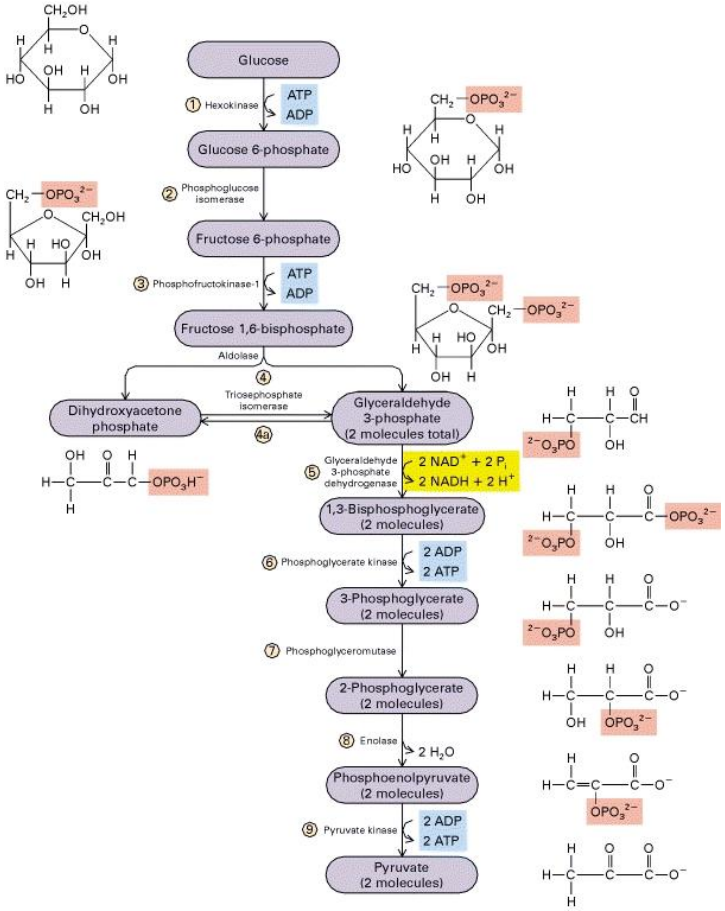

Introduction Figure 1. Schematic diagram of glycolysis. Adapted from (Lodish et al., 2000)

In the first of these processes, the pyruvate is conjugated to coenzyme A to form acetyl CoA, which also involves the reduction of an NAD^+ to NADH. Acetyl CoA can also be produced from fatty acids, with the production of 1 NADH and 1 $FADH_2$ from NAD^+ and FAD respectively.

Acetyl CoA acts as an intermediate to transfer the acetyl group into the process known as the citric acid cycle (or alternatively, the Krebs cycle, or the Tricarboxylic acid [TCA] cycle). In this cycle, the acetyl group is completely oxidised to CO_2, with the production of 6 reduced NADH and 2 $FADH_2$ molecules (along with one GTP).

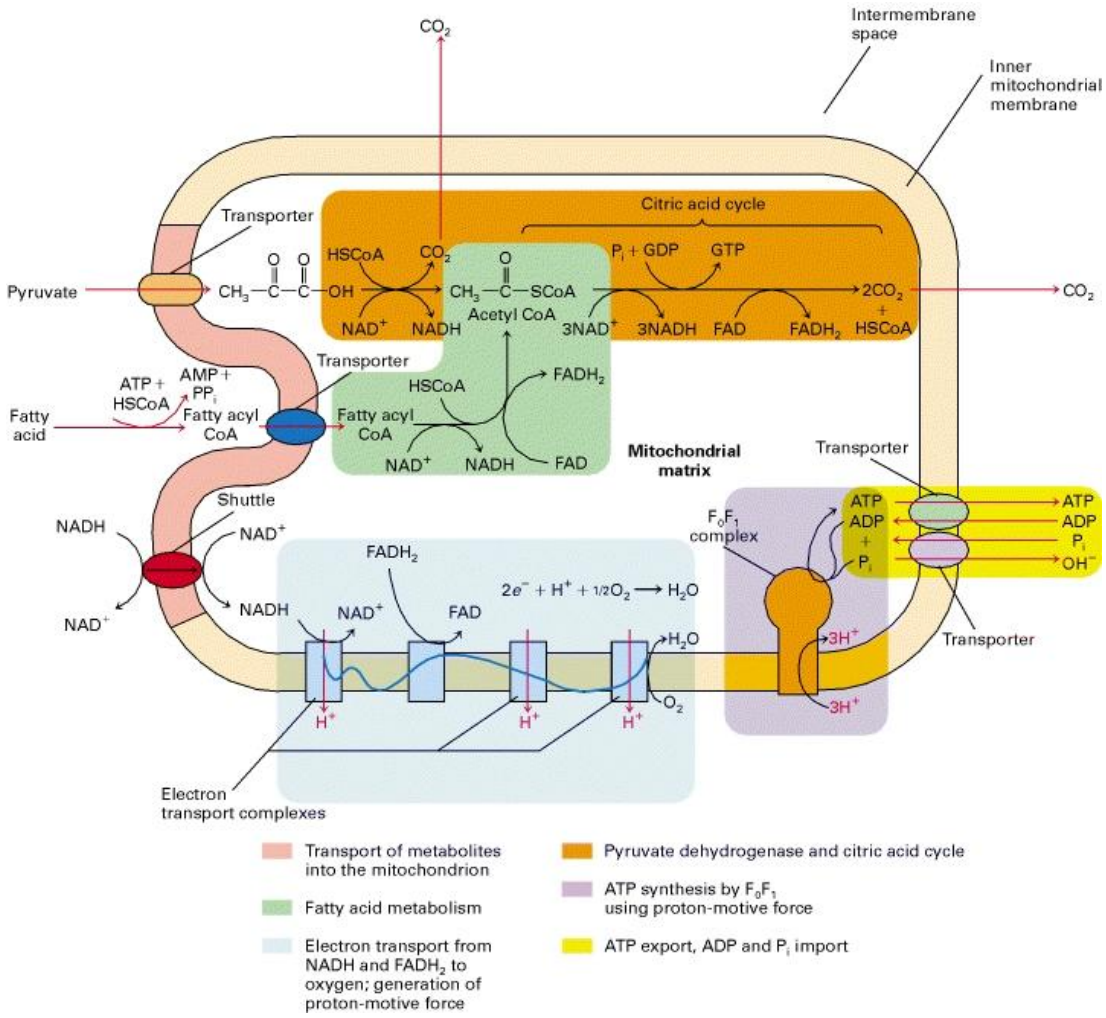

Introduction Figure 2. Schematic diagram summarising steps involved in oxidation of pyruvate (and fatty acids) in the mitochondria, and subsequent production of ATP via oxidative phosphorylation. Adapted from (Lodish et al., 2000)

The NADH and $FADH_2$ produced throughout these steps are vital to the final process which is oxidative phosphorylation. This process is carried out by a series of protein complexes (the electron transport chain) which sit in the mitochondrial inner membrane and which co-operatively act to oxidise the NADH and $FADH_2$ in a controlled fashion, and to harness the free energy released to pump H^+ ions from inside to outside the mitochondrial inner membrane. This extrusion produces a H^+ gradient across this membrane. The energy stored in this gradient is used to power the ATP-synthase enzyme. This protein complex provides a passage for H^+ to flow to the inside of the inner membrane, but their passage induces rotation and

conformational changes in the enzyme such that ADP and P_i are combined to form ATP.

The constituents of the electron transport chain (Complexes I to IV), all contribute to the controlled oxidation of the NADH and $FADH_2$ coenzymes. This allows the H^+ extrusion to proceed, but it is at complex IV, cytochrome c oxidase (or simply cytochrome oxidase), that the corresponding reduction aspect of the redox reaction occurs. Electrons, garnered from the coenzymes and passed along the electron transport chain complexes and cofactors, are transferred to oxygen along with 2 H^+ ions to form H_2O.

Therefore, oxygen acts as the ultimate acceptor of the electrons which are taken from the reduced coenzymes. It is molecular oxygen's substantial oxidising power that provides the thermodynamic drive to allow this series of electron-transferring and H^+-translocating reactions to proceed. Thus, production of ATP at the ATP synthase is completely dependent on oxygen.

Glycolysis, which does not involve molecular oxygen, produces only 2 ATP molecules per glucose molecule consumed. Conversely, the processes that converge on ATP production in the ATP-synthase can theoretically produce up to 34.6 ATP molecules (plus 1 GTP) by the complete oxidation of the two resultant pyruvate molecules to CO_2. Although the actual rate of ATP generation is approximately 30 ATP per glucose molecule consumed (Rolfe and Brown, 1997; Raichle and Mintun, 2006) (mostly due to loss of electrons along the electron transport chain and H^+ leak across the inner membrane), it is nonetheless clear that the vast majority of ATP production capability in animal cells is critically dependent on the presence of oxygen.

For each molecule of glucose that is fully oxidised, 6 O_2 molecules are consumed. The approximate number of ATP molecules produced by full oxidation of a glucose molecule is 32, of which 2 come from glycolysis, and thus 30 come from oxidative phosphorylation. This means that although the theoretical correspondence is approximately 6 ATP produced per 1 O_2 consumed, the actual ratio is closer to 5.3:1. Considering only the ATP produced via oxidative phosphorylation, the ratio is approximately 5 ATP produced per O_2 molecule consumed.

Section 2 – Oxygen in Physiology

2.1 – The physical and chemical properties of oxygen in biological systems

Oxygen can be measured in a number of different but related ways. Three essential parameters when considering oxygen in mammalian physiology are the concentration of dissolved oxygen ($[O_2]$), the partial pressure of oxygen (Po_2), which is related to the absolute number of O_2 molecules, the temperature and the local pressure, and the oxygen saturation of haemoglobin (Hb) in the red blood cells (RBCs) of the blood. This saturation is the proportion of Hb which has an O_2 molecule bound to it. It is abbreviated as So_2 and is expressed as a percentage. Hb-O2 binding, So_2 and their relationship to Po_2 will be discussed later (in section 2.2 of this chapter).

In physiology, Po_2 is typically expressed in units of millimetres of mercury (mmHg) or torr (Torr) (1 mmHg ≈ 1 Torr ≈ 133.3 kPa), and is related to the dissolved O_2 by the relationship:

$$[O_2] = (\alpha)(Po_2)$$

(Henry's law, where α is the solubility coefficient of oxygen in the solvent, often approximated as 3×10^{-5} ml O_2/ ml liquid/ mmHg, for blood plasma, intracellular fluid and interstitial/extracellular fluid [ISF]). The Po_2 influences diffusion, and spatial Po_2 differences establish diffusion gradients which are integral to gas transport in the body.

In addition to its essential role in eukaryotic metabolism (as the terminal electron acceptor in the electron transport chain), oxygen is a potent toxin. These two properties are intimately related, as they both derive from the two unpaired electrons

in molecular oxygen's valence shell. These electrons confer a very large redox potential and make O_2 the very powerful oxidising agent that it is. Production of reactive oxygen species (ROS) occurs during normal cellular and metabolic processes. Although essential in some normal physiological processes, these species are highly toxic, and are capable of oxidising essential cellular elements such as nucleic acids, lipids and proteins, inducing severe cellular and tissue damage. For this reason there are multiple mechanisms by which the body limits the formation of these chemicals and limits the damage wrought by those which are produced. However, in cases of excessive oxygenation, these protective mechanisms can be overwhelmed and oxygen toxicity can ensue. Therefore, in order to maintain sufficient aerobic production of ATP while avoiding oxygen toxicity, P_{O_2} must be tightly regulated (Acker and Acker, 2004).

The integrated operation of the cardiovascular and respiratory systems serves to facilitate controlled uptake of oxygen from the atmosphere into the body and its appropriate distribution among the various organs, tissues and cells that depend critically upon it.

2.2 – The transport of oxygen from the atmosphere to the mitochondria

Normal atmospheric P_{O_2} is around 159 mmHg (this partial pressure derives from O_2 making up ~21% of dry air, and total atmospheric pressure being 760 mmHg).

During inhalation, as air passes through the upper respiratory tract and trachea, the air is warmed and humidified, becoming saturated with water vapour. This increase in P_{H_2O}, in addition to both a loss of O_2 and an increase in CO_2 due to gas exchange with the blood means that the alveolar P_{O_2} is on average around 100 mmHg. The dense capillary network around the alveoli provides a large surface area for gas

exchange with the blood. Although a certain quantity of oxygen can dissolve in the plasma and the cytosol of red blood cells (RBCs), the vast majority (~98%) of the oxygen in blood is bound to haemoglobin (Hb) in the RBCs.

Haemoglobin is a protein made of four subunits, each containing of a haem group, which is a porphyrin with an iron atom at its centre. The iron atom is normally in the Fe^{2+} state and can reversibly bind O_2. Each iron atom can bind 1 O_2 molecule, and so a complete Hb tetramer can bind 4 molecules of O_2. In human RBCs, the Hb concentration is around 33% w/v. In theory, 1g of Hb can bind up to 1.39 ml of O_2, however, as a portion of Hb in blood is unable to bind O_2 (due to the effects of oxidation of the iron atom or binding of carbon monoxide) the empirically determined ratio *in vivo* is closer to 1.34 ml/g (Pittman, 2011). Nonetheless, with approximately 270 million Hb tetramers in each cell (Pierigè et al., 2008) , when fully saturated, a single RBC can bind and transport over 1 billion O_2 molecules.

The binding of O_2 to Hb is cooperative. Binding of O_2 to a single subunit induces a conformational change in the haemoglobin tetramer that enhances the affinity for the other subunits for O_2. Hb in which at least one of the subunits has bound an O_2 molecule has an affinity for O_2 binding that is around three times as strong as that of fully deoxygenated Hb.

This cooperativity is reflected in the characteristic sigmoid shape of the oxygen-Hb binding curve (Berg et al., 2002), which relates So_2 to Po_2 (Introduction Figure 3).

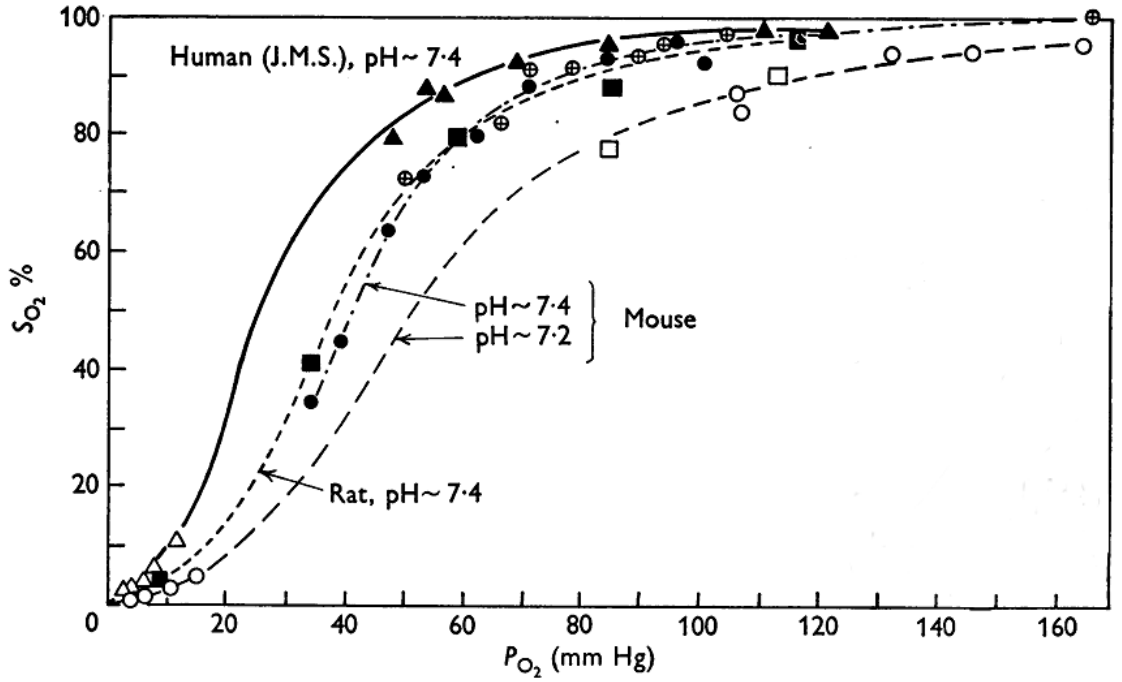

Introduction Figure 3. Oxygen-Haemoglobin binding-curves of human, rat and mouse blood. Adapted from (Gray and Steadman, 1964)

Due to the fact that in normal physiology the vast majority of O_2 in blood is bound to Hb, the oxygen carrying capacity of the blood is highly dependent on the amount of RBCs in a given volume of blood. This parameter, the volume of RBCs in a volume of blood is known as the haematocrit (expressed as a % v/v). Systemic haematocrit in humans is around 42-45%, so considering that RBCs are 33% Hb w/v, one can conclude that 100ml of fully oxygenated systemic blood (Po_2 ~100mmHg) can bind and transport ~18.7-20.1 ml of O_2 (in addition to a small amount dissolved in the plasma and the cytosol of blood cells).

The vascular system transports oxygen (primarily bound to Hb in RBCs) around the body. From the lungs, freshly oxygenated blood returns to the heart, from where it is pumped into the aorta, which gives rise to all the main arteries that distribute blood to the disparate areas of the body. In the case of the brain, this blood supply comes from the vertebral arteries and internal carotid arteries, which arise from the subclavian and common carotid arteries respectively, all of which derive their inflow

from the ascending aorta. A description of the brain vascular supply is found later in this manuscript (Chapter 2: Section 1).

Generally speaking, from the main arteries, blood is distributed into smaller arterioles and subsequently capillary beds, before progressive re-convergence through the venous network and return to the heart and lungs for re-oxygenation and redistribution.

It is primarily at the level of the microcirculation (the arterioles, capillary network and small venules within a given organ) that O_2 (and other solute) exchange occurs between the blood and the tissue. In the case of oxygen, this occurs via progressive unbinding of O_2 from Hb, and its diffusion from the RBCs into the plasma, across the vascular walls and into the tissue. The affinity that most adult human blood has for O_2 means that at normal macrocirculatory Po_2 (Arterial blood Po_2 ≈ 95-100 mmHg, mixed venous blood Po_2 ≈ 40mmHg) the haemoglobin in the blood will be largely saturated, but in the microcirculation Po_2 values fall to the range where there will be significant desaturation of HB and release of the bound O_2. In the tissue, O_2 will be dissolved in both the interstitial fluid and in cells. Within cells, O_2 finally diffuses to the mitochondria, where it is consumed by reduction to H_2O at cytochrome c oxidase (as described earlier). Representative values of Po_2 in different vascular compartments and in the interstitial fluid are presented in Introduction Table 1.

Compartment	**Mean Po_2 (mmHg)**	**So_2 (%)**	**Reference(s)**
Arterial Blood	~95 - 100	~95 - 100	(Pittman, 2011b)
Arteriolar Blood	20 - 80	50 - 80	(Tsai et al., 2003)
Capillary Blood	10 - 50	40 - 60	(Tsai et al., 2003)
Venular Blood	10 - 40	50-60	(Tsai et al., 2003)
Mixed Venous Blood	~40	~75	(Pittman, 2011b)
Intrastitial Fluid	~20	-	(Tsai et al., 2003)

Introduction Table 1. Representative values of oxygen in vascular compartments and interstitial fluid.

2.3 – Mechanisms of oxygen delivery from the microvasculature to the tissue

As it is the main site of oxygen delivery to the tissue, the mechanisms and process that govern oxygen transfer at the level of the microvasculature merit further attention.

Oxygen diffuses according to Po_2 gradients, and the difference between Po_2 in the vasculature and the tissue provides the 'driving force' for transport of oxygen between these compartments. Thus, at the level of the microvasculature, diffusion of oxygen from the vasculature to the tissue occurs at all points where there is a Po_2 gradient to induce this flow.

Most transport of oxygen to the ISF and then the parenchymal cells in a tissue occurs from arterioles and capillaries. Both Po_2 and So_2 fall progressively along the arteriolar network, with oxygen continuously being unloaded from Hb and diffusing from the RBCs through the plasma and across the arteriolar wall into the ISF. There is a similar overall longitudinal gradient in capillaries, but the situation is complicated by the fact that capillary luminal size if similar to the diameter of RBCs (Human RBC diameter = ~8μm (Rosen, 1967), mean human brain capillary diameter = ~6.5 μm (Lauwers et al., 2008). Mouse RBC diameter ~6μm (Milo et al., 2010), mean mouse brain capillary diameter ~4μm (Blinder et al., 2013) . For this reason, in capillaries, RBCs proceed in single file, with each RBC being separated from the preceding and succeeding cell by a region of plasma. As O_2 solubility is limited in the plasma, the Po_2 will be higher near the RBCs than at greater distance from them. Thus, at a given point in a capillary, there will be alternating periods of high and low Po_2 related to the passage of RBCs. This phenomenon was initially predicted by Hellums in 1977 (Hellums, 1977) and termed "erythrocyte associated transients" (EATs). These EATs were first experimentally observed in the rat mesenteric microvasculature by Golub and Pittman in 2005(Golub and Pittman, 2005) . The effect of this heterogeneous

oxygenation of capillary blood is a decrease in the effective surface area of the capillaries available for O_2 diffusive delivery of oxygen to the ISF. Only the areas near the RBCs that have a Po_2 that is greater than that of the tissue will have a net flux of O_2 out across the capillary wall. Conversely, the magnitude of the vascular-tissue Po_2 gradient will be greater in the regions near the RBCs than what would be understood by simply comparing the mean vascular and tissue Po_2.

O2 diffuses from the vasculature according to the vascular-tissue Po_2 gradient, thus, at steady state, the quantity of O_2 diffusing across the microvessel wall is equal to the quantity that is consumed by the tissue that is supplied by that vessel. Additionally, given that the ISF surrounds the cells (which consume and thus act as sinks for O_2) and the blood vessels (which are the local sources of O_2), it represents the interface between these two elements and its Po_2 in effect reports the equilibrium between O_2 supply and demand. The gradient that exists between microvascular Po_2 and mitochondrial Po_2 can be perturbed by increases or decreases in either oxygen delivery or consumption. The primary reason for changes in O_2 consumption rate is a change in tissue metabolic rate and ATP production via oxidative phosphorylation.
Delivery of oxygen to a given tissue volume can be increased either by increasing the total blood flow (and so RBC delivery) into that volume (which thereby increases convective delivery of O_2) or by increasing the fractional extraction of that O_2 which is made available by the blood flow in that volume. This can be achieved by increasing the surface area for O_2 diffusion, either by increasing the number of capillaries that are fully perfused in the region (capillary recruitment) but also by increasing the total capillary wall area that is in close apposition to RBCs. This latter mechanism will increase the diffusive flux of O_2 from capillaries by increasing the effective surface area available for diffusion from the higher Po_2 regions near RBCs. This increase in effective surface area can be achieved by increasing local haematocrit. These mechanisms have been observed in peripheral tissues (eg. skeletal

muscle) although their relative importance in oxygen delivery to these tissues is a topic of much debate(Pittman, 2011; Poole et al., 2011) .

Section 3 – Metabolism, ATP turnover and Oxygen Consumption in the Brain

The brain is very expensive metabolically. In adult humans, it makes up only 2% of the body's mass, but accounts for approximately 20% of resting metabolic rate (Attwell and Laughlin, 2001). In mice the brain makes up slightly less of the overall body weight (1.8%), but is proportionally less energetically expensive, contributing around 6.5% of total energy expenditure (Kummitha et al., 2014).

Human brain glucose consumption at rest has been measured at 23 μmol/100g/min. Average adult brain mass is around 1400g in males and 1200g in females. Thus for the whole brain, the total glucose consumption rate is 322 μmol/min for men, and 276 μmol/min for women. There are, however, regional differences in metabolic rate within the brain, with grey matter being more energetically demanding than white matter. Comparisons of metabolic rate for glucose in the human brain shows variations between structures and subregions ranging between 15 – 45 μmol/100g/min, with means of 30-40 μmol/100g/min in the grey matter and around 20 μmol/100g/min in the white matter(Heiss et al., 1984) . Measurements of glucose metabolism in the rat brain show that grey matter glucose consumption ranges between 54 and 197 μmol/100g/min, depending on regional activity levels, whereas white matter consumption rates are more homogenous with values of 33-40 μmol/100g/min(Clarke and Sokoloff, 1999). In rats the rate of cerebral glucose consumption is around 65 μmol/100g/min, which gives a whole brain consumption rate of around 1.24 μmol/min(Linde et al., 1999) (the mass of a rat brain is ~1.9g).

By considering that for each glucose molecule consumed in the brain 32 ATP molecules are generated, we can arrive at a set of values for the specific and absolute rates of ATP turnover in the brain. Thus, in humans, ATP turnover rate in the brain as a whole is 736 μmol/100g/min, the rates in the grey and the white matter are 960-1280 and 640 μmol/100g/min respectively, and in total, the human brain consumes on average 8832-10304 μmol/min. In the rat, the equivalent figures are approximately 2080 μmol/100g/min for whole brain ATP turnover rate, 1728-6034 μmol/100g/min and 1056-1280 μmol/100g/min for grey and white matter respectively, and 39.5 μmol/min for the brain's total ATP consumption.

Considering the rate of oxygen consumption, specific rates for the whole human brain have been measured as 143-156 μmol/100g/min(Madsen et al., 1995; Clarke and Sokoloff, 1999) . This rate is similar for both males and females, giving an average total rate of consumption of 1700-2200 μmol/min.

As an illustrative calculation, we can work out the amount of O_2 that could be dissolved in the brain tissue at any given moment, and compare it to the brain's rate of O_2 consumption. Taking a value of the solubility coefficient of O_2 in brain tissue of 3×10^{-5} ml O_2 (ml tissue)$^{-1}$ (mmHg)$^{-1}$(Sharan and Popel, 2002) , and a value of 30 mmHg for brain tissue Po_2 (which is towards the higher range of the mean Po_2 values that have previously been recorded in the mammalian brain, as collated by Ndubuizu and LaManna in 2007(Ndubuizu and LaManna, 2007)), dissolved O_2 in the brain can be calculated to be 9×10^{-4} ml O_2 (ml tissue)$^{-1}$. After appropriate conversions, we arrived at a value of 4×10^{-5} mol O_2 (g tissue)$^{-1}$ for the quantity of O_2 dissolved in each unit mass of brain tissue.

The resting rate of consumption of O_2 in the brain has been measured as up to 1.56 μmol (g tissue)$^{-1}$ (min)$^{-1}$ in humans(Clarke and Sokoloff, 1999) , and 3.4μmol (g tissue)$^{-1}$ (min)$^{-1}$ in rats(Nilsson and Siesjö, 1976) .

Thus, human brain is capable of consuming all the O_2 dissolved in it in around 1.5s, and the rat brain will do so in 0.7s. This suggests that there is essentially no tolerance in the brain for an interruption of oxygen supply, and that therefore the rate of consumption must be compensated for by the delivery of an equivalent quantity of oxygen.

The fact that the brain lacks the capacity to store oxygen means that it must constantly be supplied with all the oxygen necessary to support its functioning. Thus, the human brain must receive at least 36.4μmol/s (or 0.815 ml) of oxygen per second. All of this oxygen must be transported in the blood. Therefore, in the next chapter I will describe the vascular supply to the brain.

Chapter 2: Supply of Blood to the Brain, and our Model Systems.

Section 1 – Blood supply to the Brain

Given the magnitude of brain's demand for oxygen and energy substrates, and its sensitivity to interruption of their delivery (in humans, consciousness is lost within seconds of a cessation in blood supply to the brain (Raichle and Mintun, 2006)), it is imperative that it receives a large and reliable supply of blood.

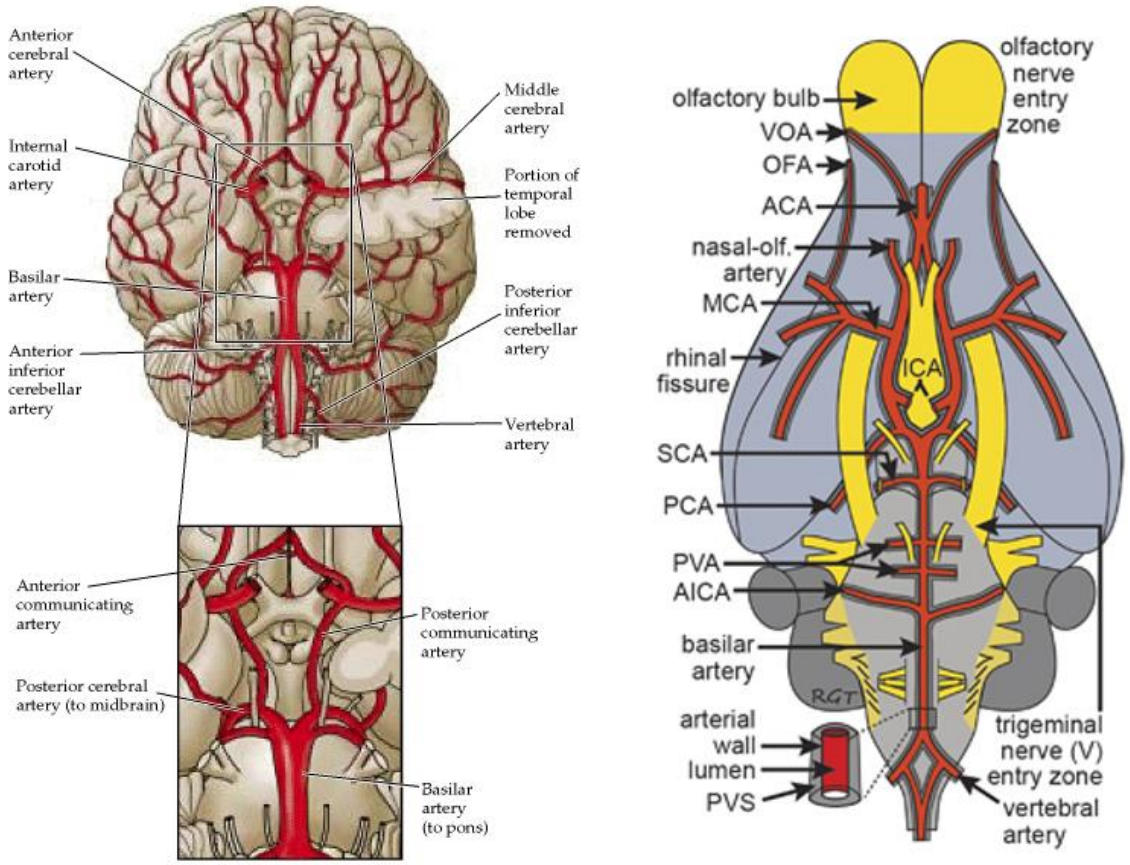

Introduction Figure 4. Diagrams of the ventral surface of the human (left panel) and mouse (right panel) brains, showing major features of the cerebrovasculature. Of note are the vessels which form the circle of Willis (see lower portion of left panel, and text for details), along with the basilar and internal carotid arteries (which supply the blood to the brain), and the major cerebral arteries (ACA, MCA, and PCA, see text for details). Left panel adapted from(Purves et al., 2001) . Right panel adapted from (Lochhead et al., 2014) .

The supply of oxygenated blood to the brain is via the two internal carotid arteries and the basilar artery (which itself is formed when the two vertebral arteries merge). In addition to giving rise to branches which supply blood to such structures as the pituitary gland, the choroid plexus and many areas of the brainstem, major output of each these three vessels is to the circle of Willis (also known as the cerebral arterial circle). This critical structure, located at the base of the forebrain, is a network of vessels which form a loop that connects the major inflows from the peripheral circulation to the major cerebral vessels that supply blood to the forebrain Introduction Figure 4. The basic structure of the circle of Willis is composed of the two posterior cerebral arteries (PCA, which diverge from the basilar artery), the two internal carotid arteries, and the two anterior cerebral arteries (ACA), along with the anterior communicating artery and the two posterior communicating arteries.

The ACA and PCA, in addition to the middle cerebral arteries (MCA), also form the major outflows from the circle of Willis. These three pairs of arteries are commonly referred to as the major cerebral arteries, and provide the bulk of the blood supplied to the cerebrum.

These vessels give off many branches which supply subcortical structures (for example the central branches of the MCA irrigate such structures as the thalamus, the striatum and the internal capsule). However, the main branches of these arteries proceed onto the cortical surface where they divide to into a network of pial arteries. Each of the major cerebral arteries has a broadly defined territory in the forebrain for which they almost exclusively provide the blood supply, although arterio-arterial anastamoses between certain downstream vessels allow for a degree of flow redistribution at the borders of these territories. Generally speaking, the ACA supplies a region that encompasses the medial portions and extends into the dorso-medial portions of the frontal and parietal lobe. Conversely, the MCA supplies a volume of the forebrain in the dorsal and lateral regions of the frontal and parietal

lobes along with the dorso-lateral areas of the temporal lobes, and the insula. Finally, the PCA supplies blood to the occipital lobe, as well as the ventro-medial areas of the temporal lobe.

The pial arteries lie on the surface of the cortex, in the subarachnoid space. From these pial vessels, descending arteries penetrate the cortex itself. They subsequently ramify extensively to generate the dense network of the cortical microvasculature.

The draining of blood from the brain is accomplished via large intracranial venous sinuses which are fed by both superficial and deep veins and have outflows which return blood to the peripheral circulation. In the case of the neocortex, microvessels in the cortical microvasculature eventually converge upon penetrating venules, which ascend to the cortical surface and allow blood to be drained to the pial venule network. From here the blood flows into collecting superficial veins and thence to the sinuses.

Section 2 – Our Model Systems

In the research presented in this dissertation, I concern myself mainly with two particular brain areas: the olfactory bulb, and the somatosensory cortex. I will thus present a more in depth treatment of these two regions, discussing their organisation and function

2.1 – The olfactory bulb

The olfactory bulb is a forebrain structure, which in humans is located to ventral to the frontal lobe but in rodents is rostral to the frontal lobes near the dorsal surface of the skull. It consists of two substructures: the main olfactory bulb and the accessory olfactory bulb. In my work I have dealt exclusively with the main olfactory bulb, will thus focus only on it during this introduction, and will refer to it simply as the olfactory bulb.

2.1.1 – Structure and basic functions

It has a relatively simple laminar structure, consisting of six well defined layers. Proceeding from the most superficial to the deepest layer they are, in order: The olfactory nerve layer (ONL), the glomerular layer (GL), the external plexiform layer (EPL), the mitral cell layer (MCL), the granule cell layer (GCL), and the internal plexiform layer(IPL).

It is the first central relay of the olfactory system, and importantly for our work, the first synaptic contact in this system occurs in the glomeruli of the olfactory bulb, which are located in the superficial GL (at a depth of approx. 40-150μm in the mouse), such that those in the dorsal portion of the bulb are accessible for *in vivo* imaging studies.

The basic circuit of the olfactory bulb is as follows: Olfactory sensory neurons (OSNs) located in the olfactory epithelium project both cilia into the nasal cavity, and axons, through the cribiform plate, towards the olfactory bulb. Axons expressing particular forms of olfactory receptors become associated into fascicles which eventually extend through the ONL to one of two specific glomeruli which are located on opposite sides of the olfactory bulb.

These glomeruli are areas of neuropil which are formed by the terminals of incoming OSN axons, and the dendrites of mitral cells and tufted cells, along with those of a heterogeneous array of juxtaglomerular neurons and the processes of GL astrocytes. They are essentially devoid of cell somata, and thus can be conceptualised as functional units composed entirely of synaptic and peri-synaptic structures.

In the mouse, the GL of each bulb contains between two- and four-thousand glomeruli (Mombaerts, 2006; Richard and Taylor, 2010) arranged in a broadly stereotyped map (Soucy et al., 2009) which contains an axis of mirror symmetry, such that the two glomeruli in each bulb that receive the axons from a specific class of OSNs are located on opposite sides of the bulb.

Each glomerulus receives input from some 5×10^3 OSNs, encompasses the axial tufts of around 25-50 mitral cells and 60 tufted cells, and are contacted by the processes of approximately 100 juxtaglomerular neurons and around 20 astrocytes(Nawroth et al., 2007) . The cell bodies of the juxtaglomerular neurons and glomerular-layer astrocytes are located in the interglomerular regions of the GL, those of tufted cells are located in the EPL, and mitral cell somata are located in the MCL.

Mitral and tufted cells are the main output neurons of the olfactory bulb, and project to numerous cortical and subcortical structures which deal with the processing and interpretation of olfactory stimuli.

Both mitral and tufted cells have extensive lateral dendritic arbours in the EPL and are contacted there by the similarly extensive processes of GABAergic granule cells to form reciprocal dendro-dendritic synapses.

Although a gross simplification, the olfactory bulb response to an odour stimulus can be described thus:

Odourant receptors on OSN cilia in the nasal epithelium are activated by the binding of the odourant molecules for which they have sufficient affinity. In response the OSNs fire action potentials, which proceed to the glomeruli. Here, pre-synaptic glutamate release is detected by the various post- and peri-synaptic elements of the relevant glomeruli. The circuit and synaptic interactions are already quite complicated at this level, potentially involving GABAergic, dopaminergic and glutamatergic inputs from varous juxtaglomerular cells and dendritic release of glutamate by both mitral and tufted cells.

Subsequent mitral and tufted cell activity is further influenced by their interactions with one another and with granule cells. Their final action potential output is then transmitted to higher areas for further treatment.

2.1.2 – Vascular supply and organisation of the olfactory bulb

Blood is supplied to the olfactory bulb by the olfactofrontal artery and the ventral olfactory artery, both of which are branches of the ACA. They each divide into a lateral and a medial branch, which proceed into the bulb, towards the dorsal regions in the case of the olfactofrontal artery and the ventral regions for the ventral olfactory artery (Coyle, 1975) . A number of anastmotic connections were observed between the medial and lateral branches of each artery, and also between the vessels of the ventral and dorsal regions. These large arterioles were situated near the surface, but give rise to smaller branches which penetrate into the bulb and supply the deeper laminae.

These observations fit with those from our own laboratory. In *in vivo* experiments, we commonly observe the existence of a small number of large vessels (both veins and arteries) on the dorsal surface of the bulb, and a larger quantity of minor

arterioles and venules in the EPL, which appear to be branches of these large vessels, some of which descend into the GL and beyond.

The organisation and distribution of vascular elements in the bulb

The vascular organisation of the olfactory bulb has yet to be thoroughly explored, particularly in the case of the deeper laminae. The density of vascular elements in the more superficial layers of the rat olfactory bulb has been studied however, initially by Borowsky and Collins (Borowsky and Collins, 1989) using histological approaches in fixed olfactory bulb slices, and subsequently here in the Charpak lab using *in vivo* 2-photon imaging(Chaigneau et al., 2007; Lecoq et al., 2009) .

The combined results of these studies show that capillary density of the glomeruli (1056 ± 72 mm/mm^3) is higher than both that of the EPL (746 ± 111 mm/mm^3) and of the ONL, the latter of which is essentially devoid of capillaries (only 45 ± 26 mm/mm^3). This value of capillary density in the GL is among the highest recorded in the brain. The calculated average distance from any given point to the nearest capillary was calculated to be 36.55 ± 1.69 μm in the ONL and 10.78 ± 0.73 μm in the glomeruli.

The density of larger microvessels, either arterioles or venules, is also low in the superficial layers of the dorsal olfactory bulb. The average distance from any given point in the ONL to a blood vessel (be it a capillary or a larger vessel) was determined to be approximately 28 ± 5 μm.

The capillary network in the GLs appears to be continuous and relatively homogenous, with no apparent functional organisation relative to the glomeruli. Indeed there are typically numerous capillaries that cross the inter-glomerular space and others which can traverse multiple glomeruli. (Chaigneau et al., 2003)

2.2 – The somatosensory cortex

2.2.1 – Structure and basic functions

The cerebral cortex is a thin layer of grey matter that forms the outermost regions of the cerebrum. The neocortex is characterised by a 6-layered structure, named layers I to VI proceeding from the pial surface to the sub-cortical white matter. The relative volumes and exact function of each layer varies somewhat with the area of the cortex considered, but nonetheless some basic parameters hold true. Classically the layers are described and distinguished based on their neuronal content. Layer I has few neuronal cell bodies, consisting mostly of axons and dendrites of cells located in deeper layers. Layers II and III both contain multiple cell types with smaller spherical neurons predominating in layer II and pyramidal cells being more prominent in layer III. Layer IV densely packed with smaller spherical cells with stellate cells being common, whereas layer V contains many large pyramidal cells which send their apical dendrites up through all the overlying layers. Layer VI, the deepest layer of the cortex, borders the underlying white matter and contains multiple different types of neurons which make connections with intracortical and subcortical structures.

The cortex as a whole is made up of vertically-oriented modules which seem to represent the basic functional unit. These modules, also known as cortical columns, consist of 200-400 μm diameter portions of the cortex that encompass the entire depth of the cortex within that area.

These columns receive and process information from either thalamocortical inputs, corticocortcal fibres or a combination of both, in addition to neuromodulatory inputs from subcortical nuclei. It is thought that the basic circuit organisation is similar across different regions of the cortex, though the input and output projections will vary according to location and function of the modules(Douglas and Martin, 2004) . A very general description of the circuit is that thalamic input to the cortical area is targeted primarily to layer IV, and that layer IV excitatory neurons synapse onto

pyramidal neurons in the more superficial layers. The axonal arbours of layer II and III neurons project to multiple targets including other Layer II and III neurons, layer IV neurons in other cortical area and also neurons in layer V of the same column, which in turn project to layer VI. Layer VI neurons then project either back to layer IV to complete a loop, or out of the cortex to the thalamus or other targets. This coarse description has been found to generally hold true for sensory and motor areas across multiple mammalian species (Douglas and Martin, 2004) .

The somatosensory cortex, located in the parietal lobe, is responsible for the initial cortical processing of sensation from the body. In humans it is located in a strip of cortex behind the central sulcus that runs from the midline to the most lateral aspect of the parietal cortex. The afferent input from the various parts of the body is organised such that there is a somatotopic representation of the body in the brain. This means that adjacent areas in the cortex receiving the input related to areas adjacent of the body, albeit with there being differences in the size of the cortical areas which represent the various regions of the body, with a correlation existing between the density of peripheral innervations and the size of the area in which it is represented. This can be clearly seen in Introduction Figure 5 (left-hand panel), in which the relative extent of cortical representation is mirrored by the apposed distorted image of a human body.

In rodents the primary somatosensory cortex is positioned in a homologous area of the cortex to that of humans, however its location is more difficult to discern based on anatomical features due to the lack of sulci and gyri in the rodent cortex. Nonetheless, the location of these areas of cortex can be approximated by use of stereotaxic co-ordinates. In adult mice, the primary somatosensory cortex covers large areas of the laterodorsal cerebral surface from around 2mm anterior to 2mm posterior to Bregma, with the areas representing the head, face and limbs lying between 0.6mm anterior and 1.2 mm posterior to Bregma and 1-4 mm either side of

the midline(Paxinos and Franklin, 2001). The primary somatosensory cortex of the rodent also displays a somatotopic representation of the body, but the relative proportions are different to that in humans, with relatively small areas receiving information from the paws and trunk as compared to those which are receive and process afferents relating to the face and especially the whisker-pad and vibrissae. The rodent equivalent to the human somatotopic homunculus is presented in Introduction Figure 5 (right-hand panel).

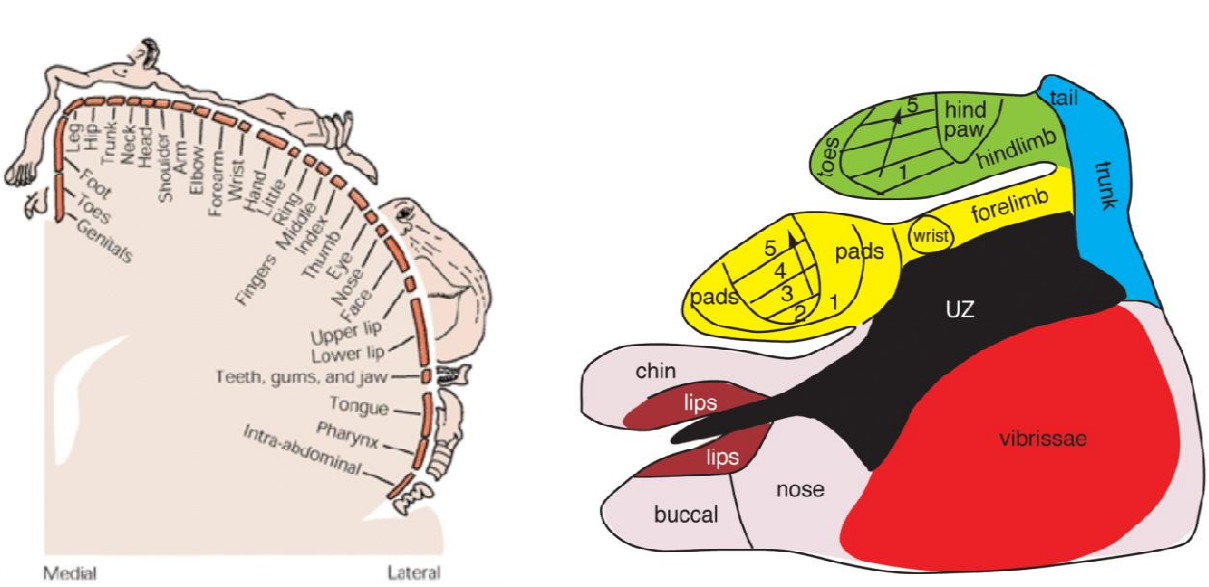

Introduction Figure 5. Diagrams showing the somatotopic representation of the body in the somatosensory cortex of the human (left panel) and rat (right panel) brains. Left panel adapted from (Kandel et al., 2000) . Right panel adapted from Seelke et al. (2012) (Seelke et al., 2012) (Originally from Chapin and Lin (1984) (Chapin and Lin, 1984).)

In the experiments which I have performed as part of my research, I have focused on the fore- and hind-limb related regions of the primary somatosensory cortex, which are located between roughly 0.5 mm anterior and 1.2 mm posterior to Bregma, and 1-3 mm either side of the midline(Paxinos and Franklin, 2001). Within this region the cortical laminar depths and thickness are as follows:

	S1 FL		S1HL	
	Thickness (µm)	Depth from Surface (µm)	Thickness (µm)	Depth from Surface (µm)
Layer I	62.7 ± 8.2	0 - 70	65.6 ± 7.1	0-75
Layer II/III	205.6 ± 14	75 - 280	191.7 ± 11.4	80-280
Layer IV	182 ± 8	290 - 480	162.9 ± 7.3	290-450

Introduction Table 2. Thickness and approximate range of depths from the cortical surface occupied by different layers I-IV in the S1FL and S1FL regions of the mouse somatosensory cortex. Laminar thickness data drawn from Altamura et al. (2007) (Altamura et al., 2007).

2.2.2 – Vascular supply and organisation of the Somatosensory Cortex

As outlined earlier, the cortex receives its vascular supply from the major cerebral arteries, which feed the pial artery network that then gives rise to the penetrating vessels and intracortical microvasculature.

The best characterised area of this cortical blood supply is the territory of the MCA, which covers large areas of the cortex, including somatosensory cortical regions such as the barrel cortex. The pial supply in this region is, as in other cortical regions, formed from a series of interconnected loops from which other branching pial vessels and penetrating arterioles arise. Within this looping structure there is a lattice-like backbone structure which allows for robust redistribution of flow within the network(Blinder et al., 2010) . The offshoots and penetrating arterioles on the other hand represent classic "end arterioles" which provide the blood supply to a particular volume of tissue(Hirsch et al., 2012). These penetrating arterioles descend from the pia into the cortex, where they ramify to form the dense network of the subsurface microvasculature.

Duvernoy et al. (1981) described the human cortical vasculature and classified both the penetrating arterioles and venules based on their penetration depth and the layers in which their branching is concentrated (Duvernoy et al., 1981) [3]. Group 1 vessels and group 2 vessels reach and ramify in layers I and II, and III respectively. Group 3 vessels are the most numerous, and branch extensively in middle layers of the cortex, primarily in layer IV but also in lower layer III and layer V. Group 4 vessels supply the lower layers of the cortex down to the border of the white matter, and group 5 are similar but with a more extensive supply of the underlying white matter. Group 6 vessels are exclusively arterioles and penetrate through the cortex without branching and only provide extensive vascularisation in the white matter.

In addition to the differences in the penetrating vessel supply to different laminae in the cortex, there are variations in the total microvascular and capillary density with

[3] The general aspects of the vascular supply to the neocortex are known to be broadly similar across multiple mammalian species (Hirsch et al., 2012) , and are likely to represent a conserved feature in mammals.

depth and layer. This has been observed in both the primate (Fonta and Imbert, 2002; Weber et al., 2008) and the rodent cortex (Tsai et al., 2009; Blinder et al., 2013). The microvascular density is lower in layer I than in deeper layers, showing a steady increase across layers II and III, reaching a peak in layer IV. In layers V and VI it is once again lower, in the range of densities seen in layers I, II, and III(see Introduction Figure 6). In agreement with the general pattern observed in the brain, vascular density is lower in the white matter than in the overlying grey matter.

Vascular density does not change only with layer and depth in the cortex. Tsai et al (2009), showed that there are variations in the total cross-laminar vascular density between different cortical areas of the same mouse(Tsai et al., 2009) . Furthermore, variations in vascular density have been observed when comparing different zones within particular cortical areas. When comparing areas which have high and low cytochrome oxidase activity (termed 'blobs' and 'interblobs', respectively) in the primate visual cortex, Keller et al. (2011) showed that there was a 4-5% greater microvascular density in the blobs than the interblobs(Keller et al., 2011) .

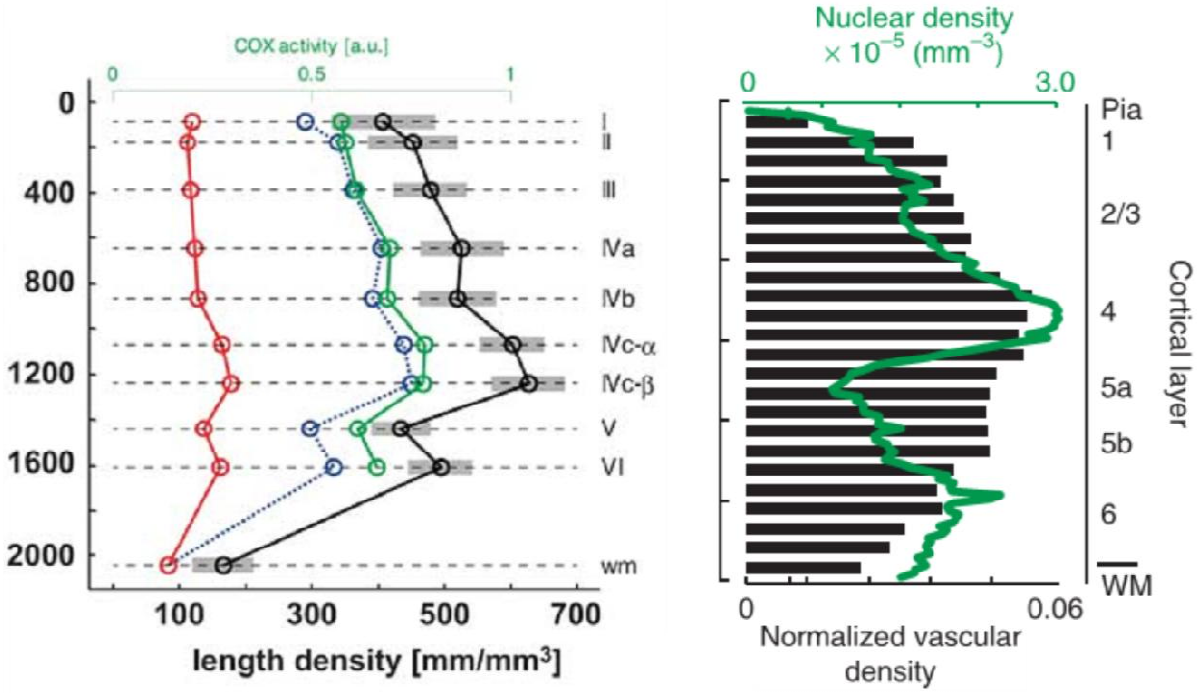

Introduction Figure 6. Plots showing the change in microvascular density across the cortical layers. *Left panel:* Variations in capillary density (blue trace), non-capillary vascular density (red trace), total vascular density (black trace) and cytochrome oxidase activity (green trace), across cortical layers and depths in the macaque striate cortex. Adapted from (Hirsch et al., 2012) . *Right panel:* Variations in capillary density (black bars) and neuronal nuclear density (green trace) across cortical layers and depth in the mouse barrel cortex. Adapted from (Blinder et al., 2013) .

As has been noted before (Hirsch et al., 2012), the idea that there is a relationship between functional neuronal columns and the vascular organisation is a tempting one, raising as it does the idea of an atomically and functionally linked neuro-vascular unit. The evidence for this form of organisation is unclear however. Two recent studies attempted to address this question by studying the relationship between vascular and neuronal organisation in the barrel cortex. The first of these, Blinder et al. (2013), examined this relationship using high-resolution all-optical histology of cortical tissue blocks followed by graph-theoretical analysis of the vascular networks revealed and their association with the barrel structures in layer IV. They found that neither the topological features of the microvascular networks nor calculated blood flow domains varied with the barrel columns. Furthermore they found no relationship between the position of penetrating vessels and the barrel structures (Blinder et al., 2013) . However, the second study, Wu et al. (2014), which employed broadly similar histological techniques, found a preferential localisation of penetrating vessels in the septa between barrels rather than in the barrels, a greater microvascular length density in the barrels than in the septa, and complex relationships between the branches of penetrating vessels and the adjacent barrels(Wu et al., 2014) . It is likely that further research in the near future will clarify if any true columnar neuro-vascular unit exits and if so what is the nature and basis of its operation.

Chapter 3: Tools and Techniques for measuring Oxygen

As discussed above (Chapter 1, Section 2.1), there are multiple parameters ($[O_2]$, Po_2, So_2, [Hb] and the rate at which O_2 is metabolised) that can be measured to garner information on tissue oxygenation and dynamics. Similarly, multiple techniques have been used to investigate tissue oxygenation, each relying on measuring a subset of these parameters or associated phenomena. In this section I will explore these methods, focusing primarily on those which directly measure tissue oxygenation (either Po_2 of $[O_2]$), but initially I will provide a brief outline of those methods which rely either on indirect indication of tissue oxygenation or only provide information on the supply or consumption of oxygen in the brain.

Section 1 – Measurements of oxygen parameters other than Po_2

1.1 – Measurement techniques based on measurement of haemoglobin and So_2

The binding of O_2 to haemoglobin induces changes in its properties such that multiple techniques can be used to differentiate oxyhaemoglobin (HbO_2) from deoxyhaemoglobin (HbR). The properties that are modified include the absorption spectra (as utilised by spectrophotometric methods and photoacoustic flowoxigraphy) and magnetic properties (as exploited by fMRI).

In methods that utilise the differences in absorbance spectra, the differential absorbance of light of different frequencies is used to obtain a measure of the total [Hb] and the ratio of HbO_2 to HbR. This allows for the So_2 to be calculated.

Depending on the exact technique used, these forms of recordings can also give information on the local blood flow (RBC delivery rate, velocity and lineal density) and So_2 gradients, and thus be used to determine the local O_2 extraction rate.

In fMRI BOLD signal based imaging, the differential magnetic properties of HbO_2 and HbR (which are dia- and para-magnetic respectively) are used to track changes in blood flow and oxygenation in the brain. The most widely used approaches depend on tracking the concentration of HbR in the blood in an area of study, with a mismatch between changes in local O_2 consumption and local blood flow leading to an increase in HbO_2 in particular areas of the brain. From these changes, interpretations about regional neural activity have been drawn. Additionally, more recent approaches (known as quantitative BOLD, or qBOLD) have attempted to use fMRI to measure So_2 in blood vessels in volumes of brain tissue.

However, although these methods can be used to measure So_2, they are unable to give information on local vascular or tissue Po_2.

1.2 – Positron Emission Tomography (PET)

This technique is based on the detection of photons emitted from positron-electron pair-annihilation, which in turn allows for localisation of the radioactive positron source. In studies of oxygen in the brain, the most common tracer is oxygen-15 (^{15}O). This tracer, when incorporated in O_2 gas and inhaled, will, as it passes through the cerebral circulation, either remain in the blood or enter the brain tissue, where it is metabolised to $H_2{}^{15}O$ (as described earlier). When combined with measurements of cerebral blood volume and cerebral blood flow, this method can give measurements of local brain tissue extraction and metabolism of O_2. It is, however, unable to provide values of vascular or tissue oxygen content.

Section 2 – Methods of Measuring Po_2

In this section, I will discuss methods that are employed to measure Po_2 in the vasculature and parenchyma of the brain. The first part of this section will deal with methods that have been used by others to assess Po_2 (Polarography, Electron Parametric Resonance, and Mass Spectrometry), and this will be followed by a more extensive section, which will explore optical measurements of Po_2, primarily those based on phosphorescence lifetime measurements which is the approach I employed during my doctoral research.

2.1 – Polarographic measurements of Po_2

This method is among the oldest and best-established methods of measuring tissue oxygenation. It is based on measurements of the current generated by the reduction of O_2 to H_2O at a noble metal (usually platinum) cathode, which can be used to determine local Po_2. In measurements of this type, the cathode is typically protected by a gas- but not liquid-permeable membrane and located within a glass micropipette. The tip of this electrode is inserted into the desired position in the tissue of interest. The electrode reports a current induced by the reduction of O_2 at the cathode, and the magnitude of this current is proportional to the Po_2 in a sphere of tissue surrounding the tip (the diameter of which is approximately double that of the tip) (Tsai et al., 2003) . This technique allows for measurements from both superficial and deep structures in the brain (which can be targeted using stereotaxic methods), and indeed can be combined with imaging approaches to allow for precise targeting within structures (for example Lecoq et al. 2009 (Lecoq et al., 2009)).

The majority of the quantitative recording of brain Po_2 has been carried out using this approach, and it has been instrumental in shaping our current understanding of brain tissue oxygenation and the factors affecting it (See Ndubuizu and LaManna 2007 for review(Ndubuizu and LaManna, 2007)).

There are, however, a number of drawbacks and limitations associated with this technique. Firstly, and importantly, the positioning of the probe in the tissue of interest is inherently and unavoidably invasive. The initial craniotomy, opening of the dura mater and subsequent insertion of the probe all involve acute disturbance of the tissue, and there is a significant risk of the probe tip damaging and rupturing microvessels in the vicinity of the recorded tissue volume. Indeed, even in experiments where the electrode is chronically implanted in the brain, experiments can be compromised by haematoma formation at the electrode tip.

A second major drawback of this method is that the recordings are limited to the volume around the electrode tip, and hence give information on only one site. This issue has been circumvented in the past by the use of an array of electrodes (e.g. Leniger-Follert et al., 1975), or by serial repositioning of the electrode tip. However, both these solutions serve to exacerbate the concerns related to tissue damage induced by the invasive nature of the technique.

2.2 – Electron Parametric Resonance (EPR) oximetry

This technique is based on measuring the difference between two spin states of unpaired electrons in a probe substance (either a soluble probe or a solid crystal probe), which is situated in a magnetic field of known strength. The probe molecules can interact with other substances which have unpaired electrons. In the case of the probes used for EPR oximetry, they interact strongly with molecular oxygen due to its two unpaired electrons. This causes a change in the measured absorption spectrum in a manner that is related to, and so reports, the local Po_2 (Dunn and Swartz, 2003; Springett and Swartz, 2007).

When solid crystals (often lithium phthalocyanine) are used as the probe, they are typically implanted into the tissue of interest 3-6 days before the first measurements are taken. This allows time for the initial trauma of their insertion to subside, and as

the crystals are almost totally biologically inert, there is typically little inflammatory response or tissue reactivity. In studies of brain Po_2, ~200μm crystals have been inserted through the skull with a fine needle. The probe will report local tissue Po_2, but if multiple different values exist around the crystal, the recorded value will be a weighted average of these distinct values. After probe implantation, the recording procedure does not require further invasive steps, and so can be used to report tissue Po_2 in the same tissue volume over widely separated times, and in either anaesthetised or awake, restrained animals.

With the use of soluble probes, a more spatially extensive range of tissue Po_2 measurements can be made. Indeed, some such probes preferentially accumulate intracellularly or even in subcellular compartments, and as such could allow for measurements of Po_2 in these specific structures. However, this type of measurement generally requires introduction of the probe to the tissue of interest at the period of recording, as they tend to be cleared over time, and so are more acutely invasive than crystal-based measurements.

This method has shown promising potential clinical applications, with implanted crystals allowing for longitudinal measurements of tumour oxygenation during anticancer therapy, but suffers from some drawbacks for neurophysiological research purposes. Firstly, there are concerns related to trauma induced by introduction of the probes to the tissue of study. Although the placement of the crystal probes in the tissue is done a number of days before recording and a number of studies report an absence of major tissue reactivity, there is nonetheless the risk of damage occurring during this procedure. This is perhaps of more importance in the brain than in peripheral tissues, as even in the absence of a classical inflammatory response, damage to neuropil and vascular elements could induce deviations from normal physiology. Indeed, the fact that this damage would most likely occur in the volume of tissue that is being measured from must represent a concern. Secondly, as alluded

to earlier, the spatial resolution of this method may be compromised by the spatial averaging of Po_2 levels around crystal probes. Thirdly, the Po_2 resolution of currently used probes is not particularly good in the lower ranges of oxygen tensions, and finally the temporal resolution of this method is quite low, at between tens of seconds to minutes (Springett and Swartz, 2007).

2.3 – Mass spectrometry for measuring Po_2

The measurement of tissue oxygen using this method involves the insertion of a cannula into the tissue of interest and the withdrawal of samples of the local milieu. These samples are then analysed using a mass spectrometer and the Po_2 measured. This can be done with acutely- or chronically-implanted cannulae. However, this method is invasive due to the need to insert the cannula into the site of measurement, and only provides information on the Po_2 at that single site, and thus suffers from the same drawbacks as polarographic measurements, while being more complicated to employ.

2.4 – Optical methods for determining Po_2

The basic principles for oxygen measurement via optical methods are related to photoluminescence (either fluorescence or phosphorescence) and its quenching.

When a photon is absorbed by a photoluminescent molecule it results in an electron in this molecule being excited and promoted from a ground state to some higher energy level. Following internal conversion processes, the excited electrons can return to the ground state via two different processes, each of which ultimately involves emission of a photon. These two processes are fluorescence and phosphorescence.

Fluorescence occurs via direct de-excitation from the excited "S_1" state to the ground state with the release of a photon, and is a fast process, with a typical lifetime on the order of ~10^{-8} s.

Phosphorescence on the other hand involves a non-radiative inter-system crossing event that involves entry into the "triplet state" (T_1). De-excitation from this state to the ground state is a much slower process than that of fluorescence, with a lifetime of between 10^{-6} and 10^{-3} s, but also involves emission of a photon.

Key to optical methods of oxygen measurement, these radiative de-excitation pathways can be circumvented by interaction of the excited molecule with certain other chemical species which allow for a radiationless de-excitation. This quenching of the photoluminescence will both decrease the intensity of the photon emission and shorten its lifetime. The most prominent quenching molecule in biological systems is molecular oxygen, O_2.

Quenching requires interactions between the excited luminophore and the quenching molecule. This process is known as collisional quenching, is diffusion limited, and has kinetics that are well described by the Stern-Volmer equation. This equation describes the relationship between the local concentration of the quenching molecule (in our case the local partial pressure of oxygen) and the degree of quenching achieved, expressed either as the decrease in luminescence intensity, or as a shortened luminescence lifetime. For the measurement of oxygen, the relationship is as follows:

$$\frac{I_0}{I} = \frac{\tau_0}{\tau} = 1 + (k_q)\,(\tau_0)\,(Po_2)$$

Where: I_0 and τ_0 are the luminescence intensity and lifetime, respectively, in the absence of the O_2; I and τ are the measured luminescence intensity and lifetime values; k_q is the quenching coefficient; and Po_2 is the local partial pressure of molecular oxygen.

Thus, in principle, by knowing the intensity or lifetime of the luminescence in the absence of O_2 and the quenching coefficient, it is possible to record the equivalent luminescence parameter in your sample or tissue of choice, and hence determine the local Po_2. In practice however, lifetime measurements are much more suitable in biological contexts, as intensity-based measurements can be influenced by a number of factors including the local concentration of the luminescent probe, the intensity of the excitation achieved by the light source, and, importantly scattering (and fluctuations in scattering) in the medium.

Conversely, measurement of the luminescence lifetime is resistant to the effects of these variables, and depends exclusively on the rate of collisional quenching, and thus local quencher availability.

Two different approaches have been used to deploy luminescence lifetime measurements in recordings of brain oxygenation. The first of these employs luminescent molecules at the tip of fibre-optic probes to allow for measurement of Po_2 in a diffusion-limited volume around the tip, whereas the second, to which I will give most attention, relies on soluble nanoprobes that can be introduced to the vasculature or the tissue (or even intra- or sub-cellularly) (Finikova et al., 2008) .

Both of these approaches could, in principle, be achieved using measurements of either fluorescence or phosphorescence lifetimes, but to date most research and development has focused on phosphorescence lifetime quenching, as it has a lifetime that is multiple orders of magnitude longer than that of fluorescence, which allows

for sensors to have a dynamic range that is much more amenable to accurate measurement.

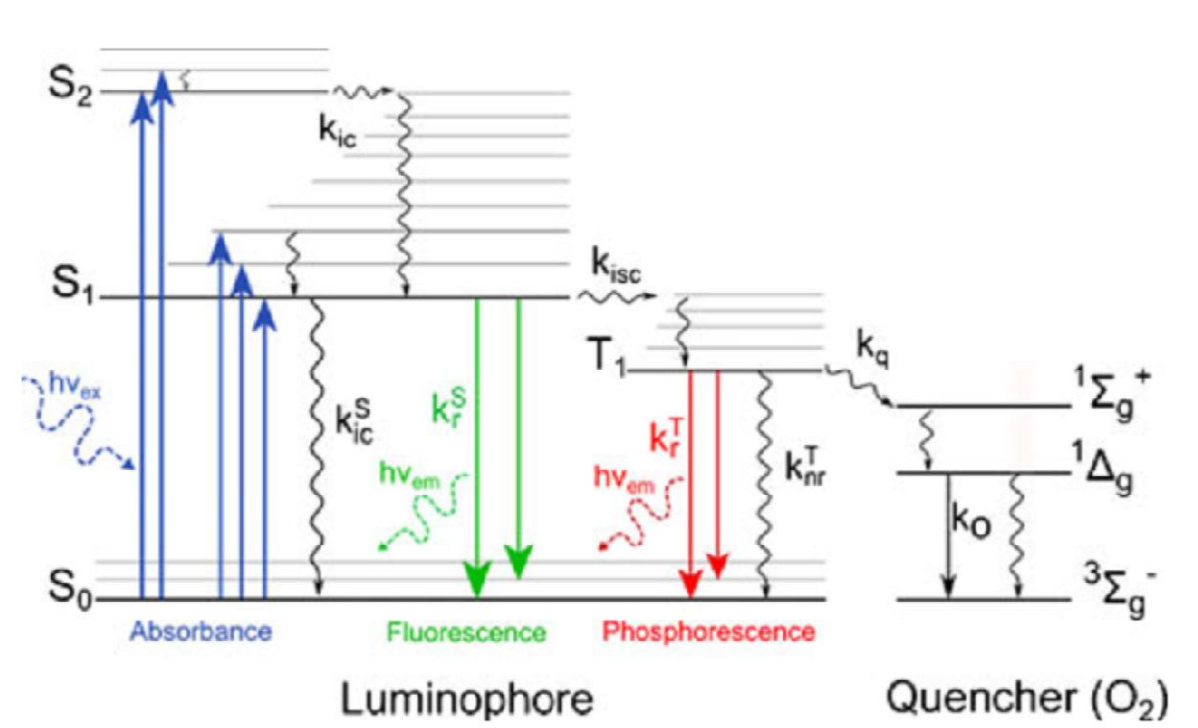

Introduction Figure 7. Perrin Jablonski diagram (from Quaranta et al., 2012) describing the excitation and subsequent possible de-excitation process in luminophores. Absorption of incident photons (See blue arrows) leads to excitation of the molecule to a higher energy level. This process takes about 10^{-15} s. Following internal conversion processes (that take approximately 10^{-12} s), the return to ground state from the excitation state can occur via either fluorescence (with a lifetime of 10^{-8} s. See green arrows), or phosphorescence (following inter-system conversion, with the total de-excitation process typically having a lifetime of longer than 10^{-6} s. See red arrows). Both fluorescence and phosphorescence involve emission of photons. As explained in the text, quenchers (e.g. molecular oxygen) can provide a non-radiative de-excitation pathway from the triplet state (T_1), thus reducing the phosphorescence lifetime and intensity.

When using solid fibre-optic phosphorescent probes, the tip of the probe is inserted directly into the tissue of interest and allowing for Po_2 measurement at this point. Although this approach has advantages over those discussed previously in that it allows for fast and reliable measurement of Po_2, it suffers from many of the drawbacks associated with polarographic measurements, primarily the risk of damage of the tissue from which recordings are made and the limitation of measurements to the area directly around the tip.

Soluble nanoprobes, on the other hand, thanks to a number of developments since their original introduction, now offer the possibility of accurate and precise Po_2 measurement, at spatially extensive but precise points and with good temporal resolution, at considerable depths below the surface of the brain.

The earliest examples of phosphorescent probes that were deployed to measure brain Po_2 were based on ruthenium, but these were later supplanted by metaloporphyrin dyes based on platinum (Pt) or palladium (Pd) porphyrins. These forms of complexes are crucial to phosphorescence based measurements as the heavy central atoms greatly increase the probability of inter-system crossing, and thus lead to high proportions of the excited state to ground state transitions occurring via phosphorescence rather than fluorescence.

Many of these dyes bind readily to biological molecules, particularly albumin, and indeed, the binding of albumin to the probes is key to their functioning. This is because, upon binding, albumin limits the access of O_2 to the porphyrin core, slowing the rate of collisional quenching. Without the restriction of access of O_2 to the porphyrin, the quenching effect at physiological ranges of Po_2 reduced the phosphorescence lifetimes to periods that are too short to be useful. The occluding effect of the bound albumin thus allowed for accurate measurements of physiologically relevant Po_2 values to be made. This however, meant that these forms

of nanoprobe were only usable in albumin-rich environments, such as the blood stream, which made them largely unsuitable for interstitial (or intracellular) measurements.

Later generations of these probes were synthesised with hydrophobic dendrimers attached, which performed the role of limiting the access of O_2 to the porphyrin and so negated the need for albumin binding. They were then further coated in hydrophobic residues (for example polyethylene glycol, PEG), which rendered them both highly soluble in aqueous media, and also insensitive to interference from organic or biological molecules that may be found in tissue or blood serum. This has the added benefit of making the probe molecules sufficiently large and hydrophilic as to limit their movement across cell membranes, avoiding leakage between vascular, tissue, and cellular compartments.

These newer probes were therefore potentially powerful tools for monitoring Po_2 in the blood stream or in interstitial tissue. They have been deployed in many studies of vascular and tissue oxygenation, primarily in peripheral tissues (including such model systems as the hamster cheek pouch, skeletal muscle, and the mesentery (see Tsai et al., 2003; Pittman, 2011a and references therein), but also in the brain (eg. Yaseen et al., 2011). In these studies, the primary imaging systems employed were either a combination of wide-field illumination and CCD (charge-coupled device) based detection or confocal laser scanning microscopy. In both cases these methods suffered from low signal-to-noise ratio (meaning that high excitation light intensities and multiple rounds of excitation and measurement of phosphorescence measurement were necessary), low spatial resolution, and in the case of wide-field illumination the measurements were limited to the surface of the tissue.

Surprising results arose from these investigations, in relation to the magnitude of Po_2 gradients across the walls of arterioles, which served to highlight one major potential

source of error that could arise from phosphorescence quenching methods of Po_2 measurement. Tsai et al. 1998, used Palladium-mesotetra-(4-carboxyphenyl)porphyrin to measure Po_2 within arterioles and in the surrounding tissue(Tsai et al., 1998). They noted a large O_2 gradient between these two compartments with arteriolar P_{O2} being on around 25 mmHg greater than that on the surrounding interstitial fluid. This gradient was at least an order of magnitude larger than what would be predicted from estimations of arteriole wall O_2 consumption (Vadapalli et al., 2000) , or from earlier polarographic measurements of transmural gradients in arterioles (Duling and Berne, 1970) . Subsequent studies determined that the major source of this gradient was not differential oxygenation of these two compartments but was in fact the result of consumption of oxygen by the quenching process (Tsai et al., 2005) .

As explained earlier, the quenching of the phosphorescent de-excitation pathway by O_2 is via a diffusion-related collisional process, during which the O_2 molecule provides a non-radiative de-excitation pathway to the probe molecule. However, inherent to this process is the transfer of the energy to the O_2 molecule which results in the generation of highly reactive singlet oxygen. This molecule very rapidly reacts with biomolecules in the vicinity, and is thus consumed. Tsai et al. 1998 provided excitation to their probe using a xenon strobe light, with flashes occurring at a rate of 30 Hz(Tsai et al., 1998) . Within the vasculature, this did not have a major effect on the measured Po_2, as the convective flow of the blood meant that the O_2 consumed by each flash was replaced in the excitation volume before the next excitation-recording cycle. However, the only means for replacement of consumed O_2 in the interstitial fluid was via diffusion from the surroundings. Given the large volume in which the probe was excited by each flash (70μm xy radius), the frequency of the flashes (30 Hz) and the relatively slow diffusion coefficient for O_2 in the tissue (1.04×10^{-5} cm^2/s (Golub and Pittman, 2008)), it is inevitable that in a period of sustained recording, there will be insufficient replacement of O_2 in the interstitial fluid to maintain a

normal level of tissue Po_2 in the recorded volume. A low Po_2 value for this region will be recorded, and give rise to apparent gradients, such as those reported by Tsai et al. 1998 (Tsai et al., 1998) .

This form of error, induced by the very nature of the recording, is obviously a major concern when using these techniques. Strategies for avoiding this pitfall that were suggested by Golub and Pittman (Golub and Pittman, 2008) include maximising the signal to noise ratio by enhancing detection, limiting the size of the excitation volume, and using a scanning excitation approach so that each area does not receive multiple excitation events in a short period of time.

The advent of newer probes has essentially overcome the limitations and concerns related to use of these earlier sensors. These new probes are excitable in a 2-photon regime. This means that Po_2 measurements can be made at depths below the tissue surface, and also that the volume in which the probe is excited can be tightly restricted. The result of this is that both the consumption of O_2 and the generation of reactive species is limited, and the source of the phosphorescence signal measured is both confined and known, lending great spatial resolution to these measurements (for example, an XY resolution of <1μm in Lecoq et al. 2011(Lecoq et al., 2011)).

The measurements that I have made over the course of my doctoral research have been carried out using the platinum porphyrin-based O_2 nanoprobe PtP-C343 (Finikova et al., 2008) . The structure of the probe and its sensitivity to Po_2 can be seen in Introduction Figure 8. Used in combination a 2-photon microscope set up, it has allowed for 2-photon phosphorescence lifetime measurements (2PLM) of Po_2.

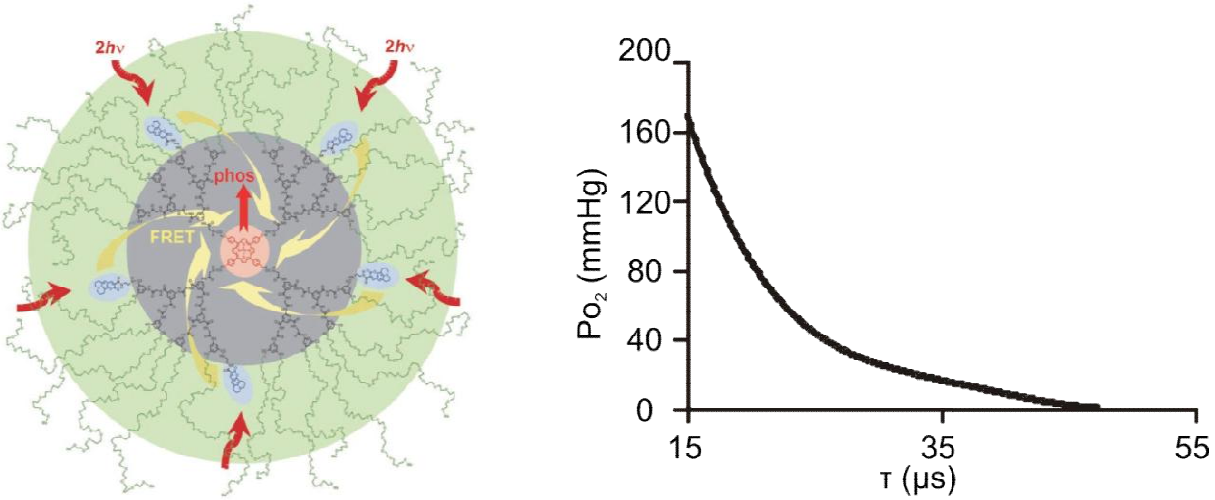

Introduction Figure 8. *Left Panel:* Diagram showing the structure of PtP-C343. The green area represents the PEG residues, which make the probe water-soluble and protect it from interactions with biological molecules. The dendrimers that help limit O_2 access to the metalloporphyrin core are represented in black, and the Pt-porphyrin core is depicted in red. The blue areas represent coumarin 343 units that, with their large 2-photon cross section, act as antennae for 2-photon excitation. The arrows on the diagram represent energy transfer: The curved red arrows represent incoming photons from the laser source, which excite the coumarin units. A FRET (Förster resonance energy transfer) based process then transfers a large proportion of this energy (~75%) to the Pt-porphyrin core (yellow arrows), which is excited and subsequently emits photons (straight red arrow) via a phosphorescence process which can be quenched by O_2 as discussed earlier.
Right Panel: Calibration curve for a particular batch of PtP-C343, showing the dependence of phosphorescence lifetime on Po_2. The calibration curves are derived from oxygen titration experiments.

This probe has been deployed in a number of studies into oxygenation of the brain, with the earliest papers (Sakadzić et al., 2010; Lecoq et al., 2011) showing the potential of this technique. Both these works demonstrated the feasibility of carrying out spatially extensive precision measurements of Po_2 in 3D volumes, at depths of hundreds of microns below the brain surface, in either the vasculature or the interstitial fluid, with high spatial and temporal resolution, and combined with the ability to visualise the local vasculature or tissue elements. Additionally, Lecoq et al. demonstrated that Po_2 values could be recorded simultaneously with measures of RBC supply rate in brain capillaries, and that this allowed for EATs to be detected and analysed. They also showed that it was possible, with these methods, to track the dynamics of vascular and tissue oxygenation in response to local neural activity and functional hyperaemia.

Thus, combining 2-photon microscopy imaging and 2PLM measurements of Po_2, is an extremely powerful method for investigating brain oxygenation. It allows for highly precise and accurate measurements of Po_2 while avoiding the drawbacks associated with many other approaches. Of particular note is the fact that when the nanoprobes are injected intravenously, measurements of vascular Po_2 can be made without directly disturbing the tissue in question. This is in contrast to the possibly confounding invasiveness associated with the other methods of directly assessing Po_2 (Polarography, EPR and mass spectrometry) as discussed above.

Therefore, this technique opens the possibility of measuring truly physiological values of Po_2 in the awake, normally functioning brain.

Chapter 4: The Current Understanding of Oxygen in the Brain

Section 1 - What is known of Po_2 in the Brain?

1.1 – Po_2 in the human brain

Given the invasive nature of most techniques for directly assessing oxygen availability, measurements of Po_2 in the human brain are sparse and those that exist are almost exclusively drawn from recordings made during neurosurgery. The results of these studies are therefore subject to a number of caveats in relation to how well they represent physiological oxygenation levels (for example, the effects of acute opening of the skull and meninges [and exposure of the brain to atmospheric Po_2] on oxygenation, the effects of anaesthetics and other pharmacological agents administered to the patients, the effect of surgical trauma to the brain tissue and of the underlying pathology itself.)

Nonetheless, those studies that did perform measurements of human brain Po_2 reported values on the range of approximately 12-50 mmHg (for example Roberts and Owens, 1972; Charbel et al., 1997)

1.2 – Po2 in the mammalian brain

Studies of Po_2 in other mammals have been performed in a number of species, with cats and rabbits featuring prominently in early research, and subsequently being largely replaced by rodent animal models (primarily rats and mice). The similarity of the distributions of Po_2 values measured across species suggests that there is a

common, characteristic brain Po_2 profile across mammalian species (Erecińska and Silver, 2001; Ndubuizu and LaManna, 2007) .

The majority of measurements are based on polarographic measurements of Po_2, but values have also been obtained using EPR, Mass spectrometry, and using phosphorescence quenching based measurements.

I will first present the current understanding of the oxygenation of the cerebral vasculature, outlining the existing data on Po_2 levels in the large cerebral arteries and veins, pial vessel network, penetrating vessels and the capillary network. In the second portion of this section, I will attempt to synthesise the known information on brain tissue Po_2 values and the variation of these values within and between brain regions. This will be followed by a section dealing with known interactions between the vascular system, blood oxygen, and tissue Po_2 in the brain. Finally, I will take a step back and outline a number of factors that have been shown experimentally to affect brain oxygenation generally.

1.2.1 – Po_2 in the brain vasculature

(a) Arteries that supply the brain

The arteries that feed the brain are highly oxygenated, with levels of Po_2 and So_2 similar to systemic arterial blood (approximately 100mmHg and >95% respectively), whereas the venous blood in the cranial sinuses and jugular veins approximates 40 mmHg (~75% So_2 in humans).

(b) Po_2 in Pial Vessels

Measurement of the vascular Po_2 in venules and arterioles of the pial network has been achieved using two different methods. Initial studies (Duling et al., 1979; Vovenko, 1999; Vazquez et al., 2010) used fine-tip polarographic electrodes, which when impressed onto large vessels can give a relatively accurate measure of the

intraluminal Po_2 (especially when correction is applied based on measured values of Po_2 consumption by the vessel walls, although there remains a potential risk of the electrode tip reporting measurements which are not exclusively from the vessel, but also to an extent from the surrounding tissue). The second approach employed phosphorescence quenching measurements, and thus exclusively samples intravessel Po_2 (Sakadzić et al., 2010; Yaseen et al., 2011) .

These studies report Po_2 values in the pial vessels that range from approximately 60-110 mmHg in arterioles and approximately 35-60 mmHg in venules. It is difficult to make comparisons of the absolute values of Po_2 reported by these studies as they derive from different animal species (cats, rats and mice), under different anaesthesia regimes (glucochloralose, pentobarbital, α-chlorolose or isoflurane depending on the study), and with differing systemic arterial Po_2 (ranging from above 130 mmHg to below 90mmHg).

These studies found that there is a correlation between vessel Po_2 and the luminal diameter of pial arterioles, and that this is not true of pial venules (for example, see Figure 2g of Yaseen et al. 2011(Yaseen et al., 2011)). However, it has also been suggested that this change in arteriolar Po_2 is primarily related to the branching order of the vessels (which is itself related to the luminal diameter) (Duling et al., 1979; Vovenko, 1999; Vazquez et al., 2010a, 2010b) .These latter studies classified the pial vessels based on branching order (with the first order being the primary branch of the middle cerebral artery, the second order being branches from the first order and so on, and the fifth order typically giving rise to penetrating arterioles), and found that the Po_2 of the higher order branches (fourth and fifth order) was approximately 20mmHg lower than in the first order branch. Venules on the other hand showed only minor (2-3 mmHg) changes in Po_2 regardless of lumen size or branching order(Vazquez et al., 2010a, 2010b; Duling et al., 1979; Vovenko, 1999) .

(c) Po_2 in penetrating vessels

Sakadzic et al. (2010), measured Po_2 in penetrating arterioles and venules in the cortex, reporting that Po_2 in descending arterioles at the pial surface was approximately 60-70 mmHg, and that of ascending venules was around 40 mmHg. They noted that, similarly to in the pial vessels, the vascular Po_2 decreased in line with increasing branching order. Moreover, they reported that there was a gradient of Po_2 in these penetrating vessels, such that the Po_2 is lower at greater depths. The magnitude of this drop in descending arterioles is on the order of 10 mmHg over the range of 0-240μm below the pial surface that was assessed, whereas ascending venules show an increase of about 7 mmHg as they approach the surface. These gradients with increasing depth were replicated in a later study by the same group, by extrapolation of vascular Po_2 from tissue Po_2 directly surrounding penetrating vessels(Devor et al., 2011). This study reported that arteriolar Po_2 at depths <100μm was around 35 mmHg greater than at depths from 200-350 μm.

(d) Capillary Po_2

In addition to the measurements performed on rat pial vessel Po_2, Vovenko (1999) made measurements from capillaries in the sub-surface microvasculature. It is unclear what parameters were used to define a capillary in this study, and it seems likely that there was a broad array of small vessels among the 19 recorded. The mean Po_2 reported for the 'arterial end' of the capillaries was 57.9±10.6 mmHg, and that at the 'venous side' of the studied capillaries was 40.9±11.5 mmHg. The average distance between the two recorded points on the capillary segments was 258±95 μm, leading to the author estimating a Po_2 drop of 0.7±.4 mmHg/μm along these capillaries, while simultaneously noting that there was no correlation between the length of the capillary segment and the measured drop in Po_2 (Vovenko, 1999).

More extensive assessments of capillary Po_2 in the brain have had to wait for the development of 2PLM. Two studies have been published which provide data on

capillary Po_2, one studying capillaries in the olfactory bulb(Parpaleix et al., 2013)*, and the other providing measurements from the parietal cortex(Sakadzić et al., 2010).

Sakadzic et al. (2010) measured Po_2 in the subsurface microvessels of mouse parietal cortex (although they didn't explicitly distinguish between capillaries and other subsurface vessels). They describe a decrease of ~10 mmHg in vessel Po_2 with increasing depth from the near the surface to -240μm. Their measurements report mean vascular Po_2 values at a given depth of between 50 and 30 mmHg, and Po_2 values of approximately 30mmHg from a small number of identified capillaries.

Parpaleix et al. (2013), on the other hand, focused their attention exclusively on capillaries in olfactory bulb glomeruli. They made measurements of Po_2 from capillaries, finding a mean Po_2 value of 30.8±0.9 mmHg. Most interestingly, by detecting and extracting EATs (See Chapter 1, Section 2.3), they were able to provide information not only on mean capillary Po_2, but also to measure the Po_2 at RBCs and at middle distance between RBCs. These parameters were both found to be significantly different to the mean capillary Po_2, with the values recorded in this study being 57.1±1.3 mmHg and 23.6±0.7 mmHg for Po_2 at the RBCs and at mid-distance between the RBCs respectively.

1.2.2 – Po_2 in brain neural tissue

Multiple studies have been published which report tissue Po_2 in the brain. These works employ a range of animal models, experimental preparations and recording techniques and explore Po_2 across a wide range of brain structures. A detailed, systematic review of the existing data was published in 2007 by Ndubuizu and LaManna (Ndubuizu and LaManna, 2007) , and I refer the reader to it for an overview of the field to that point. Of particular interest is table 1 in the review (reproduced here as Introduction Table 3), which shows the wide array of approaches used in attempts to measure brain tissue Po_2 and the widely varying values of Po_2 which they produced.

An important point that is made in this review, referring to Lubbers (1969) (Lubbers, 1969) is that in light of the fact that the tissue Po_2 is highly heterogeneous and that the Po_2 at any given point will be a product of highly variable local factors (the distance from vessels, the Po_2 in those vessels, the local diffusion coefficient and the local rate of O_2 consumption), that there is no "characteristic oxygen tension". Rather, there is an oxygen tension field in the brain tissue. Thus, although many studies report mean tissue Po_2 values for specific brain structures, the oxygenation of brain tissue, even at a local scale, is best described by an oxygen distribution curve.

More recent studies have used 2PLM to measure brain tissue Po_2 values, with Sakadzic et al. 2010 recording values in the range of 6-25 mmHg across a multiple locations ~100μm below the cortical surface, in addition to relatively elevated tissue Po_2 (~50 mmHg) around in regions surrounding large arterioles, and slightly elevated tissue Po_2 around venules (~35 mmHg) (Sakadzić et al., 2010). These general results were once again replicated in a later paper from the same group, who described a similar range of tissue Po_2 values. The distribution of the tissue Po_2 values were shifted to lower ranges with increasing depth in this study (see figure 2 of Devor et al., 2011(Devor et al., 2011)). In this second paper, these researchers also measured a radial gradient of tissue Po_2 around penetrating vessels that was of a

much greater magnitude for arterioles than for venules(Devor et al., 2011) . These gradients in tissue oxygen were in accordance with similar gradients in Po_2 that had previously been described around pial vessels (Vovenko, 1999) and for penetrating vessels near the pial surface (Sharan et al., 2008).

TABLE 1. QUANTITATIVE ESTIMATES OF BRAIN TISSUE pO_2 PARTIAL PRESSURE BY DIFFERENT TECHNIQUES AND UNDER VARIOUS CONDITIONS

PtO_2 values	*Method*	*Species*	*Status*	*Citation*
33 ± 11	Polarographic	Human	Anesthetized	Charbel, 1997 (9)
2.0–10	Polarographic	Cat	Anesthetized	Davies & Bronk, 1957 (15)
10.0–30	Polarographic	Cat	Urethane (20% sol, 1 g/kg)	Cross & Silver, 1962 (13)
10.0–20	Polarographic	Rat	Na-pentobarbital (40 mg/kg)	Metzger, 1971 (64)
0–99 (avg, 38.7 ± 0.9)	Polarographic	Cat	Na-pentobarbital (30–40 mg/kg)	Nair, 1975 (66)
0–90 (freq max 25–30)	Polarographic	Cat	Pentobarbital (25–30 mg/kg), gallaminetriethiodine (paralytic, 10 mg/kg)	Leniger-Follert, 1975 (48)
12.9 ± 0.9	Polarographic	Rat	Na-pentobarbital (35 mg/kg), D-Tubocurarine hydrochloride (10 mg/kg)	Sick, 1982 (89)
12.5 ± 1.3	Polarographic	Turtle	Na-pentobarbital (35 mg/kg), D-Tubocurarine hydrochloride (10 mg/kg)	Sick, 1982 (89)
23.3	Polarographic	G. Pig	Anesthetized	Lubbers & Baumgarti, 1997 (59)
29 ± 5	Polarographic	Rat	Control, brief isoflurane (2%), pancuronium bromide (1 mg/kg)	Seyde & Longnecker, 1986 (85)
35 ± 7	Polarographic	Rat	Isoflurane (4%), pancuronium bromide (1 mg/kg)	Seyde & Longnecker, 1986 (85)
22 ± 5	Polarographic	Rat	Sodium nitroprusside (3.8 mg/kg), pancuronium bromide (1 mg/kg)	Seyde & Longnecker, 1986 (85)
13 ± 5	Polarographic	Rat	2-Chloroadenosine (0.8 mg/kg), pancuronium bromide (1 mg/kg)	Seyde & Longnecker, 1986 (85)
1–79 (avg, 23.8 ± 12)	Polarographic	Baboon	Anesthetized	Crockard, 1976 (12)
16–59 (avg, 29.8)	Polarographic	Human	Anesthetized	Baker, 1975 (3)
0–90 (avg, 25)	Polarographic	Cat	Na-pentobarbital (30–40 mg/kg)	Whalen, 1970 (102)
24.5 ± 18	Polarographic	Rabbit	Urethane (20% sol, 1 g/kg)	Smith, 1977 (91)
18.4 ± 1.2	Polarographic	G. Pig	Na-pentobarbital (30–40 mg/kg)	Buerk & Nair, 1993 (7)
28–32 (hypothalamus)	Optical (ruthenium)	Rat	Isoflurane (1%)	Nwaigwe, 2003 (67)
10–15 (thalamus)	Optical (ruthenium)	Rat	Isoflurane (1%)	Nwaigwe, 2003 (67)
32.3 ± 0.8 (22% O_2)	Optical (Phos)	Pig	Halothane (3–4%)	Tammela, 1996 (93)
25–35	Optical (Phos)	Pig	Halothane, analgesic, tubocurarine	Wilson, 1991 (103)
42.8 ± 8.6	Optical (Fluor. PBA)	Cat	Ether, *cerveau isole*	Mitnick & Jobsis, 1976 (65)
12.0–49	Mass spectrometry	Human	Anesthetized	Roberts & Owens, 1972 (79)
16.9 ± 1.6	Mass spectrometry	Rabbit	Anesthetized	Seylaz, 1978 (86)
9.0 ± 2.1	EPR (LiPC)	Rat	Pentobarbital	Hou, 2003 (28)
13.0 ± 2.9	EPR (LiPC)	Rat	Chloralose/Urethane	Hou, 2003 (28)
16.5 ± 0.8	EPR (LiPC)	Rat	Halothane	Hou, 2003 (28)
38.0 ± 4.5	EPR (LiPC)	Rat	Isoflurane	Hou, 2003 (28)
3.5 ± 0.3	EPR (LiPC)	Rat	Ketamine/Xylazine	Hou, 2003 (28)
15.1 ± 1.8 (30% O_2)	EPR (LiPC)	Rat	Ketamine (8–10 mg/100 g), Xylazine (1.1–1.4 mg/100 g)	Rolett, 2000 (80)
55	EPR (LiPC)	Rat	Awake	Liu, 1993 (51)
45–50	EPR (LiPC)	Rat	Ketamine	Liu, 1993 (51)
20	EPR (LiPC)	Rat	Nembutal	Liu, 1993 (51)
34.1 ± 3.2	EPR (LiPC)	Rat	Awake	Liu, 1995 (50)
20–30	EPR (LiPC)	Rat	Isoflurane (1%)	Liu, 1995 (50)
12.0–20	EPR (LiPC)	Rat	Ketamine/Xylazine (100/10 mg/kg)	Liu, 1995 (50)
10.0–20	EPR (LiPC)	Rat	Pentobarbital (50 mg/kg)	Liu, 1995 (50)
26.5 ± 11	EPR (LiPC)	Rat	Awake	Dunn, 2000 (17)
26.6 ± 7.0	EPR (LiPC)	Rat	Isoflurane (1%)	Lei, 2001 (46)
30–35	EPR (LiPC)	Rat	Isoflurane (4%)	Liu, 2004 (54)
31–36	EPR (LiPC)	Rat	Isoflurane (1.75%) in 705 Nitrous	Liu, 2006 (52)
33.4 ± 6	EPR (LiPc)	Rat	Isoflurane (4%)	Liu, 2004 (53)

Introduction Table 3. "Quantitative Estimates of Brain Tissue pO2 Partial Pressure by Different Techniques and Under Various Conditions". This table, from Ndubuizu and LaManna (2007), is an overview of the various methods used to assess brain tissue P_{O2} and the results garnered.

1.2.3 – Relationship of tissue Po_2 to vascular Po_2

The blood is the source of oxygen for the brain tissue. The delivery of oxygen to the tissue can occur at multiple sites along the vascular network.

Recordings of radial oxygen gradients around pial and penetrating vessels show that arterioles supply oxygen to the surrounding tissue (as might venules, but to a lesser extent) (Sakadzić et al., 2010; Devor et al., 2011) . This is shown not only by the observation of areas of increased tissue Po_2 around these pial and penetrating vessels, but also by measurements of Po_2 and So_2 from pial arterioles (Duling et al., 1979; Vovenko, 1999; Hu et al., 2009; Vazquez et al., 2010a) , which describe longitudinal gradients in this network, with vascular oxygenation falling along consecutive vessels.

Capillaries, and small arterioles and venules (with luminal diameters close to that of capillaries), provide a large proportion of the O_2 that is delivered to the tissue. Vovenko (1999), based on calculations of So_2 decreases in each compartment, estimated that at least twice as much oxygen was unloaded from capillaries as from arterioles, and indeed the majority of the unloading that occurs in arterioles happens at the level of vessels with small luminal diameters (Vovenko, 1999) . As mentioned earlier, Parpaleix et al. (2013) recorded the Po_2 of capillaries in the OB GL, and recorded EATs and associated Po_2 values in these capillaries. Importantly, they showed that the Po_2 at mid-distance between RBC cells (which they termed the Po_2) is at equilibrium with, and thus reports the local tissue Po_2. The fact that this equilibrium between tissue and plasma Po_2 is rapidly re-established at a given point following passage of a RBC suggests that any O_2 that is unloaded from the passing RBC is rapidly delivered to the tissue. The concept that large quantities of O_2 are delivered to the tissue from capillary-scale microvessels is supported by the fact that brain structures or subregions with high Po_2 levels often also have a high density of capillaries (Cross and Silver, 1962).

It is uncertain whether ascending and pial veins serve as a sink or a source for tissue O_2. The Po_2 in ascending venules has been recorded as being slightly higher than that of the surrounding tissue, and that ascending venule Po_2 seems to rise as it approaches the tissue surface(Sakadzić et al., 2010; Devor et al., 2011) . This has been taken as representing an influx of O_2 from the surrounding tissue into the vessel and thus as evidence for an oxygen countercurrent mechanism

in the brain (Dirnagl, 2010) . Lecoq et al. (2011) directly showed that such diffusional shunting mechanisms can occur between pial vessels (Lecoq et al., 2011) but in the case of penetrating vessels, a portion of the increase in oxygenation near the brain surface could be related to convergence of blood of different oxygenation levels onto the same ascending venule.

1.3 – The effect of inspired gases and anaesthetics on brain Po_2

A number of factors have been found that affect brain oxygenation. Among the main parameters that affect the brain Po_2 is the composition of the inspired gas mix. A number of studies have addressed the effects of hypoxia and hyperoxia, and hypercapnia on brain Po_2. These studies are reviewed by Ndubuizu and LaManna (2007) (Ndubuizu and LaManna, 2007) , but the general conclusions are that hypoxia or anoxia causes rapid lowering of brain Po_2 to nearly 0 mmHg, and that various concentrations of hyperoxia increased brain Po_2 by different degrees, but that hypercapnia or hypercapnia combined with hyperoxia had the most profound effects, increasing brain Po_2 by a much greater degree than hyperoxia. This increased Po_2 is related to the dilation of cerebral arteries and increased cerebral blood flow induced by hypercapnia.

Another major factor that has been shown to impact brain Po_2 is anaesthetic agents, through influences on cerebral blood flow, cerebral metabolic rate, or both parameters (Aken and Hemelrijck, 1990; Liu et al., 1995). (Also, see Figure 18 in the Results section of this study).

Section 2 – Conclusion

Given the importance of oxygen in both normal brain processes and in pathology, the eventual aim of measurement of brain O_2 is to discover the nature and basis of optimal physiological oxygenation of in the normally functioning brain, and the mechanisms by which it is maintained. Though the measurements described above provide much information on potential regulatory mechanisms and approximations of normal brain oxygenation, they all are subject to one or more confounding factors. Some studies are invasive and potentially damaging to the brain, most lack

high spatial and temporal resolution, the majority are unable to resolve the range and variation of the tissue Po_2 field and its association with the microvasculature, and nearly all were performed under anaesthesia.

In light of the current lack of a detailed understanding of the oxygenation of the brain and the parameters that influence it, the investigations that I have carried during my doctoral research project have aimed to provide information on the oxygenation of the vasculature and the neural tissue in the awake mouse brain.

Specifically I have attempted to address the following questions:

What range of Po_2 values exist in the awake mouse brain under physiological conditions?

What are the typical levels of Po_2 that exist in microvasculature and the neural tissue?

Do the typical Po_2 values and the range of values vary between different subregions in the brain?

How do the vascular perfusion characteristics affect the local tissue and vascular Po_2?

The methods I have used to address these issues, and the results of my investigations are presented in the next chapter.

Part 2: Methods & Procedures

To address the questions outlined at the end of the introduction, I employed techniques that had been developed in the Charpak lab for 2PLM-based measurement of Po_2, and implemented them in awake, head-fixed mice with implanted chronic cranial windows.

Section 1 – Combined 2-photon Imaging and 2PLM for Simultaneous Po_2 Measurement, and RBC detection

The 2-photon microscope setup and 2PLM system used in the lab is outlined fully in Lecoq et al. (2011), and a schematic diagram can be seen in Methods Figure 1 (a). Briefly, the output from a Ti:sapphire laser (λ = 850 nm, 120 fs pulse width, 76 mHz) is gated by an acousto-optic modulator. This allows for repetitive cycles of alternating "on" and "off" periods to be generated, that correspond to periods of excitation and recording from the PtP probe in the sample. The relative duration of the excitation and recording periods can be adjusted, but for the purposes of my experiments the excitation period was 25μs and the recording period was 225μs, for a total cycle period of 250μs and a repetition rate of 4 kHz. (see Methods Figure 1, b) The scanning of the excitation light by the galvanometric mirrors is synchronised with the gating of the laser output by the acousto-optic modulator (AOM). Recordings are made as point measurements, with the excitation light focused with a water-immersion objective lens (either a x63 Leica or x40 Olympus lens).

PtP-C343 emits photons via both phosphorescence and fluorescence. The photons emitted from the sample are split at a dichroic mirror (cut off wavelength = 560 nm), and detected on one of two photomultiplier tubes (PMTs), in either the green or red channels. The photons emitted via phosphorescence (this process being sensitive to quenching by O_2) have wavelengths of ~670 nm and so are detected in the red channel PMT. The photons emitted via fluorescence have wavelengths of ~498 nm and so are detected by the green channel PMT (as are the photons emitted by fluorescein isothiocyanate dextran [λ = 518 nm], which is often co-administered with PtP to enhance imaging contrast.) The phosphorescence decays detected are averaged over a number of cycles (~3,000-40,000 decays) and the lifetime of the fluorescence is determined by fitting a single exponential curve to the data. This lifetime measurement is then converted to a value of Po_2 using a calibration curve.

The presence of PtP-C343 in the plasma following intravenous administration allows for vascular mean Po_2 to be measured. In capillaries however, RBCs flow in single file and so can be detected as transient dips in the fluorescence detected in the green channel (see Methods Figure 2). This means that both capillary RBC flow rate (RBC delivery rate, cells/s) and haematocrit (% of blood volume that is RBCs) to be measured simultaneously with capillary Po_2. Importantly, detection of the RBC borders allows for the phosphorescence decays recorded to be regrouped based on their distance from the RBCs. This allows for EATs to be detected and analysed in these capillaries.

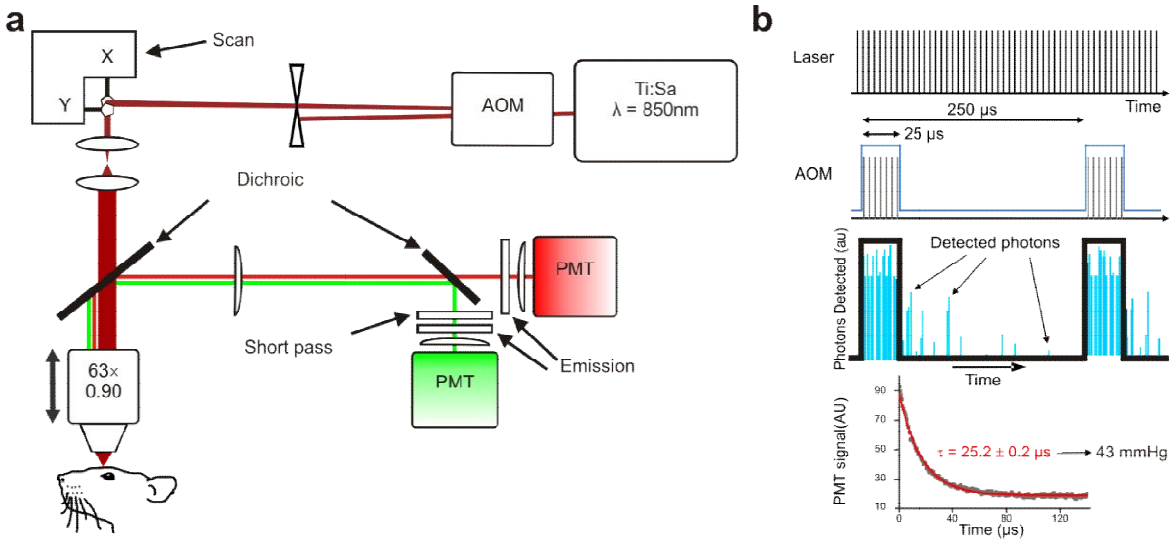

Methods Figure 1. (a) Schematic diagram of 2PLM system used in these experiments.
(b) Schematic representation of the AOM-gated excitation and detection cycles. The femtosecond laser output (top panel) is gated into µs scale On and Off periods by the AOM (panel second from top). The phosphorescent photons emitted during each Off period are detected (panel second from bottom). 3,000-40,000 such decays are averaged, a curve is fitted to determine the phosphorescence lifetime (τ), which is converted to a Po2 value using a calibration curve (bottom panel).

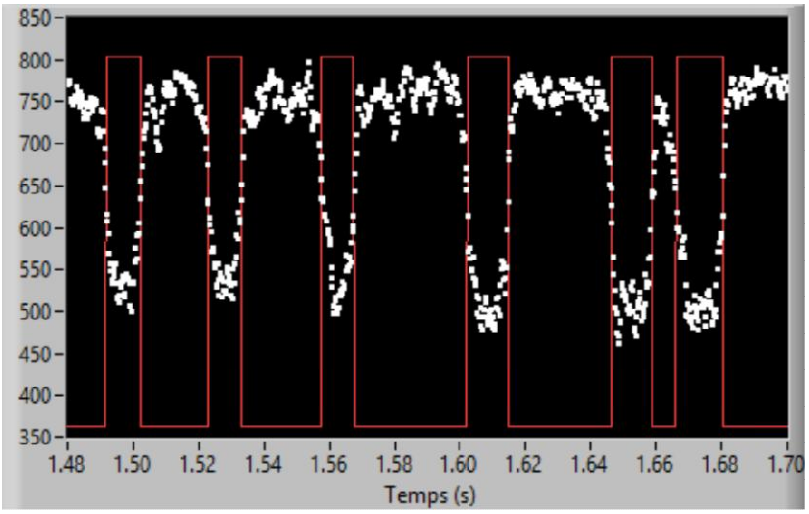

Methods Figure 2. Image of detected green-channel signal (white trace, derived from fluorescence emitted by both PtP-C343 and fluorescein dextran), showing the transient dips in fluorescence associated with the passage of RBCs through the excitation volume during acquisitions. The red lines indicate the binarised signal that is used to define RBC borders and volumes, for RBC flow, haematocrit, and EAT measurement.

As mentioned in the introduction, this capability was exploited in our lab by Parpaleix et al. (2013) to measure Po_2, RBCs flow and EATs in olfactory bulb glomerular capillaries, defining three different types of measurement that pertain to capillary Po_2. These are the mean Po_2 in the capillary plasma (Po_2Mean), the Po_2 near the border of the RBC (Po_2RBC) and the Po_2 in the plasma at mid-distance between RBCs (termed the Po_2InterRBC, see Methods Figure 3, a). One very important aspect of this work was the demonstration that this Po_2InterRBC was indicative of the Po_2 in the tissue surrounding the capillary. This was shown by comparison of the Po_2InterRBC values with the mean Po_2 in nearby tissue (See Methods Figure 3, c). Furthermore, they showed that the Po_2InterRBC was similar in capillaries up to 20-30 μm apart in spite of these pairs of capillaries having different mean Po_2 values and RBC flow rates (see Methods Figure 3, b), indicating that the tissue Po_2 around both capillaries was similar and that the Po_2InterRBC reported this tissue Po_2.

This finding, that Po_2InterRBC accurately reports local tissue Po_2, was extremely interesting, as it opened up the possibility of measuring both vascular and local tissue Po_2 in the brain in a non-invasive manner. Furthermore, it raised the possibility of performing such measurements in awake animals.

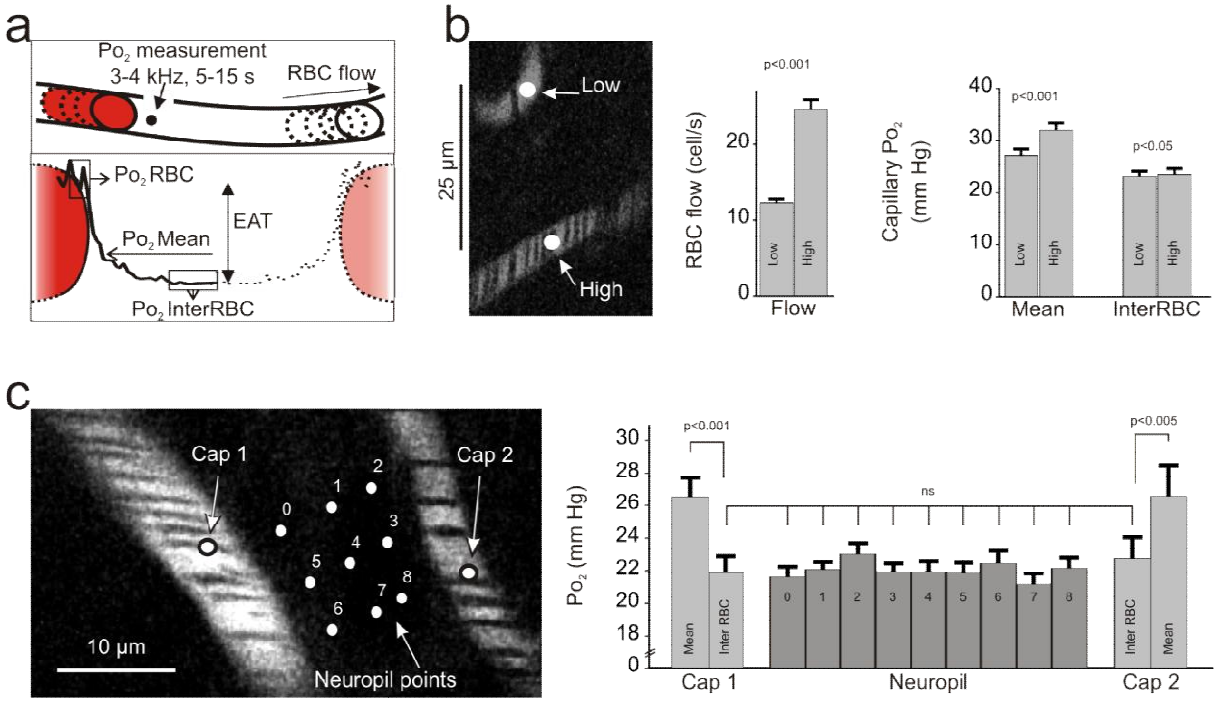

Methods Figure 3. **(a)** *Upper panel*: Schematic of how individual measurements are made, from which P_{O2} values, RBC flow, and haematocrit are determined. *Lower panel*: Schematic showing the form of an EAT (RBCs depicted, with black trace representing P_{O2} at a given distance from the RBC), and the P_{O2} parameters associated with the EAT, as defined by Parpaleix et al. (2013) and employed in the present research. **(b) and (c):** Evidence that P_{O2}InterRBC accurately reports local tissue P_{O2}. (c) EATs were measured in pairs of neighbouring capillaries (example in left panel). Subsequently, PtP-C343 was introduced directly into the intervening tissue and the tissue P_{O2} was measured. Exemplary results (right panel) show that P_{O2}InterRBC is indicative of tissue P_{O2}. (b) Capillaries with different RBC flow rates and P_{O2}Mean values had similar P_{O2}InterRBC values. This indicated that both capillaries' P_{O2}InterRBC values were at equilibrium with, and so report, a common tissue P_{O2} value.

Section 2 – Surgical Procedures

The surgical preparation consists of two main steps: the attachment of a dental cement head-cap and embedded titanium head-bar; and the craniotomy and implantation of the glass cranial window. Cortical cranial windows are stable and remain usable for many months post-surgery, but we found that windows over the olfactory bulbs tend to be less stable, with imaging quality often degrading after 2-3 weeks. The animals undergo extensive training and habituation over the course of 2-3 weeks before experimental measurements are made (see below), and so to avoid the risk that the window degraded before measurements could be made, these two steps were generally performed in two different surgical sessions a number of weeks apart (although some of the cortical cranial windows were implanted and the head-bar attached in the same session).

The mice used in the experiments were 8-12 weeks old (25-35 g) at the time of the initial surgery. They were anaesthetised with ketamine-xylazine (100 mg and 8 mg per kg body mass, respectively). Anaesthesia was confirmed regularly throughout the surgical procedures by foot pinch. The eyes were protected with hydrating ointment and the animal's head secured in a stereotaxic frame. The mice breathed air with supplementary oxygen (the final inhaled proportion of oxygen was ~30%) and the body temperature monitored by a rectal probe and maintained at ~36.5°C by a feedback-controlled heating pad.

For the head-bar attachment procedure, the fur was trimmed and the area of skin that was to be opened was cleaned with alternating swabs of 70% ethanol and betadine. An incision was made in the scalp, the skin was retracted and the connective tissue on the surface of the skull was carefully removed to make sufficient space for the head-cap to be attached. The bone was then cleaned with sterile phosphate-buffered saline and dried .The clean, dry bond was coated with a bonding agent, and then layers of light-curable dental cement were applied to all exposed areas of the skull, excepting the intended site of the cranial window. At each bonding agent or dental cement application step, the products were photopolymerised with a curing lamp (a blue light source, λ = nm, light intensity = mW). Further layers of dental cement were then applied and cured to reinforce the head cap, embed a titanium head-bar for future head fixation of the animal, and to

construct a pool to support a meniscus necessary for the water-immersion lenses used in the 2-photon imaging set-up. The edges of the incision were then rejoined and sealed to the edges of the headcap with histoacryl glue. At this stage, either the craniotomy is performed, or, in the more usual case, the area of the future cranial window is coated in a thin layer of cyanoacrylate glue to protect it, and the animal is allowed to recover and then returned to its home cage.

For the implantation of the cranial window itself, the animal was re-anaesthetised and prepared for surgery as above. The cyanoacrylate layer was removed from above the area targeted for the craniotomy, and a layer of bonding agent was applied to the exposed bone and surrounding dental cement. A thin layer of dental cement was then applied around the site of the craniotomy and cured. A craniotomy was then carried out over the brain area of interest using a hand-held drill with stainless-steel burr drill bits. Over the olfactory bulb, the final craniotomy diameter was ~2mm and those over the somatosensory cortex were ~3-4 mm. The drilling was performed with great care taken not to apply great pressure to the bone and the area was regularly flushed with cool aqueous buffer (cortex buffer, see Holtmaat et al., 2009) to avoid damage or heating of the underlying tissue.

When the craniotomy was complete, the area was covered with a drop of buffer solution and the excised bone flap was carefully removed with great care taken to not disturb the dura mater or the underlying tissue. The area was rinsed with buffer solution to removed and bone fragments that remained. Cover glasses (#1 glass, 130 to 170 μm thick) of an appropriate size (slightly smaller than the craniotomy) were chosen, and their edges coated with dental cement. The cover glass with attached dental cement was then placed into the craniotomy, with the glass resting on the dura mater, and secured in place with dental cement which linked the ring of polymerised cement on the edge of the cover glass with that which surrounded the area of the craniotomy.

For surgeries that included a craniotomy, the animals received anti-inflammatory and analgesic treatment (Carprofen, one daily 0.15 mg subcutaneous injection, administered pre-surgically and for the three days post-surgery), antibiotics (Ceftiroxone, one daily 0.25mg subcutaneous injection, administered pre-surgically and for the three days post-surgery) and dexamethasone (one daily

60μg subcutaneous injection on the day before surgery, directly before the surgery and the first post-surgical day), which has anti-inflammatory and analgesic effects and also helps prevent cerebral oedema. In surgeries where only the head-bar was attached, the dexamethasone treatment was omitted. Post-surgery, the animals were injected subcutaneously with sterile physiological saline for rehydration, kept warm, and allowed to recover from surgery in a cage with clean bedding and access to softened, moistened food. When sufficiently recovered they were returned to their home cage and allowed to recuperate for 2-3 days before training re-commenced.

Section 3 – Training procedure

In the weeks preceding surgery, the animals were supplied with a treadmill in their cages. This treadmill as similar to that which forms part of the restraint apparatus used during 2PLM recording (see Section 4), and so they became familiar with running and resting on this wheel. In the days that preceded the first surgery session, the mice were gently habituated to handling in their home cages, and provided with treats (flavoured sugar pellets) for positive reinforcement.
2-3 days after the surgery in which the head-bar was attached, restraint habituation began.

The frame used for head restraint during the habituation and imaging sessions (Methods Figure 4,a), consists of a metal frame in which the mouse's head-bar is secured, and a treadmill wheel (similar to that in the animal's home cage). This configuration allows the animal limbs and body to move freely while the head is stably fixed. All restraint- habituation sessions were carried out in the set-up that was used for imaging, with the animal kept in the near-dark at all times. The initial habituation sessions involve anaesthetising the animals briefly with isoflurane (4% in air for initiation, 2-2.5 % for maintenance. Total time of anaesthesia <5 minutes), placing the animal on the treadmill, and securing the head-bar in place in the frame. The animal was allowed to wake up, and its behaviour monitored via infra-red video camera for a period of 5 minutes. The animal was then removed from the frame and returned to a temporary holding cage, where it was provided with treats and *ad libitum* access to water. Following a period of ~30 minutes, the animal was re-anaesthetised and underwent another 5 minute habituation session. This cycle was repeated 4-5 times on the first day of restraint-habituation. The frame and all surrounding areas were cleaned with 70% ethanol and then distilled water between each session. At the end of the block of sessions the mouse was returned to its home cage.

On subsequent days, the mice were not anaesthetised, but rather were placed gently in the frame while awake. The duration of the restraint sessions were steadily increased, until after 2-3 weeks of extensive training the mice were able to remain in the restraint apparatus for periods of longer than one hour. The animals' behaviour during these sessions consisted of short bouts of locomotion (10-60 seconds) separated by longer periods of stillness (5-15 minutes). At this stage,

the animals were considered ready for use in experiments. If they already had implanted cranial windows, recordings were commenced on the subsequent days. In cases where surgery was needed to implant a cranial window, the animals underwent the procedure as describe above, were allowed to recuperate over 2-3 days, and then underwent 2-3 more days of restraint training to ensure a suitable level of habituation before experiments were initiated. These final days of habituation were often utilised to allow for the generation of image stacks of vasculature (by intravenous administration of fluorescein dextran) in the brain area of interest which aided targeting of Po_2 recordings during the experiments.

This extensive habituation schedule was implemented to minimise the potential of stress being experienced by the mice during the recordings sessions. Avoidance of stress is clearly very important as it could be a major confounding factor in experiments on awake animals, especially those concerning the vascular system, which is known to be affected by stress (Bryan, 1990). The animals did not exhibit obvious stress behaviours during the recording sessions or in the post-recording period, when upon placement in their temporary cage they typically instantly began to consume the treats provided.

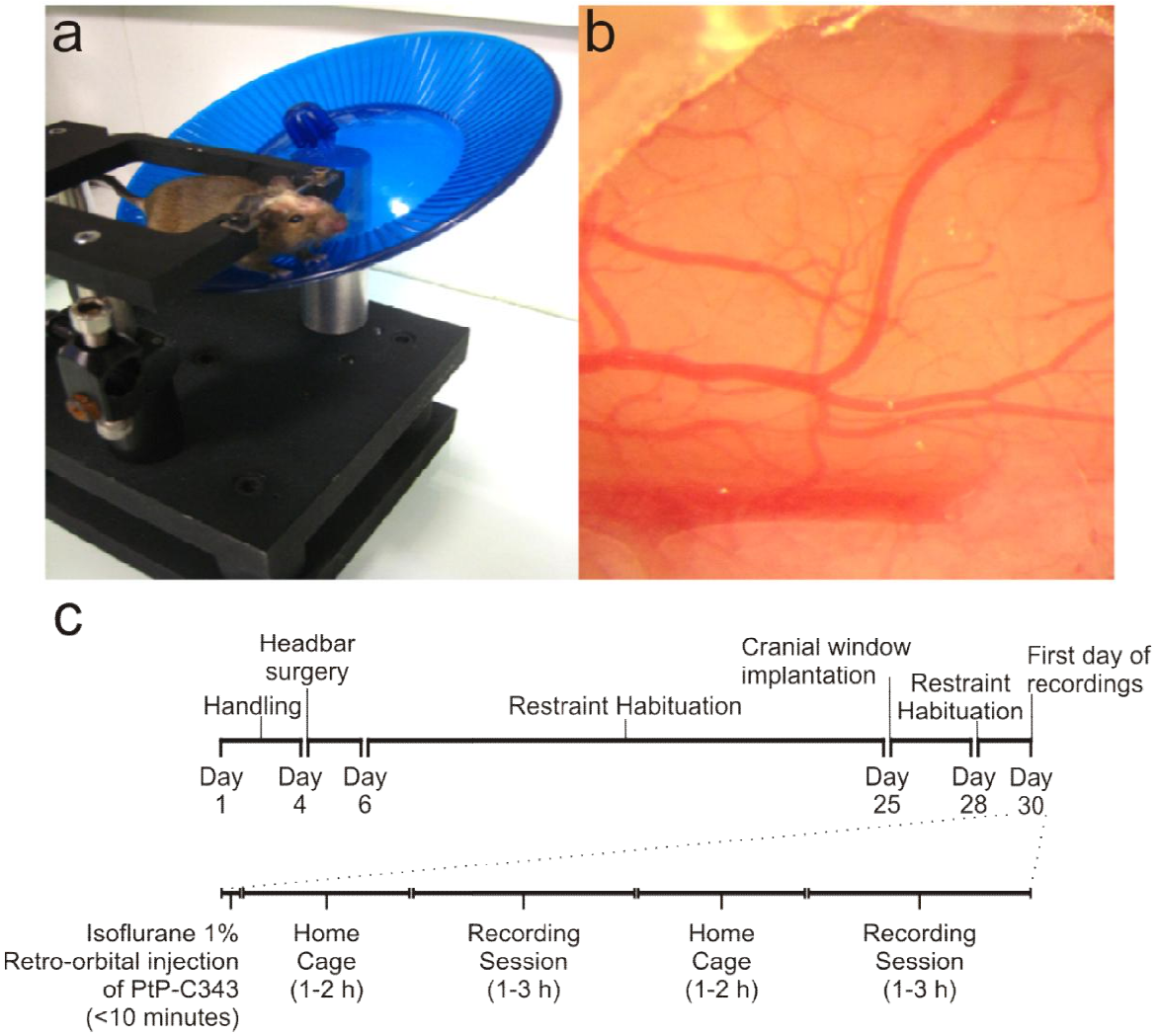

Methods Figure 4. **(a)** Image of a mouse, head-fixed in the restraint apparatus used during the habituation and recording sessions. **(b)** Image of olfactory bulb tissue and vasculature as seen through an implanted chronic cranial window. **(c)** Schematic representation of the overall procedure followed and the time-table for handling, surgical preparation, restraint habituation, and recording (upper panel), along with the pattern of PtP-C343 injection, delays and recording sessions that was followed on days in which recordings were carried out (Lower panel).

Section 4 – Procedure for recording of Po_2 and Blood flow Parameters in Awake Mice

On the days on which recordings were taken, the animals were briefly anaesthetised with isoflurane (4% for initiation, 2-2.5% for maintenance, in air. Total duration of anaesthesia <10 minutes), and PtP-C343 solution was introduced intravenously via retro-orbital injection. The injected solution was a mixture of 40µl of 5mM PtP-C343 solution and 40µl of 10mM fluorescein isothiocyanate dextran (molecular weight = 150 kDa) solution, both dissolved in physiological saline, for a total injection volume of 80µl. The final PtP-C343 concentration in the plasma is estimated to be ~100µM. After the injection, the mice were returned to their home cages for ~90 minutes, before being brought back to the experiment room, for ~30 minutes before the start of the recording session. Each recording session lasted between 1 and 3 hours, depending on the type of measurements performed and the behaviour of the animal, and each animal underwent 1-3 recording sessions per day over the course of 2-7 days, with breaks of at least 1-3 hours between each session. The overall time-course of the experiments carried out on an animal is presented in Methods Figure 4 (c).

As explained earlier, the measurement of Po_2 is based on gating the laser light into on and off periods, for excitation of the probe and recording of the emitted phosphorescence respectively. The fluorescence emitted during the on period was also recorded.

The acquisition and analysis of 2-photon imaging and 2PLM data was performed using custom build software developed using LabView (National Instruments).

Initially, fast 3D image acquisition was performed to identify and target vessels of interest. Po_2 measurements were then made by focusing the excitation point in blood vessels of interest, and recording the fluorescence and phosphorescence emitted from 10-40,000 cycles of excitation and detection of phosphorescence decays (2.5-10 seconds of measurement) at each point. Typically 4-8 measurements were performed in each capillary, with the total number of decays averaged recorded for each capillary being around 60-100,000. The first 6-7 bins (~4µs) after the end of the on-phase were discarded. The non-linear least-squares method and the Marquardt-Levenberg algorithm were used to extract the phosphorescence lifetime (τ) from these averaged decays. A

previously prepared Stern-Volmer like calibration curve was then used to convert the lifetime measurements to values of Po_2.

The fluorescence recorded during the excitation period of the cycle was analysed and the passage of RBCs through the excitation point detected based on the associated dips in fluorescence intensity. These transient reductions in fluorescence intensity were detected and quantified using a binary threshold method. This allowed for the measurement of both capillary RBC flow rate and haematocrit.

The borders of the detected RBCs were used as time-stamps, and the phosphorescence decays recorded were binned according to their distance in time from the borders of the nearest RBC. The Po_2 parameter measured are shown diagrammatically in Methods Figure 3 (a). The Po_2RBC value was calculated from the average lifetime of decays recorded in the 1-4 ms around the border of the RBC, whereas the Po_2InterRBC was determined from average value of decays at mid-distance between RBCs (averaged over a window of at least 5ms).

The results of these experiments are presented in the following chapter.

Part 3: Results

Section 1 – Oxygenation of the Olfactory Bulb Glomerular Layer

I measured Po_2 from capillaries located in the olfactory bulb GL of awake mice, using our 2PLM method to record Po_2Mean, RBC flow rates and haematocrit, and subsequently examined the EATs in these capillaries and measured the Po_2RBC and Po_2InterRBC.

3.1.1 – Capillary and tissue Po_2 in the olfactory bulb glomerular layer

The mean values of Po_2 measured were 60.6 ± 2.3 mmHg, 23 ± 1.5 mmHg, and 32.7 ± 1.9 mmHg, for Po_2RBC, Po_2InterRBC and Po_2Mean respectively (Fig. 1a). Capillary Po_2 in the GL is quite heterogeneous, with Po_2RBC, Po_2InterRBC and Po_2Mean each being spread across a range of approximately 40 mmHg (Fig. 1b). As has been previously described in anaesthetised animals (Parpaleix et al., 2013), each of these Po_2 parameters was found to be significantly different from the others.

The dispersion of the Po_2 values can also be seen in Fig. 1(c) and (d), where the range is similar whether considering the individual Po_2 measurements (d) or the mean values for each capillary derived from these measurements (c). The range of mean capillary Po_2RBC values suggests that there is a heterogeneous population of capillaries in the olfactory bulb GL, in which there is a wide range of RBC oxygenation (ranging from ~80 mmHg to ~40 mmHg, with one capillary having a mean Po_2RBC value as low as 25.6 mmHg). These two extremes (80 and 40 mmHg) correspond to So_2 values of approximately 90 and 40% respectively (Gray and Steadman, 1964), considering that Po_2RBC represents the Po_2 that equilibrates with haemoglobin inside the erythrocyte.

This heterogeneity is especially notable when considering the Po_2InterRBC value, as this is reflective of the local tissue Po_2. This suggests that most of the neural tissue of the dorsal olfactory bulb GL has steady-state Po_2 values of 20-35 mmHg, but that some regions will have Po_2 values of <15 mmHg. Indeed, in one case a mean capillary Po_2InterRBC value of <1 mmHg was recorded, indicating that the tissue in this area was within the range of what is considered severely hypoxic (Erecińska and Silver, 2001; Takano et al., 2007).

Fig. 1 (e) compares the SD of the Po_2 measurements in a given capillary to the mean of these measurements. This plot shows that although the variation in Po_2InterRBC and Po_2Mean is

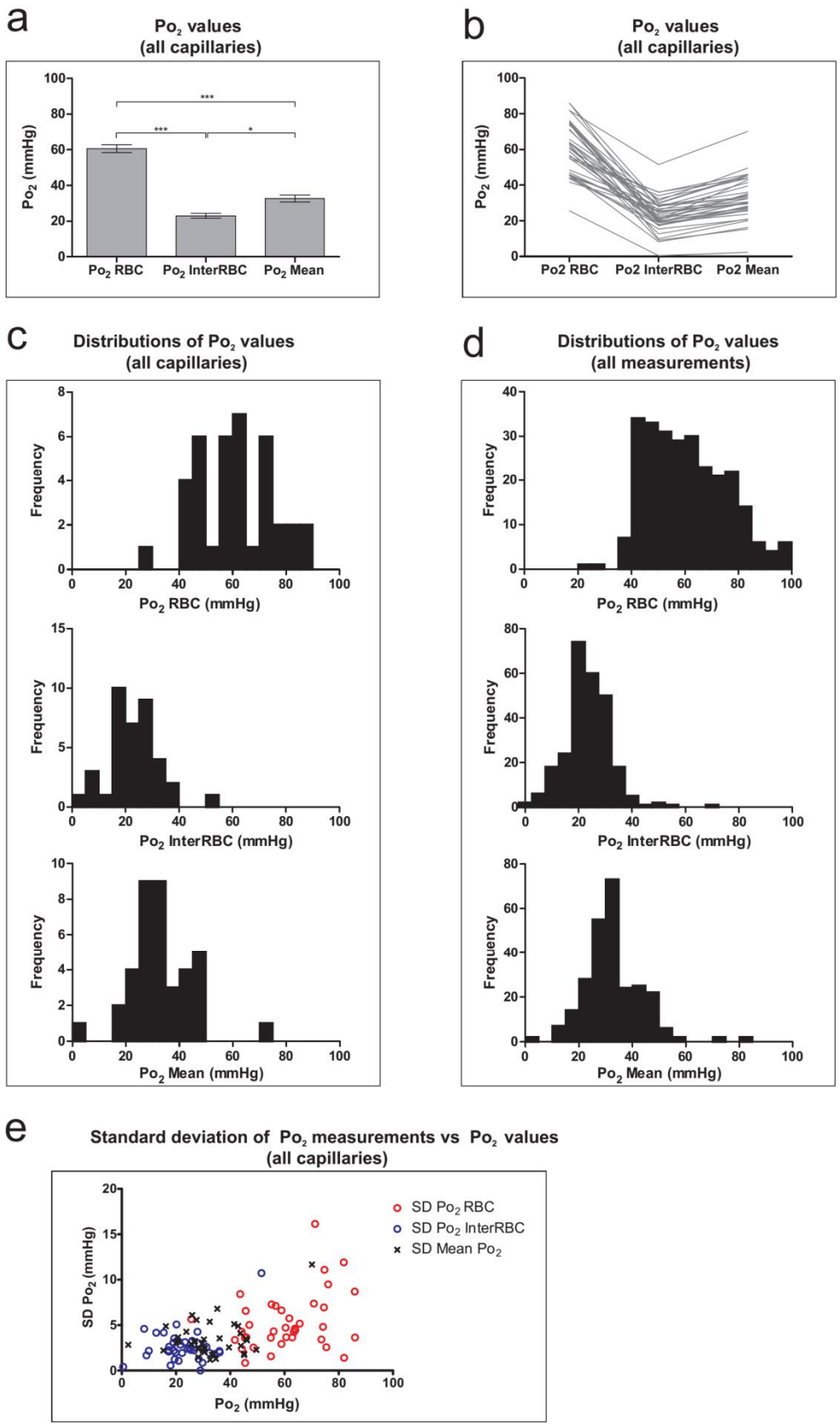

Figure 1 :Capillary and tissue P_{O_2} in the olfactory bulb GL.

(a) Mean values of P_{O_2}RBC, P_{O_2}InterRBC (= local tissue P_{O_2}) and P_{O_2} Mean from GL capillaries (n=38). Data presented as Mean ± SEM from all capillaries. * = $p<0.05$, *** = $p<0.001$, Kruskal-Wallis test with Dunn's Multiple Comparison Post-Hoc test. **(b)** All values of P_{O_2}RBC, P_{O_2}InterRBC and P_{O_2} Mean for the individual capillaries averaged in (a). **(c,d)** Comparison of P_{O_2} Mean, P_{O_2}RBC and P_{O_2}InterRBC distributions obtained from the 38 capillary mean values and from all measurements. 5 mmHg bin width. **(e)** Standard deviation of the P_{O_2} measurements in individual capillaries as a function of capillary mean values. For all plots, n = 262 measurements from 38 capillaries in 5 mice.

relatively independent of the average of these parameters measured in that capillary, the SD of the Po_2RBC measurements appears to be larger at higher average levels of Po_2RBC. This might suggest that the oxygenation of RBCs fluctuates more in capillaries that are generally more highly oxygenated. Another potential source for this variation is the fact that the Stern-Volmer type calibration curve relating the PtP-C343 lifetime and the Po_2 is steep in the higher ranges of physiological Po_2 (see Introduction Figure 6). This implies that minor errors in the fit of the curve to the phosphorescence decays recorded, or minor variations in these decays, would result in a comparatively large difference in the Po_2 value derived from these measurements. Thus, minor variations in Po_2 in a given capillary would induce greater variation on the Po_2RBC value than on the other Po_2 parameters, whose absolute values are lower and so lie in a less steep area of the calibration curve.

3.1.2 – Capillary RBC flow and haematocrit in the olfactory bulb glomerular layer

As O_2 delivery is critically dependent on RBCs, simultaneous analysis of oxygenation and blood flow parameters has the potential to allow insight into the mechanisms of oxygen delivery to the tissue. In our recordings, the identification of individual RBCs and their borders allowed for measurement of capillary RBC flow rate and haematocrit. In the olfactory bulb GL, the mean RBC flow was found to be 30.6 cells/s (Fig. 2a, left panel), which is similar to values previously measured by the Charpak lab in both anaesthetised mice and rats (Chaigneau et al., 2003; Parpaleix et al., 2013) A broad range of RBC flow rates was observed (Fig. 2a, centre panels), ranging from <10 cells/s in some capillaries to >70 cells/s in others. Once again, the range of values of each measurement is largely similar to the range of the capillary mean values. In the right-hand panel of Fig. 2(a), the SD of the measurements from each capillary indicates a trend towards greater variability in RBC flow rates in capillaries with higher RBC flow.

The mean haematocrit in GL capillaries was found to be 34.6% (Fig. 2b, left panel), but the frequency distribution histograms revealed that, in fact, there seemed to be two peaks in the frequency of haematocrit values, one around 20-25% and the other between 40 and 50% (Fig. 2b, centre panels).These two peaks were also discernible in the left-hand panel of Fig. 2(c), where RBC flow is plotted as a function of haematocrit. The presence of low RBC flow rates at high levels of haematocrit is consistent with the fact that that capillary haematocrit is an index of RBC linear density, which is, in turn, related to the RBC flow rate by the RBC velocity. Thus, the presence of low RBC flow rates at high levels of haematocrit (right-hand circle on Fig. 2c) suggests that these capillaries have low RBC velocity levels, whereas the capillaries with very high RBC flow rates (>60 cells/s) must have both high haematocrit and high RBC velocity. Note that the variability of both RBC flow and haematocrit were found to be relatively independent of the magnitude of the other parameter (Fig. 2c, centre and right-hand panels).

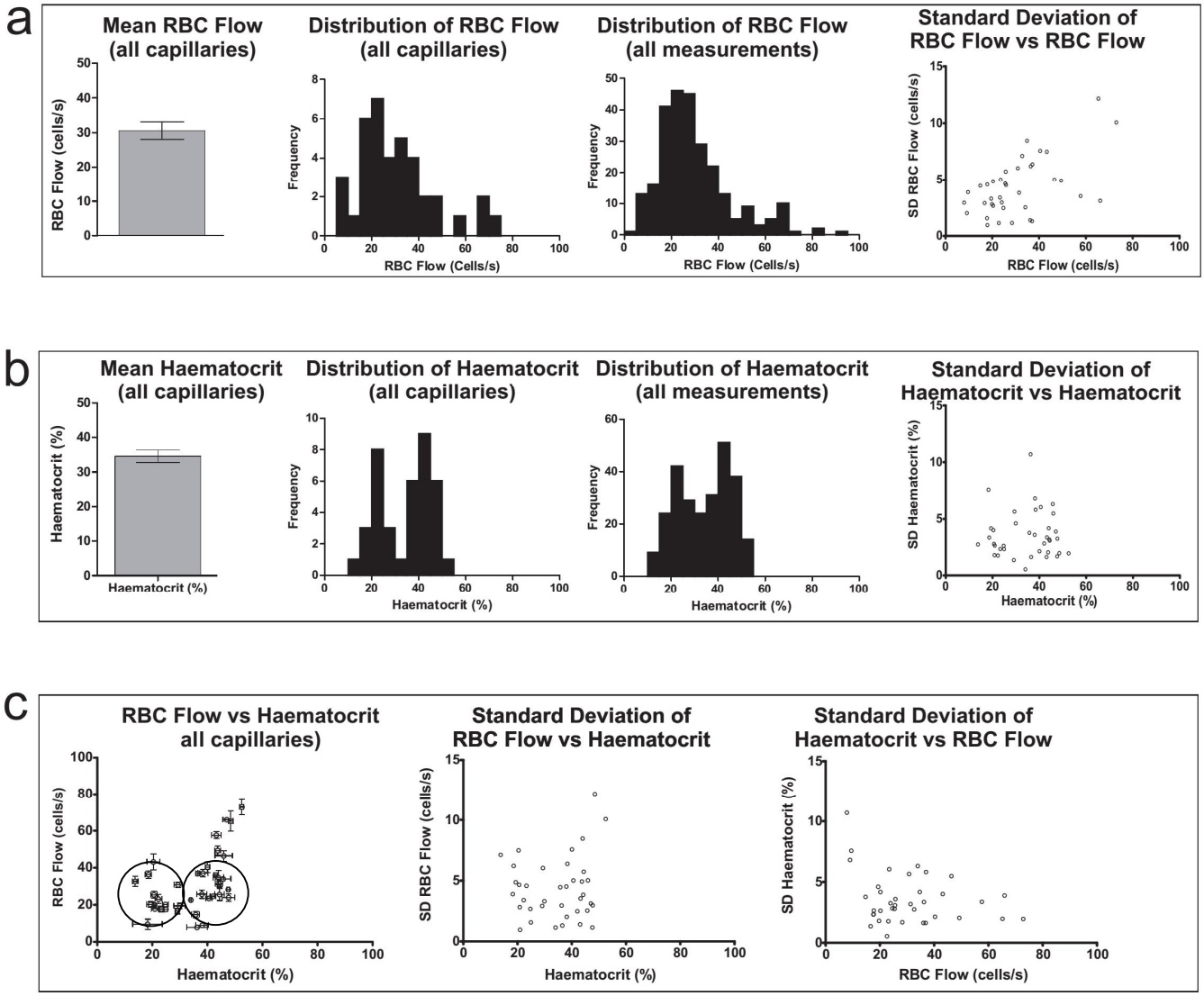

Figure 2 : Capillary RBC flow and haematocrit in the olfactory blub GL.

(a) *Left-hand panel*: Mean value of RBC flow in capillaries (Mean ± SEM). *Centre-left and centre-right panels* illustrate the comparison of RBC distributions obtained from the 38 capillaries and from all measurements. 5 cells/s bins. *Right-hand panel:* Standard deviation of RBC flow measurements in individual capillaries as a function of the mean RBC flow value. **(b)** *Left-hand panel*: Mean value of haematocrit in capillaries (Mean ± SEM). *Centre-left and centre-right panels* illustrate the comparison of haematocrit distributions obtained from the 38 capillaries and from all measurements. 5 % bins. *Right hand panel:* Standard deviation of haematocrit measurements in individual capillaries as a function of the mean haematocrit value. **(c)** *Left-hand panel*: Interaction of RBC flow and haematocrit (Mean ± SEM). *Centre and left panels:* Standard deviation of RBC flow vs. mean haematocrit, and standard deviation of haematocrit vs mean RBC Flow, in individual capillaries. For all plots, n = 262 measurements from 38 capillaries in 5 mice.

3.1.3 – The relationship between blood flow and Po_2 in the olfactory bulb glomerular layer

With this data set of simultaneously measured Po_2 and blood flow parameters, we were able to examine the correlations between these factors and uncover possible interactions.

In the upper panel of Fig. 3(a) Po_2RBC and Po_2InterRBC are plotted as functions of RBC flow, and this relationship is further examined in Fig. 3(b). It can be seen that Po_2RBC rises in tandem with RBC flow through low to moderate ranges of flow (~10-40 cells/s), but plateaus at higher rates of flow (>50 cells/s). On the other hand, Po_2InterRBC (and hence local tissue Po_2), is poorly dependent on RBC flow through a large range of flow rates, from less than 10 to around 50 cells/s, only becoming obviously related to flow rates at > 50 cells/s. Conversely, the lower panel of Fig. 3(a) shows that Po_2Mean, which depends on both Po_2RBC and Po_2InterRBC, is correlated with RBC flow throughout a wide range of flow rates. The variation each of these Po_2 parameters within a given capillary seem to be independent of the RBC flow rate in the capillary (Fig. 3c).

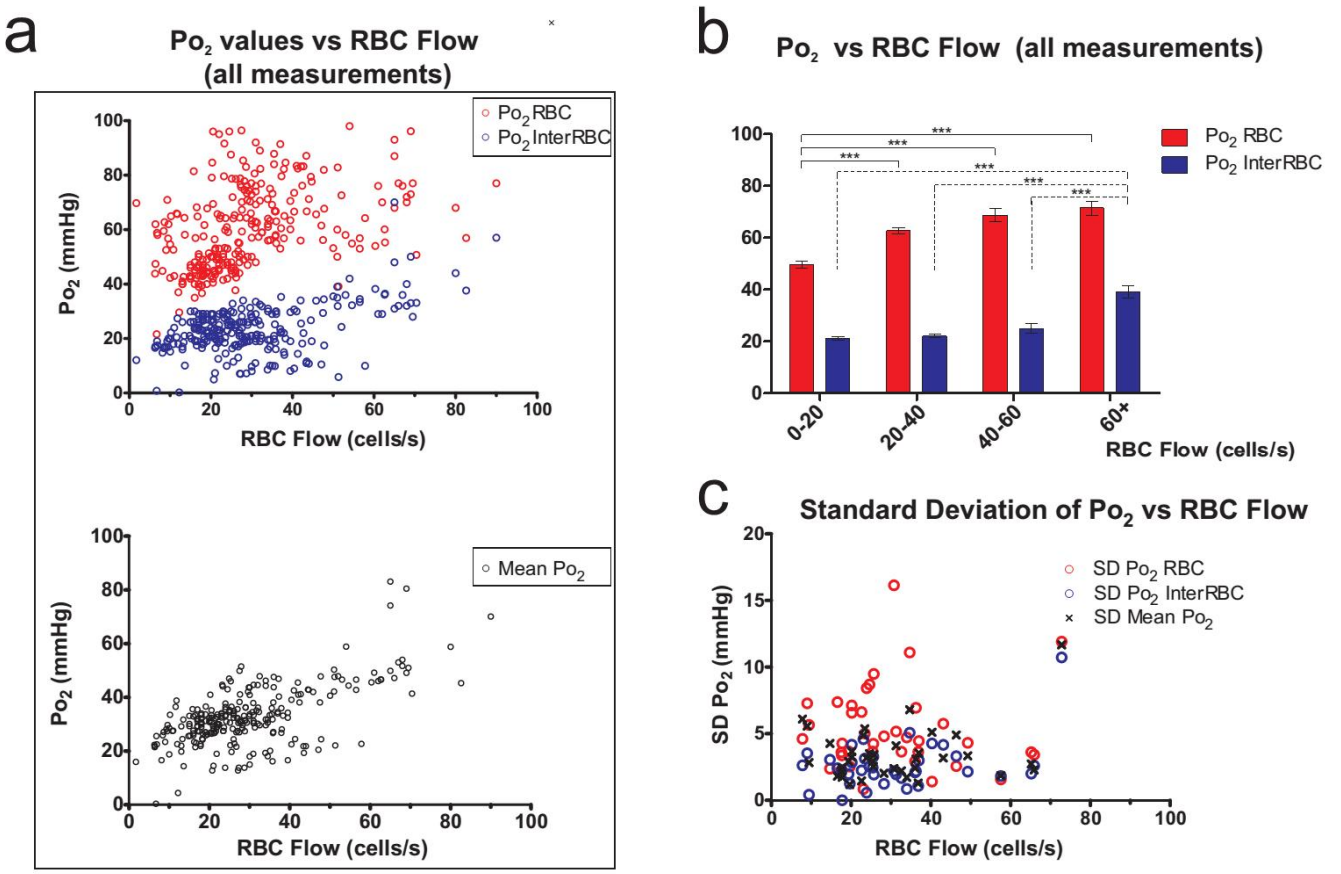

Figure 3 : The correlation of RBC flow with capillary and tissue Po_2 in the olfactory bulb GL.

(a) *Upper panel:* Po_2RBC and Po_2InterRBC (= local tissue Po_2) as a function of RBC flow. Each measurement plotted. *Lower panel:* Capillary Po_2Mean as a function of RBC flow. Each measurement plotted. **(b)** Mean Po_2 RBC and Po_2 InterRBC as a function of RBC flow, with mean values calculated per 20 cells/s bin. * = p<0.05, ** = p<0.01, *** = p<0.001. Kruskal-Wallis test with Dunn's Multiple Comparison Post-Hoc test. **(c)** Standard deviation of Po_2 measurements made in each capillary as a function of capillary mean RBC flow. For all plots, n = 262 measurements from 38 capillaries in 5 mice.

3.1.4 – The relationship between haematocrit and Po_2 in the olfactory bulb glomerular layer

From Fig. 4 (a, upper panel) and (b), it can be observed that on average Po_2RBC is greater at high levels of haematocrit, but that there is great variability in the Po_2RBC measurements observed throughout the range of haematocrit values. In contrast, the Po_2InterRBC values, which are low at low levels of haematocrit (<20%), remain relatively stable throughout a large range of haematocrit values (from approximately 20 to 45%), and show a moderate increase at haematocrit values >50%. A notable feature is the relatively small variation of Po_2InterRBC throughout most of this range of haematocrit (the average SD of the Po_2InterRBC measurement values from 20-45% = 6.5 mmHg). Similarly to the relationship seen with RBC flow, Po_2Mean correlates quite well with haematocrit (Fig. 4a, lower panel). The SD of the Po_2 measurements was unrelated to the capillary haematocrit (Fig. 4c).

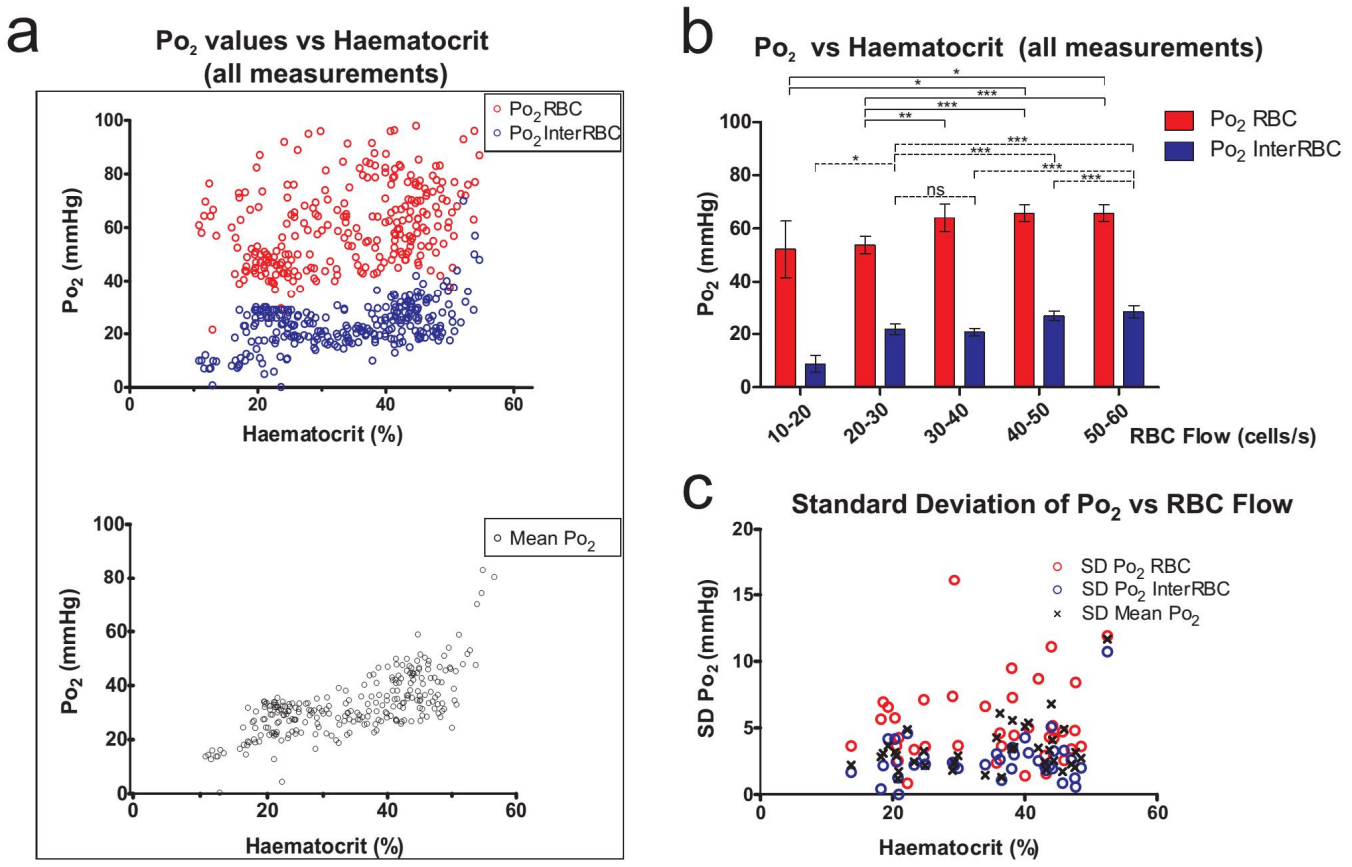

Figure 4 : The correlation of haematocrit with capillary and tissue Po_2 in the olfactory bulb GL.
(a) *Upper panel:* Po_2RBC and Po_2InterRBC (= local tissue Po_2) as a function of haematocrit. Each measurement plotted. *Lower Panel:* Capillary Po_2Mean as a function of haematocrit. Each measurement plotted. **(b)** Mean Po_2 RBC and Po_2 InterRBC as a function of haematocrit, with mean values calculated per 10% bin. * = p<0.05, ** = p<0.01, *** = p<0.001. Kruskal-Wallis test with Dunn's Multiple Comparison Post-Hoc test. **(c)** Standard deviation of Po_2 measurements made in each capillary as a function of capillary mean haematocrit. For all plots, n = 262 measurements from 38 capillaries in 5 mice.

3.1.5 – Capillary blood flow parameters in areas of low tissue Po_2 in the olfactory bulb glomerular layer

In figures 3 and 4, the relationship between Po_2 and both RBC flow and haematocrit are explored. On examination of these relationships, it can be seen that there were a number of capillaries (n=5), in which the Po_2InterRBC is noticeably low (<15 mmHg). We decided to focus on these capillaries and assess the dependence of these low Po_2InterRBC (and therefore local tissue Po_2) values on RBC flow or haematocrit. As can be seen from Fig. 5(a), these low Po_2InterRBC values can be found across a wide range of RBC flow rates. In contrast, these low Po_2 values were all associated with relatively low haematocrit values (<25%, Fig. 5b). This suggests that tissue areas of very low Po_2 are supplied by capillaries in which the haematocrit is low. The relationships of Po_2RBC to RBC flow and to haematocrit are also contrasting. Po_2RBC seems uncorrelated to haematocrit, but rises almost linearly with RBC flow rate. This suggests Po_2RBC is strongly related to RBC velocity. These measurements provide insight into the capillary and tissue oxygenation of the olfactory bulb GL in awake mice, and the way in which blood flow influences Po_2 values in this structure.

To answer the question of whether these values and relationships are specific to the olfactory bulb, or if they are more generally true for the mammalian brain, we decided to investigate Po_2 in the cerebral cortex.

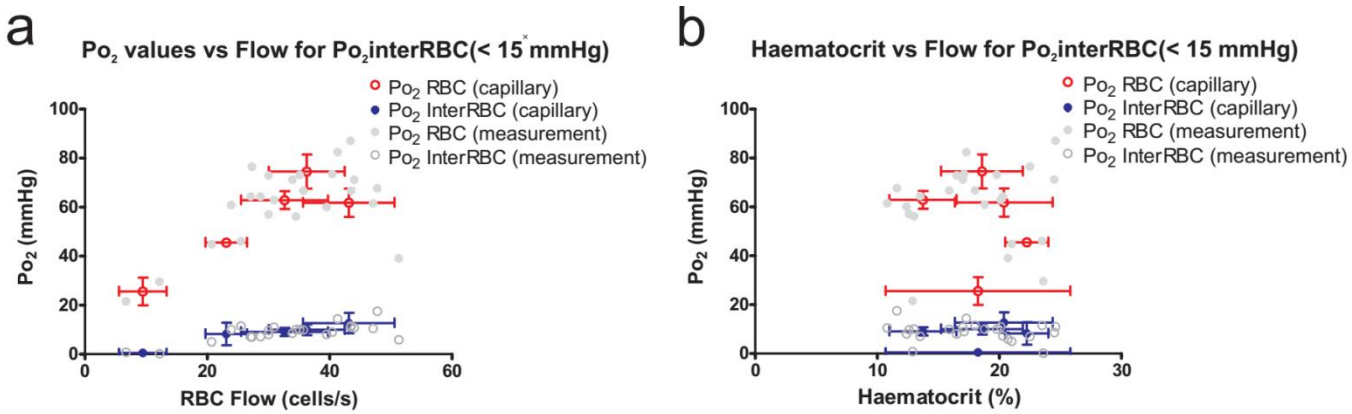

Figure 5 : The correlation of RBC flow and haematocrit with capillary Po_2 in low- Po_2InterRBC capillaries (Po_2InterRBC <15 mmHg) in the olfactory bulb GL.

(a) Po_2RBC and Po_2InterRBC as a function of RBC flow. **(b)** Po_2RBC and Po_2InterRBC as a function of haematocrit. Single measurement values and mean ± SD of all measurements in each capillary shown. n = 24 measurements in 5 capillaries.

Section 2 – Oxygenation of the superficial layers of the somatosensory cortex

We turned our attention to the somatosensory cortex, with the goal of investigating regional differences in the basic values of Po_2 and blood flow parameters in a brain area particularly prone to ischemic events. A random sample of (n=81) capillaries were targeted at depths of up to 410µm below the pia mater in the somatosensory cortical areas representing the fore- and hind-limbs (S1FL and S1HL) and (n=526) measurements of Po_2, EATs, RBC flow and haematocrit were made.
It is important to note that the mean from any point in the tissue to the nearest capillary has been reported to be higher in the cerebral cortex than in the olfactory bulb glomeruli (Lecoq et al., 2009; Sakadžić et al., 2014). As a result it is uncertain how well the Po_2InterRBC represents the total variation in tissue Po_2. It is possible that, in the cortex, Po_2InterRBC is only an accurate measurement of tissue Po_2 to a certain radius from the capillary where it is measured. The extent to which cortical tissue Po_2 is reported by capillary Po_2InterRBC is yet to be fully determined (See Discussion), so currently we consider that Po_2InterRBC reports peri-capillary tissue Po_2 rather than a general tissue value, though for the sake of simplicity we continue to refer to is as local tissue Po_2.

3.2.1 - Capillary and local tissue Po_2 in the somatosensory cortex

We initially analysed the complete data set, collating measurements acquired from all the capillaries assessed regardless of their depth in the cortex.

In figure 6, the data relating to the Po_2 parameters measured in all of these capillaries is presented. The mean Po_2 values recorded were 66.3 ± 1.6 mmHg, 23.3 ± 1.1 mmHg, and 36.3 ± 1.3 mmHg for Po_2RBC, Po_2InterRBC and Po_2Mean respectively (Fig. 6a). As in the olfactory bulb GL, the three Po_2 parameters were significantly different from each other, and the Po_2 values recorded in the cortex were distributed widely outside the mean values.

The range of the distribution of the Po_2RBC and Po_2Mean values were similar in the cortex to those recorded in the GL, although there was a higher relative frequency of Po_2RBC values greater than 60 mmHg, with Po_2RBC values between approximately 55 and 70 mmHg being most common (Fig. 6, b, c, d). The Po_2InterRBC values, representative of local tissue Po_2, are most frequently in the range of 15-25 mmHg, a slightly lower value than that observed in the GL, although the full range (~0-40 mmHg) was similar. Just as in the olfactory bulb, the relationship between SD Po_2 for the measurements from a capillary and the mean of these measurements suggested that Po_2RBC was more variable in a capillary at a high absolute Po_2RBC (Fig. 6e), but similarly, an explanation related to the intrinsic properties of the 2PLM Po_2 measurement technique is possible.

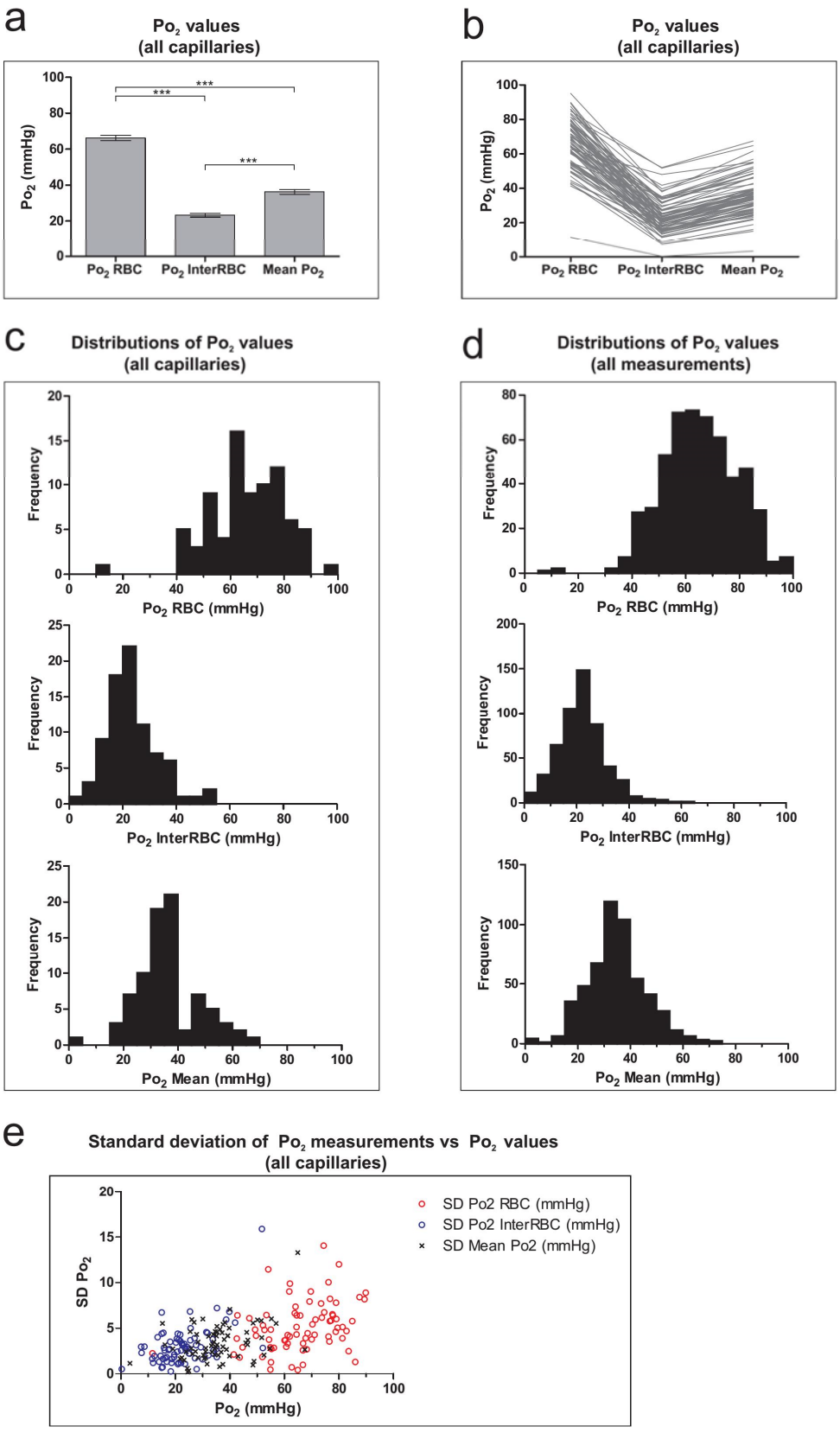

Figure 6 : Capillary and tissue P_{O_2} in the somatosensory cortex. Data from all capillaries assessed.

(a) Mean values of P_{O_2}RBC, P_{O_2}InterRBC (=local tissue P_{O_2}) and P_{O_2} Mean from cortical capillaries (n=81). Data presented as mean ± SEM from all capillaries. *** = $p<0.001$, Kruskal-Wallis test with Dunn's Multiple Comparison Post-Hoc test. **(b)** All values of P_{O_2}RBC, P_{O_2}InterRBC and P_{O_2} Mean for all the individual capillaries averaged in (a). **(c,d)** Comparison of P_{O_2} Mean, P_{O_2}RBC and P_{O_2}InterRBC distributions obtained from the 38 capillary mean values and from all measurements. 5 mmHg bin width. **(e)** Standard deviation of the P_{O_2} measurements in individual capillaries as a function of capillary mean values. For all plots, n = 526 measurements from 81 capillaries in 3 mice.

3.2.2 – Capillary RBC flow and haematocrit in the somatosensory cortex

The fact that measurements of Po_2 parameters in the cortex revealed a pattern of values that was broadly similar to that in the olfactory bulb GL would perhaps suggest that there is also a similarity in the blood flow parameters between these two regions. However, this supposition was not borne out by the data.

The mean value of RBC flow recorded in the cortex (41.9 ± 1.8 cells/s, Fig. 7a, left-hand panel) was higher than that in the olfactory bulb GL, and the distribution of RBC flow values in the cortex was right-shifted relative to that in the GL (frequency peak ~25-40 cells/s in the cortex, as opposed to ~15-30 in the GL), when either individual capillary means or single measurements were considered (Fig. 7a, centre panels). This was also the case for haematocrit where the mean value from all capillaries measured is 47.3 ± 0.9 % (Fig. 7b, left-hand panel). In addition to being right shifted relative to the equivalent distribution in the olfactory bulb GL, the frequency distribution of the haematocrit observed in the cortical capillaries did not display multiple peaks. Rather, the most frequent haematocrit values lay in the range of 40-60 % (Fig. 7b, centre panels).

The relatively narrow distribution of both RBC flow and haematocrit values is reflected in the dense clustering observed on the plot of RBC flow as a function of haematocrit(Fig. 7c, left panel), from which no clear relationship is discernible. The SD of the RBC flow and the haematocrit measurements from a capillary seem to be largely independent of each of these parameters mean values for that capillary (Fig. 7,a and b, right-hand panels, and Fig. 7c, centre and right-hand panels).

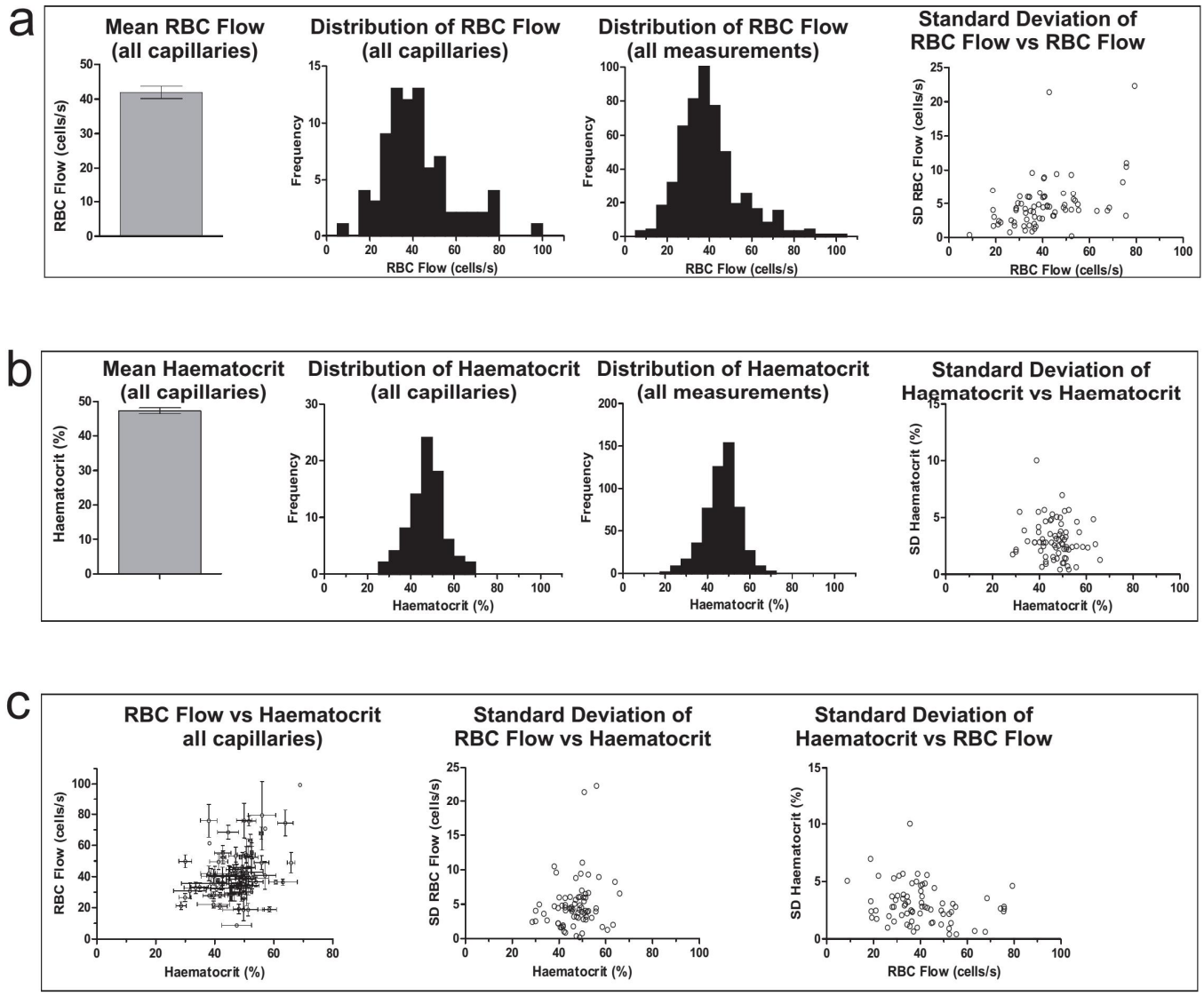

Figure 7 : Capillary RBC Flow and haematocrit in the somatosensory cortex. Data from all capillaries assessed.

(a) *Left-hand panel:* Mean value of RBC flow in capillaries (Mean ± SEM). *Centre-left and centre-right panels* illustrate the comparison of RBC distributions obtained from the 81 capillaries and from all measurements. 5 cells/s bins. *Right-hand panel:* Standard deviation of RBC flow measurements in individual capillaries as a function of the mean RBC flow value. **(b)** *Left-hand panel:* Mean value of haematocrit in cortical capillaries (Mean ± SEM). *Centre-left and centre-right* panels illustrate the comparison of haematocrit distributions obtained from the 81 capillaries and from all measurements. 5 % bins. *Right-hand panel:* Standard deviation of haematocrit measurements in each capillary as a function of the mean haematocrit value. **(c)** *Left-hand panel: Interaction of RBC flow and haematocrit (*Mean ± SEM). *Centre and right panels:* Standard deviation of RBC flow vs mean haematocrit and standard deviation of haematocrit vs mean RBC flow, in individual capillaries. For all plots, n = 526 measurements from 81 capillaries in 3 mice.

3.2.3 – The relationship between capillary blood flow and Po_2 in the somatosensory cortex

The relationship between capillary RBC flow, and both Po_2RBC and Po_2InterRBC in the cortex is illustrated in Fig. 8(a, upper panel) and (b). Po_2RBC shows increases through low to moderate ranges of RBC flow (from ~15-70 cells/s), but stabilises above around 70 cells/s. Conversely, the Po_2InterRBC (local tissue Po_2) displays a constant increase across the range of RBC flow values measured, a general pattern that is replicated by the relationship between Po_2Mean and RBC flow (Fig. 8a, lower panel). The SD of Po_2 parameters measured in each capillary appears to be independent of the average RBC flow measured in that capillary (Fig. 8c).

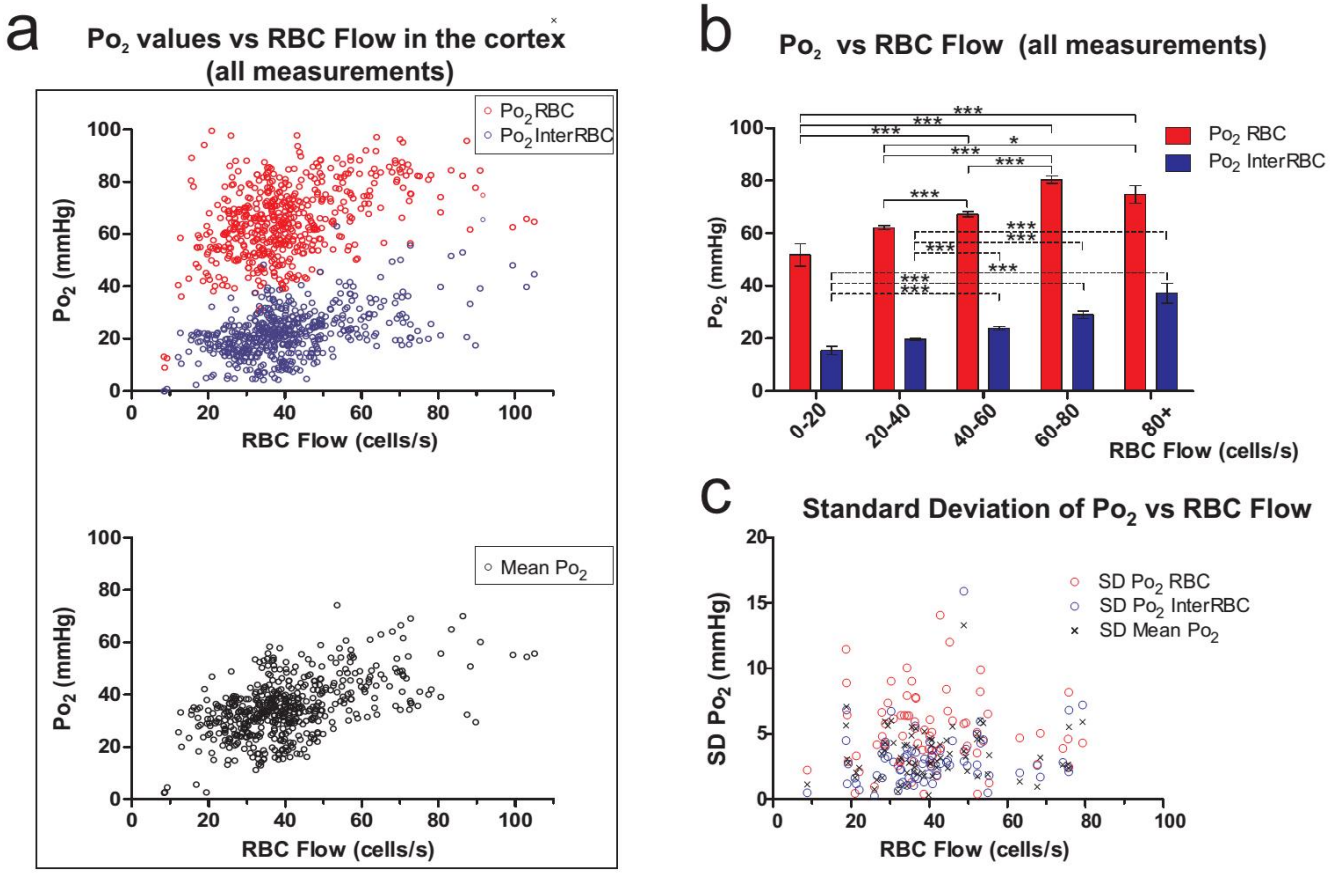

Figure 8 : The effect of RBC Flow on capillary and tissue Po_2 in the somatosensory cortex. Data from all capillaries assessed.

(a) *Upper panel:* Po_2RBC and Po_2InterRBC (= local tissue Po_2) as a function of RBC flow. Each measurement plotted. *Lower panel*: Capillary Po_2Mean as a function of RBC flow. Each measurement plotted. **(b)** Mean Po_2 RBC and Po_2 InterRBC as a function of RBC flow, with mean values calculated for each 20 cells/s bin. * = $p<0.05$, ** = $p<0.01$, *** = $p<0.001$. Kruskal-Wallis test with Dunn's Multiple Comparison Post-Hoc test. **(c)** Standard deviation of Po_2 measurements made in each capillary as a function of the capillary mean RBC flow. For all plots, n = 526 measurements from 81 capillaries in 3 mice.

3.2.4 – The relationship between capillary haematocrit and Po_2 in the somatosensory cortex

The plots of Po_2RBC and Po_2InterRBC as a function of haematocrit suggest that the mean Po_2RBC and Po_2InterRBC both rise with increasing haematocrit (Fig. 9b), although this increase is less steep in the case of Po_2RBC than for Po_2InterRBC. It is also the case, however, that there is significant variation around this mean value, especially in the case of Po2RBC, where at any given haematocrit level, there is a wide range of Po_2RBC values recorded (up to ~50 mmHg difference, Fig. 9 a, upper panel). A similar relationship is observed between Po_2Mean and haematocrit, with a quite steep linear relationship (Fig. 9 a, lower panel), but with a range of ~20 mmHg visible in the distribution of Po_2 values at any given haematocrit level. As for RBC flow, there seems to be little relationship between the SD of Po_2 values measured in a capillary and the mean haematocrit in that capillary (Fig. 9c).

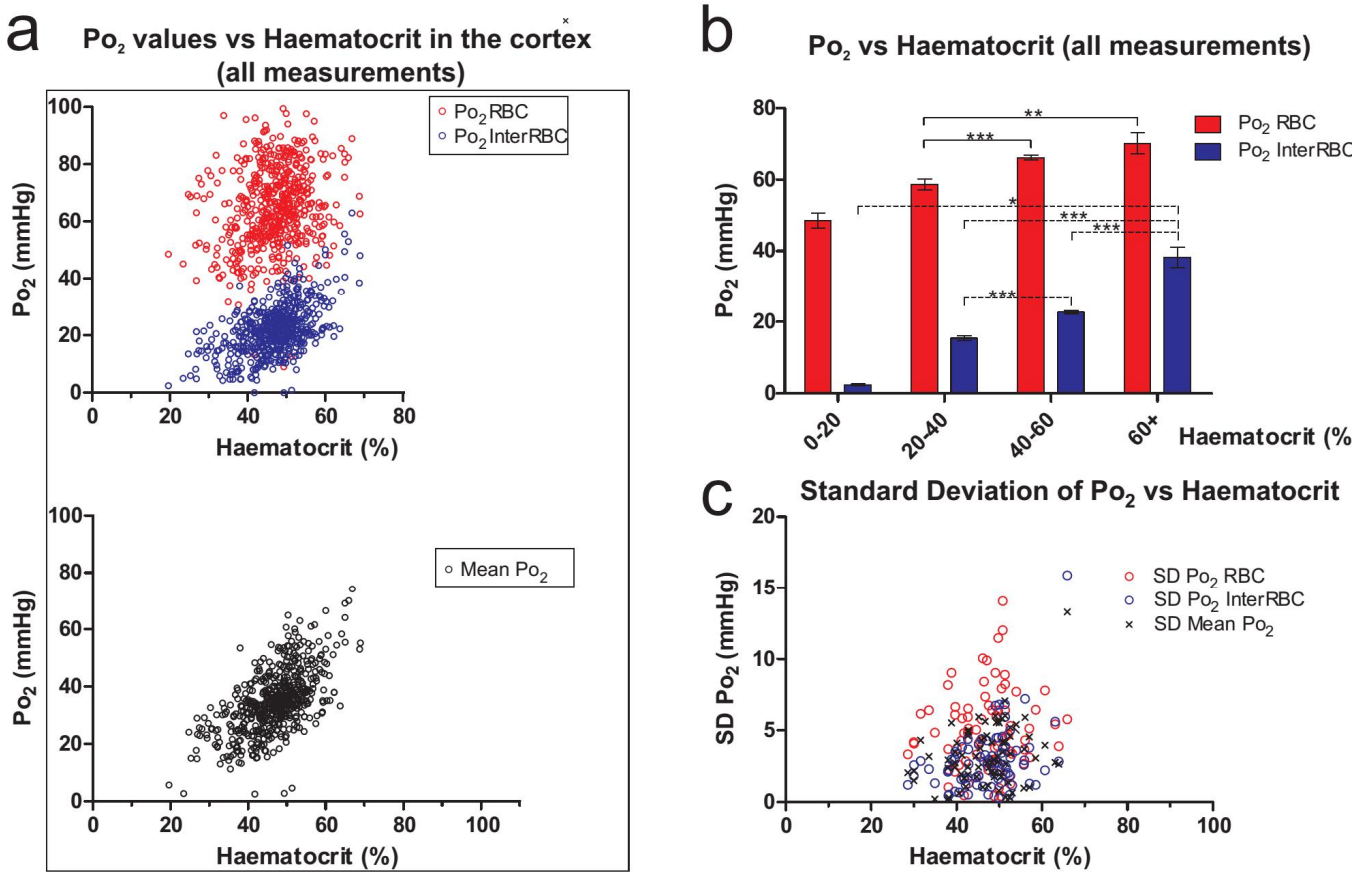

Figure 9 : The effect of haematocrit on capillary and tissue Po_2 in the somatosensory cortex. Data from all capillaries assessed

Upper panel: Po_2RBC and Po_2InterRBC (= local tissue Po_2) as a function of haematocrit. Each measurement plotted. *Lower panel:* Capillary Po_2Mean as a function of haematocrit. Each measurement plotted. Mean Po_2RBC and Po_2InterRBC as a function of haematocrit, with mean values calculated per 20 % bin. * = $p<0.05$, ** = $p<0.01$, *** = $p<0.001$. Kruskal-Wallis test with Dunn's Multiple Comparison Post-Hoc test. (c) Standard deviation of Po_2 measurements made in each capillary as a function of the capillary mean haematocrit. For all plots, n = 526 measurements from 81 capillaries in 3 mice.

3.2.5 – Capillary blood flow parameters in areas of low tissue Po_2 in the somatosensory cortex

In the cortex, capillaries with a low mean value of Po2InterRBC (<15 mmHg, n=13 capillaries), display both a wide range of RBC flow (capillary mean RBC flow rates from 8.7 to 50.4 cells/s, Fig. 10a) and haematocrit values (capillary mean haematocrit values of 33.5 - 51.5% [Fig.10b]. Unlike in the olfactory bulb, there was no clear correlation between capillary haematocrit and Po2InterRBC values in capillaries with low Po2InterRBC. However, the majority of these capillaries (n=10) were located in layer I of the cortex (<60µm below the cortical surface, see section 3.2.6), suggesting that low Po2InterRBC capillaries exist primarily in this layer.

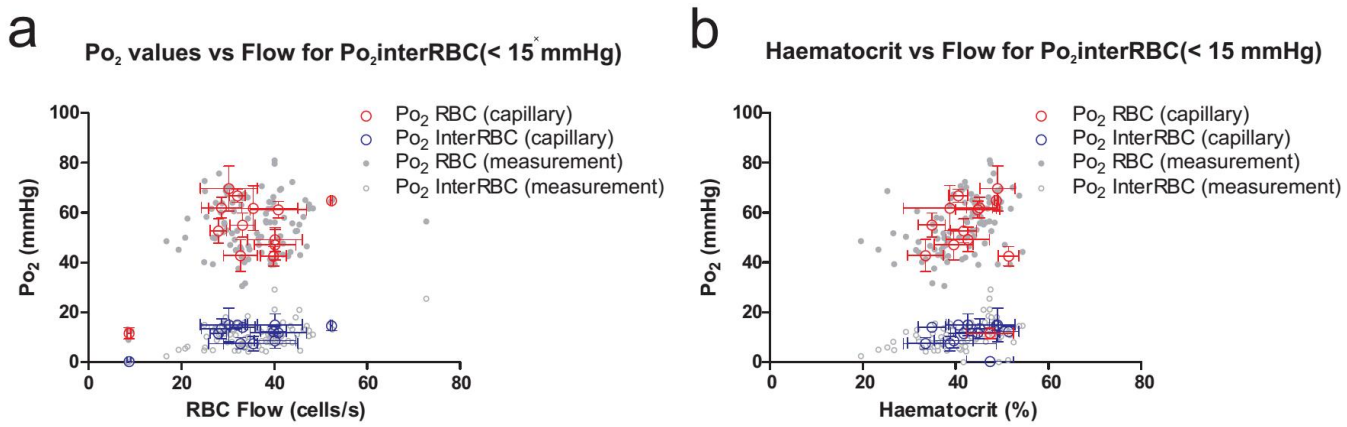

Figure 10 : The correlation of RBC flow and haematocrit with capillary Po_2 in capillaries with low Po2InterRBC (Po2InterRBC <15 mmHg) in the somatosensory cortex.

(a) Po2RBC and Po2InterRBC as a function of RBC flow. (b) Po2RBC and Po2InterRBC as a function of haematocrit. Single measurement values and mean ± SD of all measurements in each capillary shown. n = 101 measurements in 13 capillaries.

3.2.6 – Laminar variations in capillary Po_2 in the somatosensory cortex

Thus far, recorded capillaries in the cortex have been considered together. However, the range of depths at which capillary parameters were measured (0-410μm below the cortical surface) encompasses all of layers I and II/III, along with the upper portions of layer IV in S1 FL and S1 HL (Altamura et al., 2007) . To determine whether laminar differences exist in the oxygenation and blood flow of the awake somatosensory cortex, we analysed and compared Po_2 and associated blood flow parameters of capillaries in each of these layers. The capillaries associated with each cortical layer can be distinguished according to their depth below the cortical surface. In our experiments, capillaries less than 60μm below the surface were considered to be in layer I, those from 90-260μm below the surface were classified as layer II/III capillaries and those deeper than 340μm (and down to maximum measured depth of 410μm) were considered layer IV capillaries.

Comparing the mean Po_2RBC, Po_2InterRBC (local tissue Po_2), and Po_2Mean observed in these different layers (Fig. 11a), it can be seen that in layer I Po_2InterRBC and Po_2Mean are both lower than in layers II/III and IV. In contrast, Po_2RBC is higher in layer II/III than in either layer I or layer IV. The laminar differences in Po_2InterRBC and Po_2Mean are visible in the frequency distribution plots of these measurements, which have similar ranges, but different peaks. Several possible explanations could account for the lower Po_2InterRBC and Po_2Mean values in layer I: a higher rate of O_2 consumption; lower RBC flow and/or haematocrit values; or a lower capillary density (Blinder et al., 2013), each of which could lead to a lower tissue Po_2 level. This finding of lower Po_2 in layer I, is, however, at odds with previous reports, which describe tissue Po_2 as being higher near the cortical surface (Masamoto et al., 2003; Devor et al., 2011) .

In the case of Po_2RBC, in spite of the fact that the mean values are similar between layers I and IV (Fig. 11a), the distribution (Fig. 11b, top row) in layer IV (mean capillary Po_2RBC ranging from 49.2 to 70 mmHg) is narrower than in layer I (mean capillary Po_2RBC ranging from 11.6 to 81.4 mmHg). This suggests that the oxygenation of the RBCs flowing in different capillaries is less heterogeneous in layer IV than in more superficial layers. The recording of multiple relatively low Po_2RBC values in layer I could be related to the high probability density of venule branching in the uppermost regions of the cortex (see figure 5e in Blinder et al. (2013)), which would suggest that many layer I capillaries are located only a small number of vascular branches from venules and thus tend to have more deoxygenated RBCs.

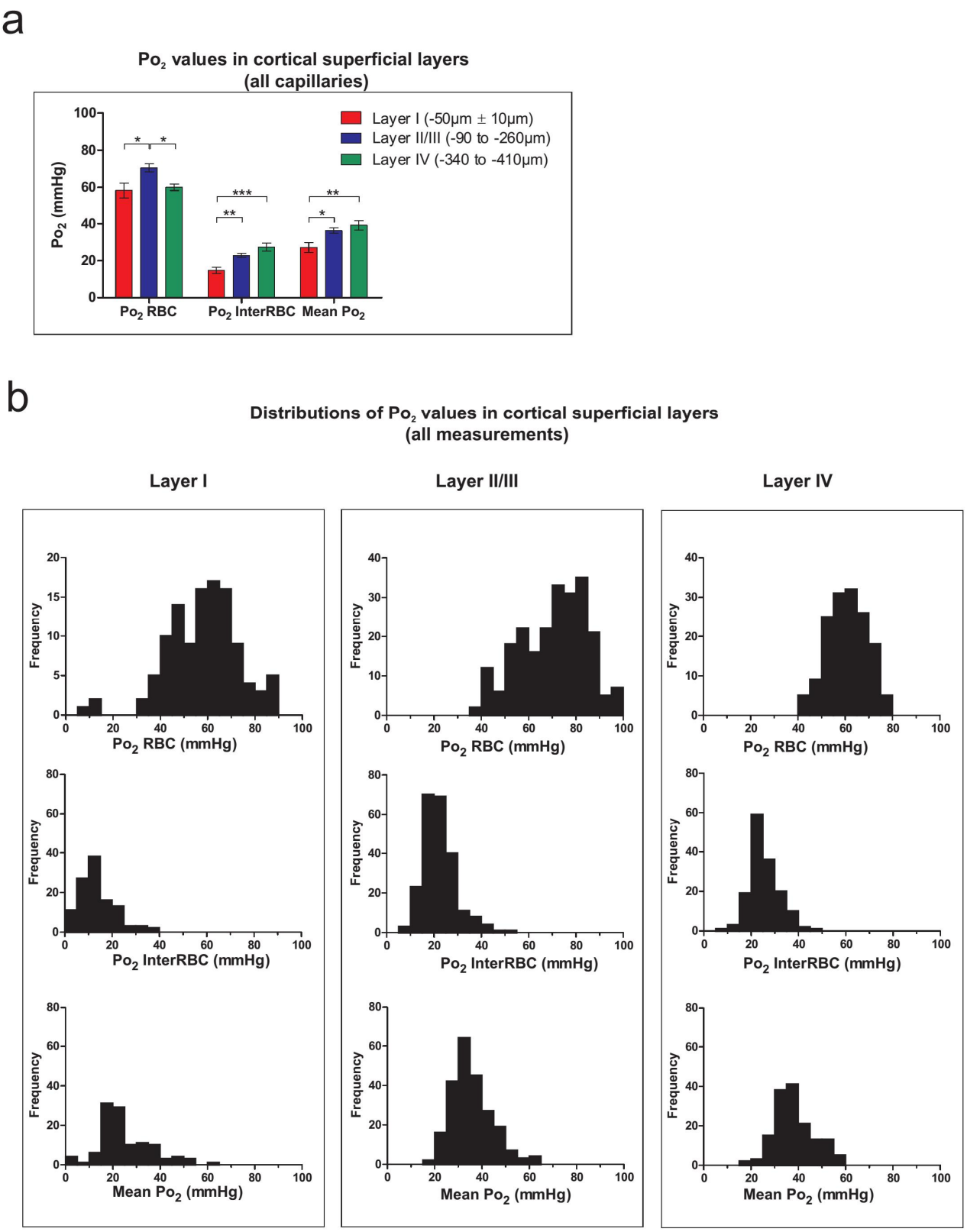

Figure 11 : Capillary and tissue P_{O_2} in layers I-IV of the somatosensory cortex.

(a) Comparison of capillary P_{O_2}RBC, P_{O_2}InterRBC and P_{O_2}Mean in Layers I, II/III and IV of the somatosensory cortex. Data presented as Mean ± SEM. * = $p<0.05$, ** = $p<0.01$, *** = $p<0.001$, Kruskal-Wallis test with Dunn's Multiple Comparison Post-Hoc test. (b) Frequency distribution plots (5 mmHg bin) of P_{O_2}RBC (Top row) P_{O_2}InterRBC (Tissue P_{O_2}, middle row) and P_{O_2}Mean (bottom row), comparing the values recorded in layer I (Left-hand column), layer II/III (centre column) and layer IV (right hand column). All measurements from all capillaries. For all plots, Total n = 526 measurements from 81 capillaries in 3 mice; Layer I = 113 measurements in 17 capillaries, Layer II/III = 230 measurements in 41 capillaries, Layer IV = 151 measurements in 15 capillaries

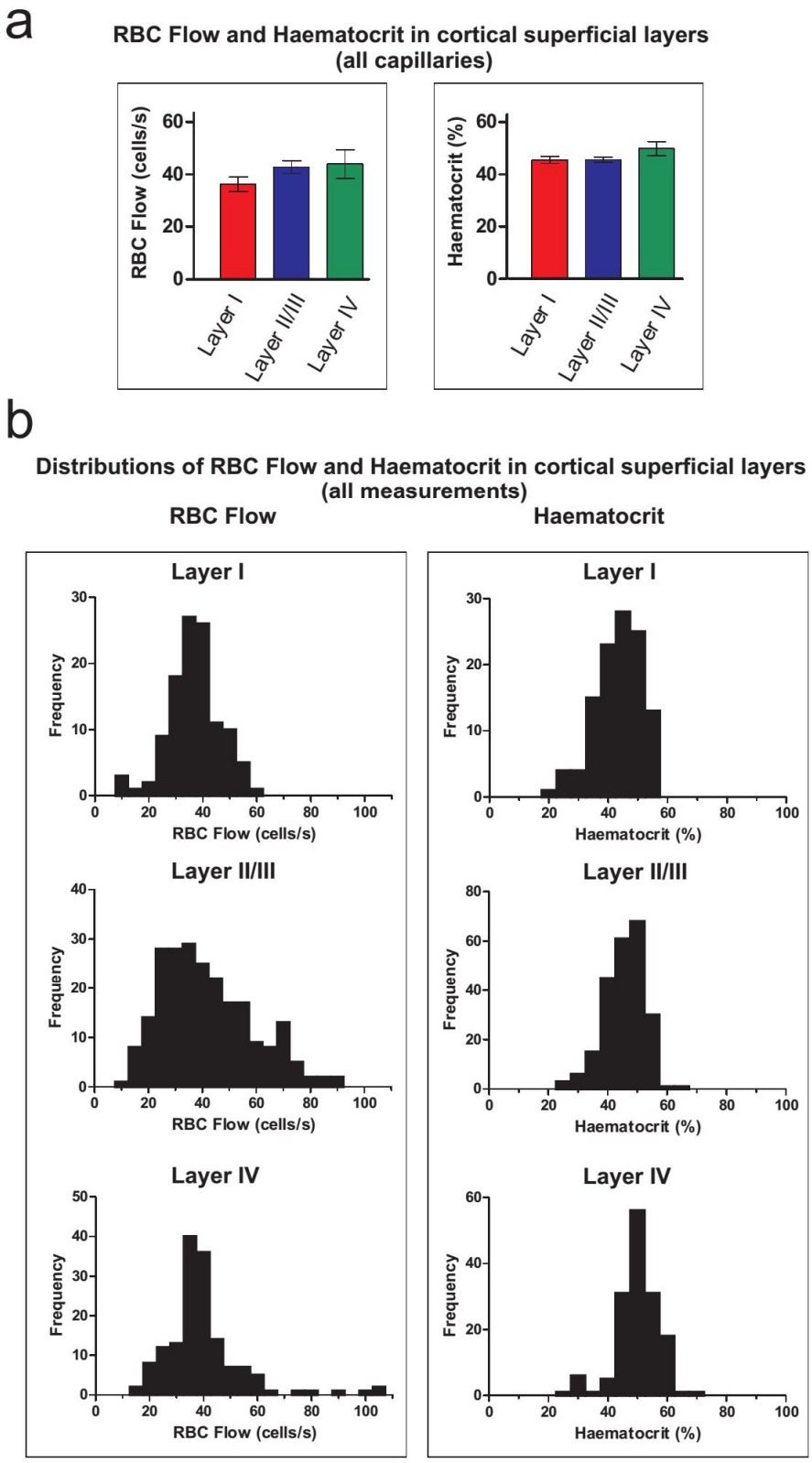

Figure 12 : Capillary RBC flow and haematocrit in layers I-IV of the somatosensory cortex.

(a) Comparison of capillary mean RBC delivery rate and haematocrit in Layers I, II/III, and IV. * = $p<0.05$, ** = $p<0.01$, *** = $p<0.001$. Kruskal-Wallis test with Dunn's Multiple Comparison Post-Hoc test. (b) Frequency distribution plots of RBC Flow (left-hand column, 5 cells/s bin) and Haematocrit (right-hand column, 5% bin) for capillaries in cortical layers I-IV, comparing the values recorded in layer I (top row), layer II/III (middle row) and layer IV (bottom row). All measurements from all capillaries. For all plots, Total n = 526 measurements from 81 capillaries in 3 mice; Layer I = 113 measurements in 17 capillaries, Layer II/III = 230 measurements in 41 capillaries, Layer IV = 151 measurements in 15 capillaries.

3.2.7 – Laminar variations in capillary RBC flow and haematocrit in the somatosensory cortex

Considering the blood flow in these cortical laminae, no significant differences in the mean RBC flow or haematocrit are observed between capillaries of layer I, II/III or IV (Fig. 12a, left- and right-hand panels). Similarly, the distributions of RBC flow and haematocrit values measured do not differ greatly between the layers (Figure 12b, left and right columns), although RBC flow in layer II/III seems to be more evenly distributed within its range. Note that there is also an apparent absence of very high RBC flow rates (>65 cells/s) in layer I.

3.2.8 – Laminar variations in the relationship between capillary blood flow parameters and Po_2 in the somatosensory cortex

The relationship of Po_2RBC and Po_2InterRBC to RBC flow was compared in each layer.

In layer I and II/III, Po_2InterRBC (and hence local tissue Po_2) increases throughout the range of RBC flow rates recorded (Fig. 13, both top and middle panels). Po_2InterRBC also increases with RBC flow in layer IV in the range from ~20-60 cells/s. Although this trend appears to continue above this range, the interpretation of the data (circled on plot) is questionable as it is derived from only two capillaries, in which the fluctuations in RBC flow were unusually large.

Po_2RBC rises with RBC flow across the entire range of flow rates in layer I (Fig. 13, top panels of both left and right columns). In layer II/III, the mean value of Po_2RBC rises with increasing flow rates in the low to moderate ranges of RBC flow measured (10-60 cells/s), but stabilises above ~80 cells/s (Fig. 13, middle panels of both left and right columns). The range of Po_2RBC values is greater at rates of flow <50 cells/s, spanning approximately 60 mmHg, as opposed to around 30 mmHg at flow rates >60 mmHg. Surprisingly, in layer IV, Po_2RBC seems to be independent of RBC flow, with the mean value and distribution being broadly similar across the range of RBC flow rates measured (Fig. 13, lower panels of both left and right columns). However, concerns exist in relation to the data at high flow rates, as for Po_2InterRBC.

We also examined the relationship of both Po_2RBC and Po_2InterRBC with haematocrit in each layer. Fig. 14 shows that the haematocrit appears to be strongly related to the Po_2InterRBC in all layers, with higher haematocrit levels being associated with higher Po_2InterRBC (local tissue Po_2)

levels (Fig. 14, all panels). In contrast, only in layer I did the mean value of Po_2RBC increase across the full range of haematocrit values measured (Fig. 14, top panels of both left and right columns), although low Po_2RBC measurements persist at high levels of haematocrit. In layer II/III and layer IV, on the other hand, Po_2RBC seemed to be independent of haematocrit (Fig. 14, middle and bottom panels of both left and right columns). Thus, surprisingly, it appears that in layer IV, Po_2RBC is independent of both RBC flow and haematocrit.

In all layers, the relationship between Po_2Mean and both RBC flow and haematocrit is clearer: higher levels of each parameter are associated with a higher Po_2Mean value, although the slope of the correlation varies according to the cortical layer (Figs. 15 and 16) However, low values of Po_2Mean exist across the full range of haematocrit values in each of the layers, with the spread of the Po_2Mean values broadening at higher haematocrit levels. In layer IV, the fact that in the Po_2Mean rises with increasing haematocrit, whereas the Po_2RBC is independent of haematocrit suggests that Po_2Mean follows Po_2InterRBC.

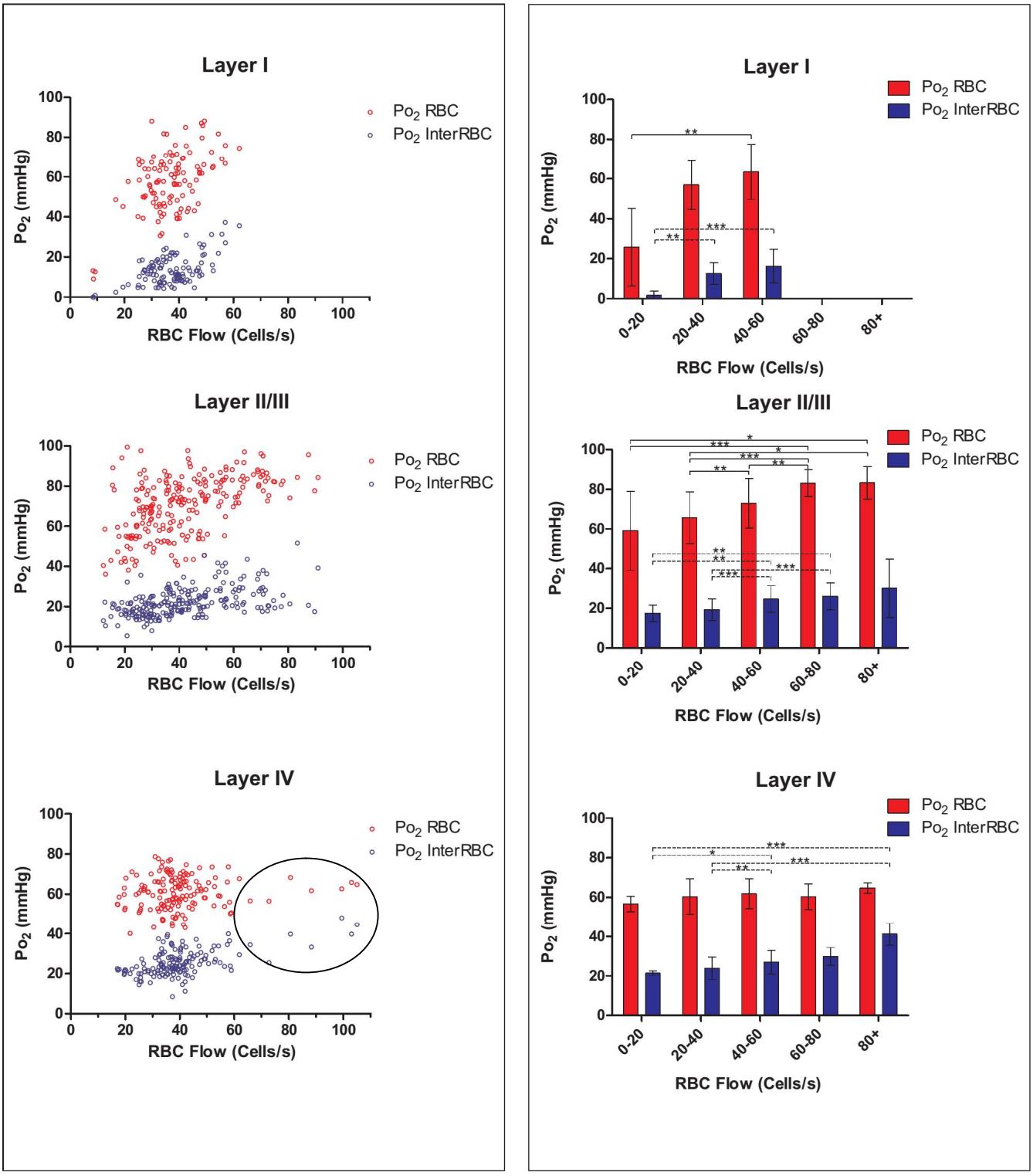

Figure 13 : Capillary P_{O_2}RBC and P_{O_2}InterRBC as a function of RBC Flow, in layers I-IV of the somatosensory cortex.

Scatter plots (left-hand column) and bar plots (right-hand column) of P_{O_2}RBC and P_{O_2}InterRBC as a function of RBC flow in layer I, layer II/III, and layer IV (Top, middle, and bottom row respectively). For all plots, Total n = 526 measurements from 81 capillaries in 3 mice; Layer I = 113 measurements in 17 capillaries, Layer II/III = 230 measurements in 41 capillaries, Layer IV = 151 measurements in 15 capillaries. * = $p<0.05$, ** = $p<0.01$, *** = $p<0.001$. Kruskal-Wallis test with Dunn's Multiple Comparison Post-Hoc test.

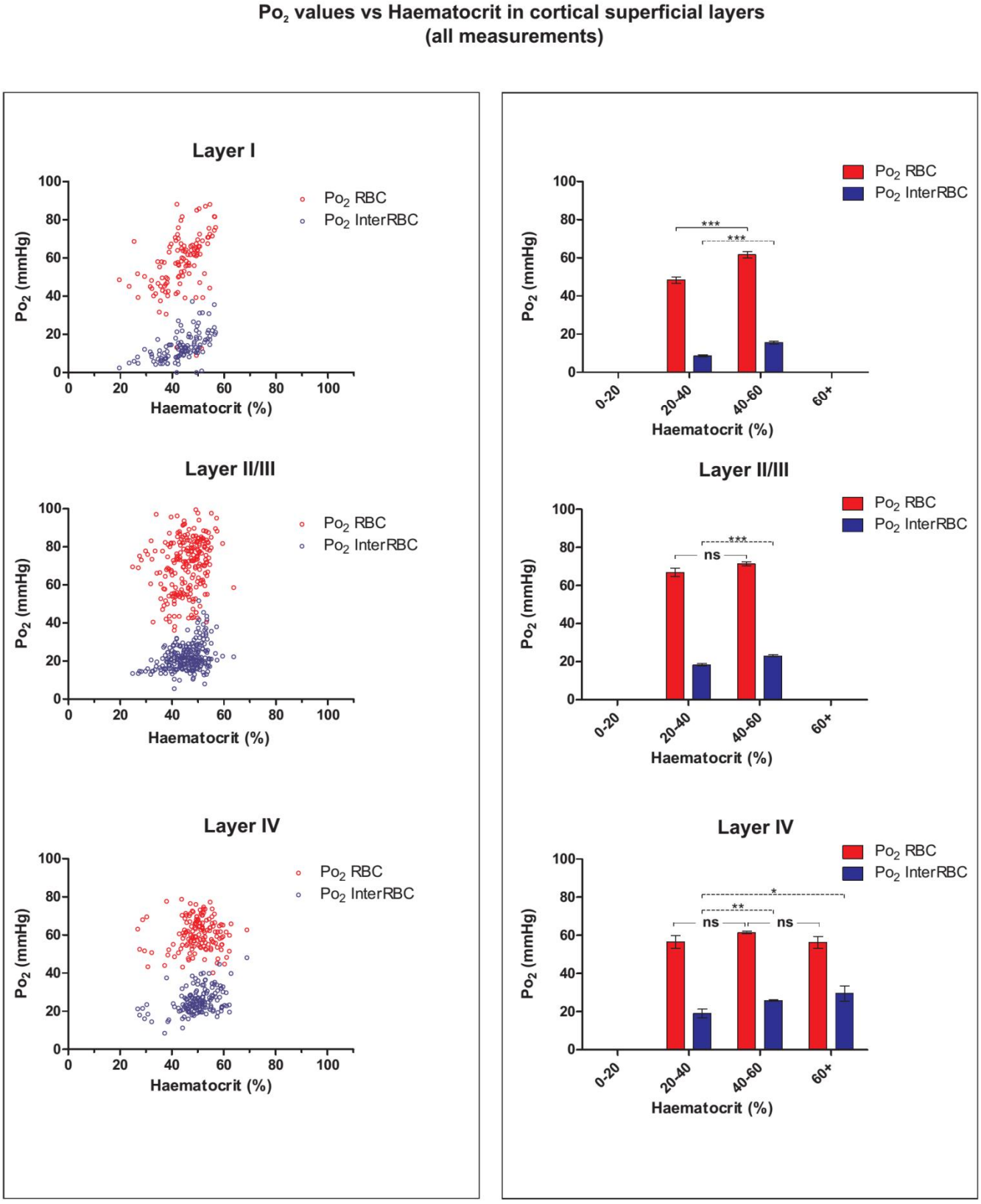

Figure 14 : Capillary P_{O2}RBC and P_{O2}InterRBC as a function of haematocrit, in layers I-IV of the somatosensory cortex.

Scatter plots (left-hand column) and bar plots (right-hand column) of P_{O2}RBC and P_{O2}InterRBC as a function of haematocrit in layer I, layer II/III, and layer IV (Top, middle, and bottom row respectively). For all plots, Total n = 526 measurements from 81 capillaries in 3 mice; Layer I = 113 measurements in 17 capillaries, Layer II/III = 230 measurements in 41 capillaries, Layer IV = 151 measurements in 15 capillaries. * = $p<0.05$, ** = $p<0.01$, *** = $p<0.001$. Kruskal-Wallis test with Dunn's Multiple Comparison Post-Hoc test.

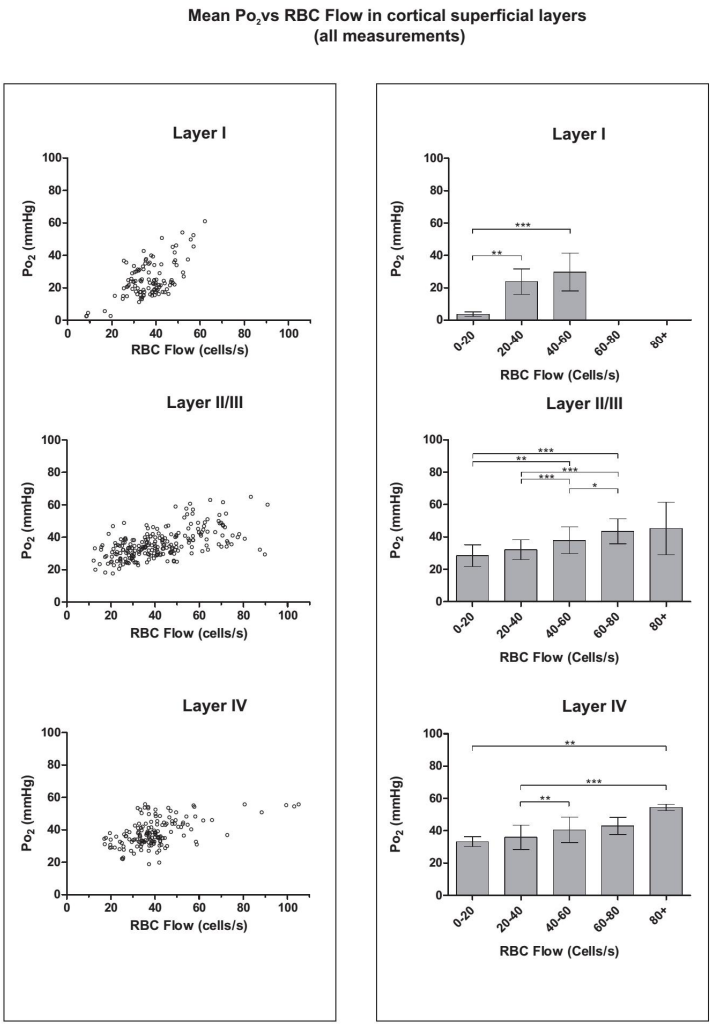

Figure 15 : Capillary P_{O2}Mean as a function of RBC Flow, in layers I-IV of the somatosensory cortex.

Scatter plots (left-hand column) and bar plots (right-hand column) of P_{O2}Mean as a function of RBC flow in layer I, layer II/III, and layer IV (Top, middle, and bottom row respectively). For all plots, Total n = 526 measurements from 81 capillaries in 3 mice; Layer I = 113 measurements in 17 capillaries, Layer II/III = 230 measurements in 41 capillaries, Layer IV = 151 measurements in 15 capillaries. * = p<0.05, ** = p<0.01, *** = p<0.001. Kruskal-Wallis test with Dunn's Multiple Comparison Post-Hoc test.

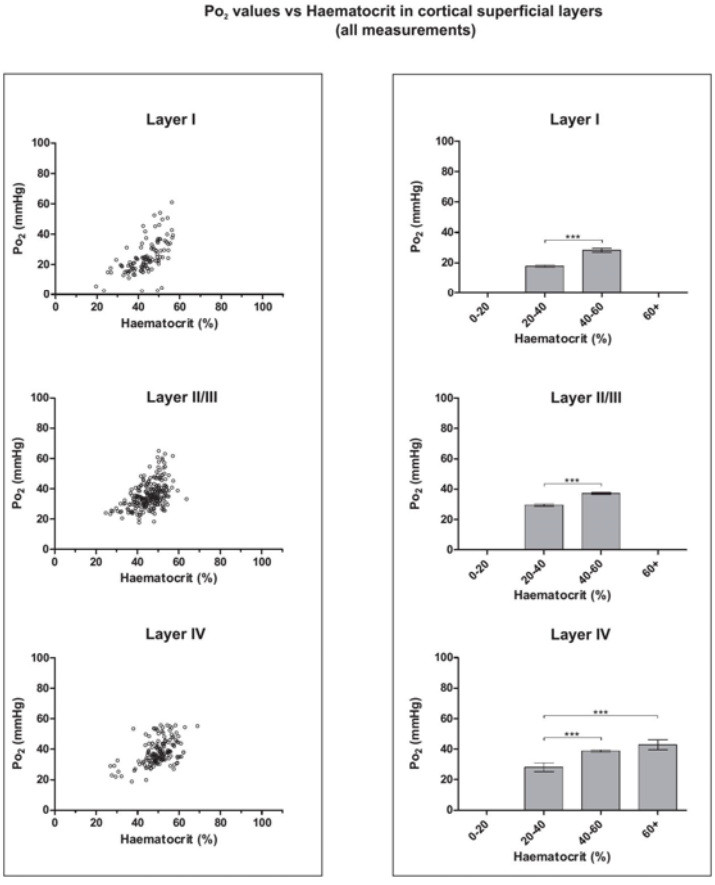

Figure 16 : Capillary P_{O2}Mean as a function of haematocrit, in layers I-IV of the somatosensory cortex.

Scatter plots (left-hand column) and bar plots (right-hand column) of P_{O2}Mean as a function of haematocrit in layer I, layer II/III, and layer IV (Top, middle, and bottom row respectively). For all plots, Total n = 526 measurements from 81 capillaries in 3 mice; Layer I = 113 measurements in 17 capillaries, Layer II/III = 230 measurements in 41 capillaries, Layer IV = 151 measurements in 15 capillaries. * = p<0.05, ** = p<0.01, *** = p<0.001. Kruskal-Wallis test with Dunn's Multiple Comparison Post-Hoc test.

3.2.9 – Po_2 in penetrating arterioles and venules in the somatosensory cortex

The blood that perfuses cortical capillaries both enters and exits this structure primarily via larger gauge penetrating vessels. Additionally, although the total length density and surface area of capillaries in the cortex far outweighs that of these larger-diameter vessels, it is likely that they directly influence tissue oxygenation, at least in their immediate environs. Therefore, in addition to measuring Po_2 and blood flow parameters in cerebral cortex capillaries, Po_2Mean measurements were made in larger penetrating vessels (descending arterioles and ascending venules). It was not possible to simultaneously detect the passage of RBCs in these large diameter vessels as they do not travel in single file. For this reason, no RBC flow, haematocrit measurements or Po_2RBC or Po_2InterRBC values could be recorded. Penetrating vessels (13 arterioles, 14 venules) were traced from the point where they descended into the cortex to the point at which they ramified into smaller vessels. For a small number of vessels (3 arterioles and 4 venules), the trunk of the vessel was still present at ~410µm below the surface, and proceeded further downwards below the maximum depth at which we made recordings. The vessel mean Po_2 was measured at 30-50µm z-steps, with multiple point Po_2 measurements being made from different areas of the lumen at each depth. The Po_2 was found to be 65.5 ± 0.6 mmHg for arterioles and 39.5 ± 0.5 mmHg for venules (Mean of all measurements ± SEM). From our recordings, no gradient in arteriole or venule Po_2 is seen in relation to increasing depth in the cortex, to at least a depth of ~400µm (Fig. 17, (a) and (b)). This finding is once again in contrast findings from other groups who observed decreases in both arteriolar and venular Po_2 with increasing depth in the cortex in anaesthetised animals (Sakadzić et al., 2010; Devor et al., 2011).

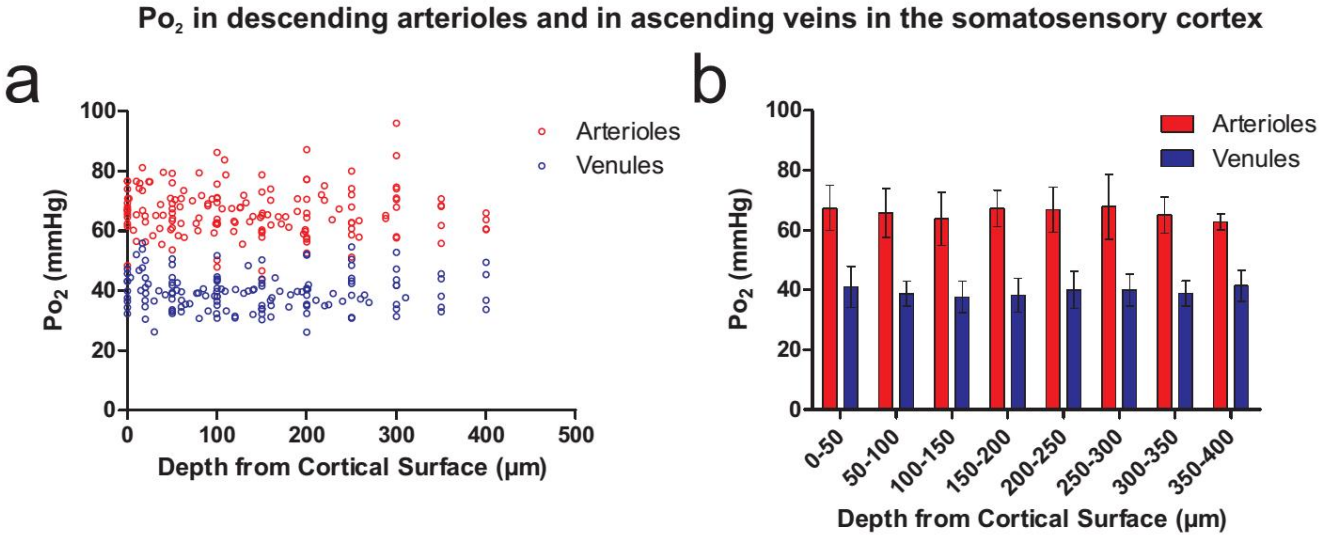

Figure 17 : Penetrating vessel P_{O2} as a function of depth below cortical surface.

(a) P_{O2} measurements in penetrating arterioles and venules as a function of depth below the cortical surface. Each point represents the average P_{O2} of 5-10 measurements made at different positions in the lumen at each depth. Arteriolar P_{O2} = 65.5 ± 0.6 mmHg, venular P_{O2} = 39.5 ± 0.5 mmHg (Mean ± SEM of P_{O2} measurements at all depths). (b) Mean P_{O2} measured in all arterioles and all venules recorded as a function of depth from the cortical surface (50µm bin size). For both plots, n = 159 P_{O2} values in 13 arterioles and 148 P_{O2} values in 14 venules.

Section 3 – The effect of isoflurane anaesthesia on capillary Po_2 and RBC flow rates in the brain

On examination of the results of the Po_2 measurements made in olfactory bulb GL capillaries, we were surprised to observe that the average Po_2 (Po_2RBC, Po_2InterRBC and Po_2Mean) values in GL capillaries that were measured in awake mice in this study are broadly in line with those measured previously by Parpaleix et al. (2013). This was unexpected, as these earlier results from our group, measured using the same techniques, were derived from animals anaesthetised with ketamine-xylazine and breathing air supplemented with O_2 (the final O_2 proportion being 30%). It seems that in that particular condition, the cardiopulmonary depression induced by xylazine is compensated for by an increase in O_2 loading in the lungs (due to the augmented percentage of O_2 inspired [$FiO_2 \approx 30\%$]) resulting in this surprising absence of a difference in capillary Po_2. I therefore wished to establish that capillary Po_2 and EAT parameters can be altered by anaesthetic agents. For this reason, I measured EATs and RBC flow in a specific set of GL capillaries in both the awake state and when the animal is anaesthetised with isoflurane (~0.75% as measured at the animals snout, delivered in pure air, with no supplementary O_2, $FiO_2 \approx 21\%$), which is a volatile anaesthetic commonly used in the study of cerebral oxygenation (Hu et al., 2009; Sakadzić et al., 2010) .

As can be seen from Fig. 18 (a), GL capillary Po_2Mean, Po_2RBC and Po_2InterRBC are all significantly elevated under isoflurane anaesthesia. This effect is associated with an increase in RBC flow observed in these vessels. This elevation of vascular and tissue Po_2 is likely to be largely related to isoflurane's known cerebral vasodilatory effects (Matta et al., 1999) , although altered neural activity patterns might also exert an effect. We subsequently replicated this type of experiment in cerebral cortex layer I capillaries (Fig. 18b), similarly observing increases in capillary RBC flow and all Po_2 values during isoflurane anaesthesia. Notably the ratio of the increase in Po_2InterRBC to the increase in RBC flow under isoflurane is different between the two regions studied.

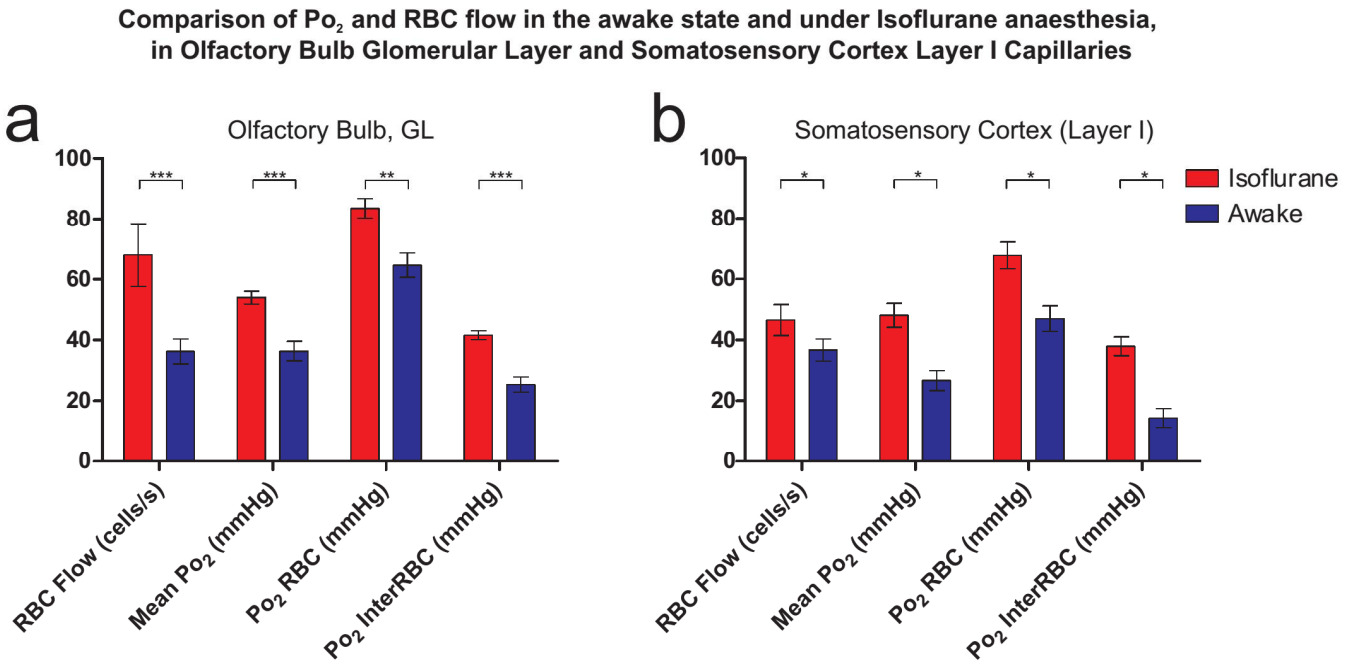

Figure 18 : Comparison of capillary P_{O_2} and RBC Flow in the awake state and under isoflurane anaesthesia.
RBC flow and P_{O_2} were measured in a set of capillaries in two different imaging sessions, one when the animal was awake, and another when the animal was anaesthetised with isoflurane (0.75%, delivered in air).

(a) Olfactory bulb GL capillaries: RBC delivery rate is increased under isoflurane anaesthesia as compared to the awake state (68 ± 10.4 vs 36.3 ± 4.1 cells/s, $p<0.01$, paired Wilcoxon signed rank test), as were P_{O_2} Mean (54 ± 2.1 vs 36.4 ± 3.2 mmHg, $p<0.01$, paired Wilcoxon signed rank test), P_{O_2}RBC (83.5 ± 3.2 vs 64.6 ± 4 mmHg, $p<0.01$, paired Wilcoxon signed rank test), and P_{O_2}InterRBC (41.6 ± 1.4 vs 25.4 ± 2.5 cells/s, $p<0.01$, paired Wilcoxon signed rank test), the latter indicating that local tissue P_{O_2} was elevated to the same extent under isoflurane. n = 142 measurements under each condition, from 16 capillaries in 3 mice. Data presented as Mean ± SEM.

(b) Somatosensory cortex capillaries: RBC delivery rate is increased under isoflurane anaesthesia as compared to the awake state (46.5 ± 5.1 vs 36.7 ± 3.6 cells/s, $p<0.05$, paired Wilcoxon signed rank test), as were Po2 Mean (48.1 ± 3.9 vs 26.7 ± 3.3 mmHg, $p<0.05$, paired Wilcoxon signed rank test), P_{O_2}RBC (67.8 ± 4.4 vs 47.1 ± 4.1 mmHg, $p<0.05$, paired Wilcoxon signed rank test), and P_{O_2}InterRBC (37.9 ± 3.1 vs 14.4 ± 3.1 cells/s, $p<0.05$, paired Wilcoxon signed rank test), the latter indicating that local tissue P_{O_2} was elevated to the same extent under isoflurane. n = 36 measurements under isoflurane and 26 when awake, from 5 capillaries in 1 mouse. These 5 capillaries were in layer I. Data presented as Mean ± SEM.

Section 4 – Summary

The results and data obtained from these experiments provide extensive information, not only on the Po_2 values present in awake brain, but on the inter- and intra-areal variations in the distribution of these values, and on how blood flow influences these patterns of oxygenation.

We present data on capillary RBC flow and haematocrit values in the olfactory bulb GL and upper cortical layers in the awake mouse; RBC, vascular and tissue Po_2 in these regions; and how the fashion in which these blood flow parameters impact the oxygenation parameters differs within and between these areas.

Furthermore, we provide evidence that brain vascular and tissue Po_2 can be drastically different in the awake state than it is under isoflurane anaesthesia, indicating that the vasodilatory effects of this volatile anaesthetic can profoundly impact the oxygenation state of the brain, potentially deviating it significantly from physiological conditions.

Part 4: Discussion

The primary importance of this research lies in the provision of data on basic physiological parameters of the cerebrovascular system and brain oxygenation in the awake, normally functioning mammalian brain at rest. This data represents the first high-resolution measurements of brain vascular and tissue Po_2, along with the first published values of RBC flow rate and haematocrit in the microvasculature of the awake brain.

Section 1 – The olfactory bulb glomerular layer

1.1 – Po_2 in the olfactory bulb GL

In the olfactory bulb GL, the values of the Po_2 parameters that we measured are similar to those found by Parpaleix et al. (2013), which were recorded in animals anaesthetised with ketamine-xylazine and breathing air supplemented with oxygen (FiO_2≈30%). We believe that the correspondence between the data derived from the two studies is due to the compensatory effects of this supplementary inhaled oxygen, which counteracts the cardiopulmonary depressive effects of xylazine. Notably, this similarity in Po_2 values is in direct contrast to the stark changes induced in the current study by a different anaesthetic, isoflurane, in which all Po_2 parameters are increased.

The Po_2 measurements that we performed are reliable and stable, with the SD of the measurements in each capillary typically <5 mmHg for Po_2InterRBC, and <15 mmHg for Po_2RBC. We thus consider that the Po_2InterRBC values are a good representation of the local tissue Po_2 values. As outlined earlier, the larger SD values for Po_2RBC may be related to a greater effect of fluctuations in RBC flow or haematocrit in the capillary, but may also be due to a technical issue, whereby minor errors in the fit of the curve to the phosphorescence decay recordings could cause larger errors in the Po_2 value extracted in the higher ranges of physiological Po_2.

The capillaries in the olfactory bulb GL are a heterogeneously oxygenated population, presenting a wide range of Po_2RBC and Po_2InterRBC values. In our study the mean Po_2RBC of capillaries in this region was 60.6 mmHg, and the most frequent values lay between approximately 40 and 65 mmHg, although values as low as 25.6 mmHg and as high as 86 mmHg were also recorded. The mean of the Po_2InterRBC values we recorded was 23 mmHg. The values observed generally lay between 15 and 30 mmHg, although measured capillary Po_2InterRBC ranged from <1 to 51.5 mmHg. This suggests that in the GL, tissue generally has Po2 levels of 15 – 30 mmHg, but that some areas experience Po_2 values outside these values.

The wide distribution of Po_2InterRBC values recorded indicates that there is significant heterogeneity in Po_2 values in the tissue of the GL. Some of this variability could arise from the fact that we did not distinguish between intra- and juxta-glomerular regions in our recordings, and it is possible that these two regions have different resting levels of O_2 consumption and tissue Po_2. Another explanation for the great spread in this data could be that different glomeruli have different resting rates of O_2 consumption and resting tissue Po_2.

1.2 – RBC flow and haematocrit in the olfactory bulb GL

As for Po_2 measurements, mean values of both capillary RBC flow rates (30.6 ± 15.7 cells/s, Mean ± SD) and haematocrit (34.6 ± 11%, Mean ± SD) that we determined in the GL were similar to those found by Parpaleix et al. (2013), indicating that there is a close association between all these parameters. However, we found that two populations of capillaries could be distinguished based on their haematocrit levels, although their RBC flow values overlapped at lower rates of flow (Fig. 2c in Results). The results of these measurements raise two interrelated points: 1) The haematocrit may differ greatly between capillaries that exhibit similar RBC flow rates, implying that the velocity must be lower in the high haematocrit capillaries, and 2) Nonetheless, on average, capillaries with higher haematocrit values have higher rate

of RBC flow. What the existence of these two populations represents is unclear, but it may be related to the possible existence of two populations of capillaries distributed throughout the GL which would be distinguished by their diameter. Ongoing work in the Charpak lab aims to generate comprehensive 3D reconstructions of the olfactory bulb vasculature, which could allow these hypothetical populations to be unearthed.

1.3 – Correlations of Po_2 with capillary haematocrit and RBC flow in the GL

Our correlations of Po_2InterRBC with RBC flow and haematocrit (Figs. 3 and 4 in Results) imply that tissue Po_2 is independent of both of these factors over a large range of values. There is little change in Po_2InterRBC in the range of RBC flow from ~10-50 cells/s, and in the range of haematocrit levels from ~20-45%. This suggests that in the resting GL, tissue Po_2 remains rather constant and that vascular fluctuations are buffered.

1.4 – Low tissue Po_2 in the GL is linked to low capillary haematocrit

In the GL, Po_2InterRBC values are low when the capillary haematocrit is very low. Indeed, the GL capillaries in which we measured low Po_2InterRBC values (<15 mmHg) all had low haematocrit levels (<25%), whereas their RBC flow values were distributed across a wide range (Fig. 5 in Results). This relationship of low Po_2InterRBC and low haematocrit is in contrast to the case in the cortex (as will be discussed later).

1.5 – Are there hypoxic regions in the GL?

Most low capillary Po_2InterRBC measured lay between 10 and 15 mmHg, but one capillary had a Po_2InterRBC value of <1 mmHg, indicating that the local tissue Po_2

was also similarly close to 0 mmHg. This raises the question as to whether this tissue region is hypoxic. Similarly low values of Po_2InterRBC were previously observed by Parpaleix et al. (2013), but their existence was thought to be related to problematic effects of the anaesthetised state.

1-6 – Why are capillary haematocrit levels low in the GL?

The mean capillary haematocrit (34.6 ± 11%, Mean ± SD) levels in the GL are lower than those seen in the superficial cortical layers (Layer I = 45.6 ± 5.7%, Layer II/III = 45.6 ± 6.1%, Layer IV = 49.9 ± 10.3%. All Mean ± SD). Given the dependence of tissue Po_2 on haematocrit that has been described in many tissues (Pittman (2011), and see Introduction Chapter 1, Section 2.3 of this work), it is surprising that Po_2InterRBC is similar between the GL and both layer II/III and IV in the cortex in spite of this lower haematocrit level. That this is the case is perhaps due to the extremely high density of capillaries in the glomeruli (Lecoq et al., 2009) , which means that although the total number of RBCs traversing a given volume of tissue is sufficiently high to support a certain level of oxygen, the number of RBCs (and hence the haematocrit) in each capillary is lower.

It might be the case that this enhanced density of capillaries in the glomeruli serves an important functional role in the delivery of O_2 to the neural tissue of these structures. The glomerulus is a very energetically demanding structure, and as such consumes a great quantity of oxygen to support this high metabolic rate. It has been estimated that, at rest, the glomerular tissue consumes ~2.5 times more oxygen than does cerebral cortical tissue (~0.045 μmol/g/s as opposed to ~0.02 μmol/g/s in the rat (Clarke and Sokoloff, (1999) ; Nawroth et al. (2007)). One consequence of this very high oxygen consumption rate is to limit the distance over which diffusion from a blood vessel can supply a sufficient quantity of oxygen to support cellular function (the effective diffusion distance).

Thus, to ensure an adequate supply of oxygen to all areas of these structures, a more spatially extensive and denser network of capillaries would be advantageous. This would bring RBCs into closer association with a larger proportion of the tissue and so shorten the diffusion paths for O_2 molecules to any given point in that tissue. The end effect would be to augment convective flow of oxygen within the tissue volume, to ensure that adequate quantities of oxygen are supplied to all areas of the tissue when the effective diffusion distance is limited or reduced.

Another possible effect of a very dense capillary network is to enhance the effective surface area for diffusion of O_2 from RBCs across the capillary wall and into the ISF and tissue. The importance of this large capillary surface area could be even greater in times of elevated neuronal activity and associated functional hyperaemia. Indeed having a very large number of capillaries would allow for a higher maximal number of total RBCs in the tissue volume at any moment, as even relatively small elevations in the haematocrit of multiple capillaries would outweigh the haematocrit increase possible in any single capillary.

Section 2 – The cerebral cortex

In addition to the data we gathered from the olfactory bulb GL, we also measured Po_2 and blood flow parameters in the microcirculation of the superficial layers of the somatosensory cortex, presenting the first data of this type measured in awake animals.

We initially analysed the data we derived from all cortex capillaries together, regardless of their depth. The values of the Po_2 parameters that we found in cortical capillaries do not differ greatly to those we found in the olfactory bulb GL, with the mean, SD and range of values for each of Po_2RBC, Po_2InterRBC and Po_2Mean being similar between the two regions (See Figs. 1 and 6 in Results).

The range of Po_2RBC values encountered in the cortical capillaries is in direct and strong contrast to the results of supposedly similar recordings in this brain area which have recently been published (Sakadžić et al. (2014) as will be discussed further later.)

2.1 – Capillary haematocrit in the awake cortex is higher than previous estimates from anaesthetised mice

Mean RBC flow rates and haematocrit levels are both higher in cerebral cortex capillaries than in the olfactory bulb GL, and unlike in the GL there is no evidence for the existence of two distinct capillary populations based on haematocrit. These capillary haematocrit values (47.3 ± 7.9%, Mean ± SD) are significantly higher than those that have previously been reported for the cerebral cortex (~24 ± 9% Mean ± SD, for review see Hudetz (1997)). On the other hand, the RBC flow values we recorded (41.9 ± 16.3 cells/s, Mean ± SD), fall within the (wide) range of RBC flow measurements recorded in the anaesthetised brain (eg. 36 ± 28 cells/s (Villringer et al., 1994) and 56 ± 39 cells/s (Kleinfeld et al., 1998) , both Mean ± SD).

2.2 – Cortical tissue Po_2 is correlated with both capillary haematocrit and RBC flow

Although in the olfactory bulb GL, tissue Po_2 was independent of RBC flow and haematocrit over a large portion of the range of values, this is not the case in the cortex. Po_2InterRBC was found to increase steadily, though modestly, with RBC flow (Fig. 8 in Results), and to rise more dramatically with increases in haematocrit (Fig. 9 in Results). Unlike in the GL, no association was seen between low Po_2InterRBC values (<15 mmHg) and low capillary haematocrit levels. Rather, in capillaries with very low Po_2InterRBC values, both the haematocrit and RBC flow levels were distributed around the mean values for these parameters. Notably, the majority of the capillaries in which these low Po_2InterRBC values were recorded were located in layer I (see below).

Laminar differences in the Po_2 and blood flow of the cerebral cortex

Rather than treating the superficial regions of the cortex as homogenous, interesting features of cerebrovascular function can be identified by treating the capillaries associated with the different cortical layers separately. Thus, we analysed the capillaries located in layers I, II/III and IV separately.

2.3 - Tissue Po_2 is lower in layer I than in underlying layers

Tissue Po_2 (Po_2InterRBC) was found to be lower in layer I than in either layer II/III or layer IV. Though one could imagine that is due to high rates of O_2 consumption in the apical tufts of pyramidal neurons with their somata in deeper layers, we propose that this lower tissue Po_2 level is due to the reduced capillary density in layer I compared to other layers of the cortex (Tsai et al., 2009; Blinder et al., 2013) , and the relative abundance of capillaries that are a small number of branches from venules (Blinder et al., 2013) . This would also provide an explanation as to why the majority

of the capillaries that we found with low Po_2InterRBC values were located in layer I. Although lower than the values recorded in layer II/III and IV, the distribution of Po_2RBC values in layer I was higher than those seen by Sakadzic et al. (2014) (Discussed in detail later, in Discussion Section 6).

Capillary RBC flow and haematocrit values were higher in layer I than those measured in the olfactory bulb GL, and not significantly different from those measured in deeper cortical layers. In this layer the relationship of Po_2 values to RBC flow or haematocrit shows increase in both Po_2RBC and Po_2InterRBC with increases in these vascular parameters.

2.4 - The correlation of Po2 and blood flow parameters in layers II/III and IV

In both of these layers, Po_2InterRBC and Po_2Mean are higher than that in layer I (*Po_2InterRBC*: Layer I = 14.7 ± 1.7 mmHg, Layer II/III = 22.9 ± 1 mmHg, Layer IV = 27.4 ± 2.3 mmHg. *Po_2Mean*: Layer I = 27.2 ± 2.7 mmHg, Layer II/III = 36.3 ± 1.4 mmHg, Layer IV = 39.2 ± 2.5 mmHg).

In both of these layers, Po_2InterRBC (local tissue Po_2) varies consistently, albeit modestly, with both RBC flow and haematocrit (Figs. 13 and 14 in Results). Thus the relationship between Po_2InterRBC and either flow or haematocrit differs greatly between the different brain regions studied, and so merits discussion. As outlined above, in the GL the Po_2InterRBC is stable throughout most of the ranges of both haematocrit and blood flow, in cortical layers II/III and IV it shows a consistent but modest positive correlation across the whole range of these parameters, whereas in layer I it rises quite steeply with increases in both blood flow parameters.

It is unclear what the basis of this different relationship between the local tissue Po_2 and these blood flow parameters in the different areas is. A possible explanation for this difference could lie in the distance (both in space and along the vascular paths) between the site of (activity dependent) blood flow regulation and the capillary in which we measure the Po_2 and blood flow parameters. In the brain generally, local O_2

consumption is determined primarily by local synaptic activation (Thompson et al., 2003; Lecoq et al., 2009; Howarth et al., 2012) .

In the glomerulus, the site of regulation by activity must be primarily local, as studies have shown that the functional hyperaemia response is generally confined to single glomeruli (Chaigneau et al., 2003) (although uncoupling can also occur (Chaigneau et al., 2007; Jukovskaya et al., 2011)). This means that the site of O_2 consumption and the site of blood flow increase coincide. Thus, the levels of oxygen delivery and consumption will be closely associated to one another via their coupling to local neuronal activity. Therefore, at rest, through a wide range of haematocrit or RBC flow, local tissue Po_2 will be stable.

In the superficial layers of the cortex, the vascular paths on average consist of 6 vascular segments from the descending arteriole to the ascending venule (Sakadžić et al., 2014) . In the cortex, the site at which the levels of neuronal activity that will affect blood flow in a given capillary could be at any position on its vascular path. Thus, for many capillaries (such as our recorded capillaries, which were chosen at random, irrespective of the neuronal organisation) there will possibly be a significant mismatch between the local oxygen delivery in the blood flow (as measured by RBC flow or haematocrit levels) and the local oxygen consumption. For this reason the local Po_2InterRBC in cortical capillaries could vary in response to a change in blood flow that is being regulated at a site distant to the capillary being measured. This phenomenon could be more prominent in layer I where the general rate of O_2 consumption might be lower than in underlying layers, and many capillaries are a small number of branches from venules (Blinder et al., 2013). This could explain the steeper correlation between blood flow parameters in this layer than in either layer II/III or layer IV.

2.5 – Po_2RBC is independent of blood flow parameters in layer IV

In layer IV, Po_2RBC seems to be independent of both RBC flow and haematocrit, which is very surprising. It is difficult to offer a satisfactory explanation for this observation. A recent paper (Sakadžić et al., (2014), which is discussed more fully later) postulates that capillaries which are high number of vascular branches from a penetrating arteriole do not contribute much oxygen to the cortical tissue, claiming that little oxygen is extracted and little change in near-RBC Po_2 occurs in such capillaries. If this were the case then one would expect little change in Po_2RBC in spite of alterations of blood flow in these capillaries. It however seems unlikely that all the capillaries we recorded are such 'high-branching order' capillaries, and furthermore the recorded Po_2RBC values (40-80 mmHg) indicate a higher range of So_2 than that reported by Sakadzic et al. (2014).

2.6 – Penetrating arterioles and venules in the cortex

In our measurements from descending arteries and ascending venules we do not observe a Po_2 gradient with increasing depth below the cortical surface. Please note that in these measurements the acquisition points were distributed throughout the entire lumen of the vessels. This absence of change in penetrating vessel Po_2 with depth in the cortex is in contrast with previous reports of the existence of such a gradient (Sakadzić et al., 2010; Devor et al., 2011) in different conditions. These previous studies were performed in anaesthetised animals following acute surgical procedures and craniotomy. In Devor et al. (2011) the intravascular Po_2 in penetrating vessels of the rat somatosensory cortex was estimated from Po_2 values measured in the ISF surrounding these vessels. The difference in descending arteriole Po_2 at >100μm and at 200-300 and below the cortical surface was estimated at ~35 mmHg. In Sakadzic et al. (2010), the intravascular Po_2 was measured in penetrating vessels in the mouse cortex with a decrease in Po2 was observed with increasing

depth in the cortex. This gradient was ~10 mmHg in descending arterioles and ~7 mmHg in ascending venules between the cortical surface and a maximum depth of ~240μm. We believe that although there is likely to be diffusion of O_2 from penetrating vessels to the surrounding tissue, that in the awake animal the loss of O_2 from these vessels is small in comparison to the delivery of O_2 by the blood and thus a drop in Po_2 along the course of the vessel is not large enough to be measurable.

Section 3 – Comparison of Po_2 and RBC flow in the awake state and under isoflurane anaesthesia

Anaesthesia alters the consumption and supply of oxygen to the brain in a fashion that can be difficult to disentangle completely (e.g. Lei et al. (2001)). In the GL, the magnitude of the increase in Po_2InterRBC associated with the increase in RBC flow is similar to the increase in Po_2InterRBC with an equivalent rise in RBC flow in the awake state (according to the correlation seen in Fig. 2 a and b, in Results). Conversely, in the capillaries in layer I of the cortex, the increase in Po_2InterRBC is of a much greater magnitude than would be predicted from the change in RBC flow observed (see the upper left panel of Fig. 13, in Results). This difference between ratio of the increase in Po_2InterRBC and the elevation in RBC flow rate could be related to the vasodilatory effects of isoflurane on large pial vessels, which would lead to increased blood flow and Po_2 levels in these vessels. This could result in a loss of O_2 from these vessels directly into the tissue of layer I, which would elevate the tissue Po_2 and hence the Po_2InterRBC in layer I capillaries. This difference in Po_2InterRBC effects could be also potentially be explained by differential effects of isoflurane on neuronal activity (and so O_2 consumption) in the cortex and the olfactory bulb GL. If isoflurane reduced neuronal activity in the cerebral cortex to a greater extent in the cortex than in the GL, this could help account for the increased Po_2InterRBC in the cortex.

Section 4 – Comparison of my data with previous measurements of P_{O2} in the awake brain

Measurements of mean vascular and tissue P_{O2} in the brain has been heretofore primarily carried out in anaesthetised animals (Ndubuizu and LaManna, 2007; Sakadzić et al., 2010; Devor et al., 2011) . Most of the small number of studies which carried out measurements in unanaesthetised animals (for example Liu et al. (1995); Rolett et al. (2000); Dunn et al. (2011)) used EPR oximetry, which has severely limited resolution and involves invasive probe implantation and tissue trauma (See Introduction Chapter 3, Section 2.2 for details). Other studies that have assessed brain tissue P_{O2} in awake animals used implanted probes, with the inherent invasiveness and lack of information on the local cerebrovasculature providing major limiting and confounding factors.

One particularly interesting study (Ortiz-Prado et al., 2010) used a chronically implanted fibre-optic probe in which tissue P_{O2} measurement was based on oxygen's quenching effect on fluorescence of a Pt-porphyrin dye embedded in the probe tip, which was excited with blue LED light. This fibre-optic probe assembly (total size: 1.8 mm length, 250μm diameter) was implanted in the cerebral cortex of rats. Although this implantation is invasive and causes damage to the tissue, the recordings of tissue P_{O2} were made at least 7 days after implantation, thus perhaps avoiding some of the effect of the acute tissue trauma. In 5 of the 6 animals for which individual data is presented, the single point bulk tissue P_{O2} value (at ~21% FiO_2) was between 18 and 22 mmHg, which is similar to the typical P_{O2}InterRBC values in my data. The value recorded from the remaining rat was ~35 mmHg, which would skew the mean P_{O2} value from these 6 rats to a higher level than might be typical in the tissue. This single elevated point P_{O2} value could potentially arise due the proximity of the probe tip to a highly-oxygenated blood vessel. This possibility emphasises the importance of the measurement of P_{O2} from multiple, spatially extensive sites, at high resolution, and with access to information on the local vascular structure and

properties. This, therefore, highlights the power of 2PLM based P_{O2} measurements in understanding both cerebral oxygenation and the factors that influence it.

Section 5 - Comparison of my data with similar measurements made under anaesthesia

A wide array of tissue P_{O2} mean values and distributions have been previously reported (See Table 1 from Ndubuizu and LaManna (2007), reproduced here as Introduction Table 3). This means that it was inevitable that my data would approximate the results of at least one earlier study. The tissue P_{O2} levels that I infer from measured P_{O2}InterRBC values in the olfactory bulb and the cortex have mean values of around 23 mmHg, with the most frequent values lying between 18 and 30 mmHg. However, the tissue P_{O2} recorded in the two structures encompasses the range of from almost 0 mmHg to greater than 60 mmHg. These values all fall within the broad range previously reported, but they are especially congruent with the results reported by groups who carried out a very large number of point measurements at different positions with polarographic electrodes, and so sampled a significant portion of the tissue oxygen field (Cross and Silver, 1962; Nair et al., 1975; Smith et al., 1977). 2PLM based measurements of cortical tissue P_{O2} (Sakadzić et al., 2010; Devor et al., 2011), carried out in rats, found values ranging from around 5 – 90 mmHg, with values from tissue near large arterioles and venules being elevated in comparison to the tissue at distance from such vessels.

The average and distribution of my research's P_{O2}Mean values (Mean ~36 mmHg, with most values lying between 15 and 55 mmHg, with the peak at 30-40 mmHg) are in general agreement with Sakadzic et al (2010) (Average capillary P_{O2} of ~30 mmHg, and a microvessel P_{O2} range of ~30-50 mmHg). On the other hand, the average values of P_{O2} from the arteriolar and venular ends of a set of capillaries, reported by Vovenko (1999), were 58 to 41 mmHg respectively, so the average capillary P_{O2} is higher than that from the two 2-PLM based studies. However, as noted in the

introduction, the criteria used to identify capillaries was not clear, so it is possible that at least some of these capillaries are more akin to small-bore arterioles and venules.

Discrepancies between the existing literature and the brain P_{O2} distribution described in this work become clear when one considers the differing data on the relationship of vascular and tissue oxygenation to depth in the cortex. This disagreement can be seen when comparing the P_{O2} recorded in every intracortical vascular compartment and also the cortical tissue. The constant intravascular P_{O2} that is observed in penetrating arterioles and venules throughout the superficial cortical layers (Fig. 17, in Results) is in stark contrast to the gradients described by Sakadzic et al. (2010) and Devor et al. (2011) (Dirnagl, 2010; Sakadzić et al., 2010; Devor et al., 2011). Similarly, Sakadzic et al. (2010) describe decreasing P_{O2} in the subsurface microvessels, with the average P_{O2} at 240μm below the surface of the mouse cortex being 10-20 mmHg lower than that near the surface. This is once again in direct conflict with our data, which indicates that capillary P_{O2}Mean is higher in the deeper layers than in layer I (Fig. 11, in Results). Furthermore, Figure 17 shows that tissue P_{O2} is also higher in layers II/III and IV than in layer I, which is in contrast with the findings of Devor et al. (2011), who recorded lower tissue P_{O2} ranges at greater depths. Aside from 2PLM based studies, decreasing P_{O2} with increasing depth in the cortex has also been described in studies employing polarographic electrodes (for example (Nair et al., 1975; Masamoto et al., 2003). At present it is unclear what underlies these incompatible findings, although it is likely that the effects of anaesthetic agents or of acute surgical trauma could play a role in the processes responsible for this discrepancy.

Thus, although some aspects of the cortical P_{O2} distribution in the awake brain uncovered in this research are mirrored in the existing literature from anaesthetised animals, the areas of disagreement are quite substantial and indicate the importance of experiments in awake animals in furthering our understanding of brain physiology.

Section 6 – Appraisal of Sakadzic et al. (2014) "Large arteriolar component of oxygen delivery implies a safe margin of oxygen supply to cerebral tissue"

A new study (Sakadžić et al., 2014) has recently been published by a group of researchers that utilises 2PLM to measure microvascular P_{O_2} in the cerebral cortex. They combine these measurements with 2-photon imaging based morphological measurements, optical coherence tomography based measurements of blood flow and numerical modelling to examine microvascular oxygen in this brain region. This study purports to show that S_{O_2} falls rapidly along the microvascular paths in the brain at 'baseline', with ~50% of the total O_2 extraction reported to occur in descending arterioles and their proximal arteriolar branches and the majority of the remaining efflux of O_2 from the blood occurring in the first few capillary segments of the network. In this schema, high branching order capillaries (≥4 branch points from pre-capillary arterioles) provide little or no O_2 to the tissue at 'baseline' conditions (in spite of representing >50% of the total capillary segments).

The nature of their research (e.g. Sakadzić et al., 2010; Devor et al., 2011), means that this group are in direct competition with the Charpak lab, and this most recent study, Sakadzic et al. (2014), presents measurements which are directly comparable with those presented in this thesis. For these reasons it is worthwhile at this point to take some time to critically assess this study. I will compare and contrast the findings that should be comparable between my research and Sakadzic et al. (2014), and attempt to account for discrepancies that exist. In this spirit it must be initially stated that the methodology employed by Sakadzic et al. differs from my own in a number of key respects.

6.1 – Experimental animal preparation

My measurements are made in awake, unstressed mice, freely breathing normal air (FiO_2 ≈21%), with chronically implanted cranial windows and hence minimally disrupted neurophysiological and neurovascular functioning. Sakadzic et al.,

conversely, carried out their work in isoflurane-anaesthetised (0.7 – 1.2% during the recording period) mice, which were tracheotomised, with an FiO_2 > 21% (due to the inspired gas being a mixture of air and O_2, although the exact figure is not defined in the article), and which had undergone acute surgical procedures (tracheotomy, femoral artery catheterisation, and the opening of a 2.5 x 2.5 mm craniotomy directly over the area of study. In addition, the dura mater was removed in the area of the craniotomy). This form of preparation is associated with greatly reduced $CMRO_2$ (Isoflurane anaesthesia reduces $CMRO_2$ by >50% compared to the awake state (Myburgh et al., 2002)), and abnormally high arterial P_{O2} (due to the elevated FiO_2). Additionally isoflurane is a potent vasodilator, although its exact effects on the cerebral microvasculature under acute craniotomy are not well described. Given the departures from normal physiology inherent to this preparation, it would perhaps be surprising if no major divergence existed between the results described by Sakadzic et al. and my own.

6.2 – Measurement of near-RBC P_{O2} and its difference from P_{O2}RBC

Sakadzic et al. attempt to employ the procedure developed in our lab (Parpaleix et al., 2013) to measure P_{O2} near RBCs in capillaries, and to derive the mean S_{O2} in the capillary from this value. These P_{O2} measurements should therefore be comparable to my measurements of P_{O2}RBC in cortical capillaries. Comparison of the frequency distributions of capillary RBC P_{O2} from my study with that of Sakadzic et al., however, reveals a stark contrast.

Sakadzic et al.'s study (in their Fig. 6) shows that, in their preparation, the majority of capillaries' 'P_{O2}RBC' lie between approximately 15 and 55 mmHg, with only very few having 'P_{O2}RBC' values of >60 mmHg. The highest frequency P_{O2}RBC values were between 20 and 40 mmHg. In my data set, on the other hand, there are very few capillary P_{O2}RBC values <40 mmHg, with most values lying between 50 and 80 mmHg.

It is not certain that the measurement of P_{O_2}RBC is being performed in the same way by Sakadzic et al. as it is in the Charpak lab. They do not report specific parameters that they employ to define the site of P_{O_2} measurement near the border of the RBCs. Given the much lower range of P_{O_2} values they report as being equivalent to 'P_{O_2}RBC' it seems likely that the criteria they use might not assess P_{O_2} in as restricted a region near the RBC as those that we employ. We consider only phosphorescence decays that were recorded in a period of 1-4 ms around the RBC border when measuring P_{O_2}RBC (See Section 4 of Methods and Procedures). This possible underestimation of the magnitude of P_{O_2}RBC would tally with the fact that these researchers do not detect significant EATs in their recordings, measuring only fluctuations of only ~5 mmHg below their near-RBC P_{O_2} values (David A. Boas, personal communication) as opposed to the EAT amplitudes of >>20 mmHg that we typically observe.

Adopting the assumption that the extraction of 'P_{O_2}RBC' is appropriately performed in the Sakadzic et al. paper, and that their "capillary P_{O_2}" is in fact reflective of near RBC P_{O_2}, this is a very surprising finding. It suggests that the majority of the RBCs in the cortical capillary network of the mice in Sakadzic et al's study are largely desaturated (with S_{O_2} values of > 50%) at what they term 'baseline' cerebral activity and CBF levels. The authors claim that this is evidence for their proposed model of cortical tissue oxygenation, where most capillaries play a very minor role in oxygen delivery, and most O_2 is supplied by arterioles of low-branch-order capillary segments.

The P_{O_2}RBC distributions that I observe in cortical capillaries in awake, physiologically normal, mice are more closely mirrored by the values that Sakadzic et al. recorded in conditions of hypercapnia ($FiCO_2$ ~5%) than those in what they term "baseline" conditions. In the mice exposed to hypercapnia, total blood flow (total fluid flow, in nl/s, as measured by OCT in arterioles and venules) was 30% higher than in the normocapnic mice. In this condition of elevated CBF, the 'P_{O_2}RBC' distribution was right-shifted, with most values falling in the range of 35-65 mmHg, and many capillaries having values >70 mmHg. This could suggest, quite

paradoxically given the known vasodilatory effects of isoflurane (Matta et al., 1999) , that CBF is reduced below normal physiological levels in the "baseline" state of Sakadzic et al.'s invasive and acute surgical preparation. If this is the case, a restricted CBF at the "baseline" condition, in addition to suppresses $CMRO_2$, could compromise the validity of the results garnered and the interpretations proposed. For instance, if CBF significantly reduced, the number of RBCs delivered to the cerebrovasculature per unit time will also be diminished. Thus, (even with a dampened $CMRO_2$) at a constant rate of O_2 extraction, there will be a greater desaturation of each RBC, which might lead to large drops in S_{O2} in the early portion of microvascular paths. This would help account for the patterns of oxygen extraction observed by Sakadzic et al., and explain why they are altered by the increase in CBF induced by hypercapnia.

6.3 – Change in 'P_{O2}RBC' with depth in the cortex

When examining the distribution of "capillary P_{O2}" with depth in the cerebral cortex, Sakadzic et al. (in their Supplementary Fig. 7) see an overall trend for 'P_{O2}RBC' to rise with increasing depth in the cortex, with a mean value of ~34 mmHg at depths from 0 to 50μm below the cortical surface, to a peak of ~42 mmHg at 250–300μm in depth. P_{O2}RBC values at depths of 300-400 μm below the pia mater were recorded as ~36-38 mmHg. The general pattern of capillary 'P_{O2}RBC' distributions with depth could be considered to be superficially similar to that which I observe with measurements at a similar range of depths (P_{O2}RBC in Layer I < Layer II/III > Layer IV), but there is great disagreement in the absolute P_{O2}RBC values which reflects that seen in the differing frequency distribution plots of this P_{O2} parameter.

6.4 – Evidence for a large supply of oxygen to the cortical tissue from arterioles

The schema that Sakadzic et al. propose is based on their measurements of P_{O_2} and S_{O_2} estimations in the microvasculature, and on the output of the simulations they derive from this data. This proposal suggests that the majority of the O_2 that is delivered to the cerebral cortex is supplied by the arterioles and proximal capillaries. Their primary lines of evidence for this edifice arise from phenomena interpreted to represent very large efflux of O_2 from arterioles. In the case of penetrating arterioles, dense grid-like measurements over the luminal cross-section revealed that P_{O_2} was higher in the centre of the lumen than at the area directly abutting the vessel wall. This was interpreted as representing a P_{O_2} gradient established by large rates of O_2 efflux into the surrounding tissue. Although it is almost certain that there is some diffusion of O_2 from arterioles into the surrounding parenchyma (Sharan et al., 2008; Sakadzić et al., 2010; Devor et al., 2011; Lecoq et al., 2011), it is perhaps mistaken to view intra-luminal P_{O_2} gradients as being evidence for the presence and magnitude of such a diffusive flow. Another mechanism that could give rise to a significant intra-luminal gradient like that observed by Sakadzic et al. is the existence of a cell-free layer near the internal wall of the vessel (see Hightower et al. (2011) for a review). This phenomenon describes how as blood flows in narrow tubes (in a range of diameters from approximately 300 – 10 μm), the RBCs tend to flow in the centre of the lumen, with the production of a cell-free layer near the vessel wall where there is only plasma. Due to the lack of RBCs and hence peri-RBC plasma, a lower P_{O_2} value would be expected to be observed in this region. In vessels on the range of ~10 to 50μm (such as those assessed in Sakadzic et al.), the cell-free layer has been measured to be ~0.8 to 2.9 μm on each side of the flowing RBCs (Kim et al., 2007), which is similar to the size of the area of lower intra-luminal P_{O_2} in the data presented by Sakadzic et al.

The second line of evidence they draw on in the S_{O_2} gradient in the arteriolar and proximal capillary networks. The P_{O_2} and S_{O_2} gradients in arteriolar networks were said to be steep, with a rapid decrease in O_2 levels downstream, which correlated strongly with vessel luminal diameter. However, on careful examination of the plot

of the correlation between arteriolar diameter and P_{O_2}, it can be seen that a major proportion of this drop in P_{O_2} and S_{O_2} is observed in vessels with diameters of less than 15μm. This is interpreted by Sakadzic et al. as being indicative of large O_2 extraction rates at the level of these vessels. However, an alternative possible explanation is as follows: This range of luminal diameters, below ~15μm, is also the range at which the ~6μm diameter RBCs might be expected to begin to flow in a linear fashion rather than being superimposed in the lumen. If this is the case, then it is at this point on the path through the microvasculature that one would expect to see EAT-like effects. This is to say that with the RBCs flowing linearly in the plasma, there will begin to be points in the axis of the vessel where there is only plasma. These plasma gaps may be more pronounced in capillaries, and their influence more obvious, but if they exist at all, then any measurement technique that doesn't account for them will record a P_{O_2} signal that consists of both RBC and non-RBC P_{O_2} values (similar to the P_{O_2}Mean measurement in capillaries). In such a situation, the P_{O_2} values measured would show a sudden drop at the transition point from overlapping RBC flow to linear RBC flow. Some supporting evidence for this proposal arises from examination of the pre-capillary arteriole P_{O_2} and S_{O_2} changes in either "baseline" or hypercapnia conditions. This class of vessels (which should be almost identical in the different mice used for each condition), is dilated in hypercapnia (~50% greater diameter, ~15μm as opposed to ~10μm) and this dilation (with an assumed increase in superimposition and decrease in separation of RBCs) is associated with a reduced magnitude of P_{O_2} and S_{O_2} decline in these vessels. Furthermore, the P_{O_2} and S_{O_2} gradients observed in the pre-capillary arterioles and low-branching-order capillaries could be related to the possible effect of a potentially reduced CBF induced by the acute surgical preparation, as discussed earlier.

Another factor that might influence the observation of much higher P_{O_2} values at arterial-end microvascular segments than elsewhere is the elevated FiO_2 (>21%) in Sakadzic et al.'s study. It has been noted many times that an increased FiO_2 can induce a rise in brain tissue P_{O_2}, but that it does so to a lesser degree than mild

hypercapnia or combined hypercapnia and hypoxia (See Ndubuizu and LaManna (2007) for review). However, Metzger et al. (1971) also showed that hyperoxia (induced by augmented FiO_2) caused increased tissue P_{O2} only at the arterial ends of capillaries, whereas hypercapnia results in increased P_{O2} at all sites (Metzger et al., 1971), a finding which seems to be reflective of Sakadzic et al's recorded microvascular P_{O2} distribution.

6.5 – Conclusion

In summary, the data presented and the mechanisms of microvascular O_2 supply proposed by Sakadzic et al., although potentially interesting, are far from definitive and are called into question by viable alternative explanations of their data on the one hand, and more profoundly undermined on the other by serious caveats and concerns related to the experimental approach and preparation, which call into question the physiological relevance of the data itself.

Section 7 – A perspective on the applicability of anaesthetised animal preparations in cerebrovascular research

Anaesthetised *in vivo* preparations are used extensively in cerebrovascular research and in physiology and neuroscience research generally. They offer the possibility of carrying out investigations in intact systems, while often allowing for the use of experimental manipulations that are impossible or impractical in unanaesthetised animals.

As discussed in Results, Section 3.2.8, the most comparable study for the olfactory bulb GL data presented in this thesis, is Parpaleix et al. (2013). This earlier work from the Charpak lab uses the same techniques as the current research to measure the same P_{O2} and blood-flow parameters in the olfactory bulb of ketamine-xylazine anaesthetised rodents. Parpaleix et al. found comparable P_{O2}RBC, P_{O2}InterRBC and P_{O2}Mean values, as well as broadly similar RBC flow and haematocrit values as those presented in this work. However, measurements in the same population of capillaries under isoflurane anaesthesia and in the awake state in this study (Fig. 18, in Results), show that isoflurane anaesthesia can drastically alter blood flow and P_{O2} in the brain.

The comparison of these two cases indicates that results of measurements of cerebrovascular function carried out in anaesthetised animals need not necessarily differ greatly from those in the awake, normally functioning brain. More specifically, it suggests that with appropriate compensation (e.g. supplementary inspired oxygen to counteract the cardio-pulmonary depressive effects of xylazine), P_{O2} in the brain under anaesthesia can approach the levels existing in more physiological conditions. However, this comparison also demonstrates that without appropriate compensation, anaesthetics can cause brain P_{O2} and blood flow to be greatly perturbed. Thus, the interpretation of the physiological relevance of such information derived from experiments in anaesthetised animals must be done with great care. Furthermore, such experiments should be carried out with due attention paid to the

potential confounding effects of anaesthetics, and appropriate compensation employed where possible.

I would suggest that integrative data on physiological parameters garnered from awake, *in vivo* experiments could be used as a benchmark for such compensations.

Section 8 - Potential application of the present data to theoretical studies of oxygen dynamics

Given the difficulty in controlling all relevant factors that can affect oxygen supply and consumption in an experimental setting, the application of theoretical modelling to the problem of understanding oxygen dynamics is an important endeavour. The ability to manipulate single variables and identify their importance, gives these approaches great power to provide insight. As with all simulations, however, models of oxygen transport in the cerebrovasculature and distribution and consumption in the brain are only as robust as the data with which the key parameters are constrained. The P_{O2} and capillary blood flow data reported in Parpaleix et al. (2013) has been used in a recent modelling study (Lücker et al., 2014). This study involved generation of a model of oxygen transport from capillaries in which RBCs are flowing, and compared the predictions of their model against Parpaleix et al.'s measurements. The model was able to reproduce EATs of a similar amplitude to those observed by Parpaleix et al., and longitudinal gradients along single capillaries which they had also observed. The fact that there has until now been a dearth of information on the steady state P_{O2} in the awake brain has been an impediment to the progress of theoretical studies ability to accurately model P_{O2} dynamics in this state. Data provided by this study, on capillary RBC flow, haematocrit, and P_{O2} values could potentially be useful in such efforts. Additionally, the reported values and the correlations between them could provide useful targets for theoretical studies to reproduce as tests of the accuracy of the models created.

Section 9 - Remaining questions and future directions

Although the results of the research presented here represent an enhancement of our knowledge of P_{O_2} in the brain under physiological conditions and the mechanisms by which blood flow and oxygen delivery influence brain tissue oxygenation, a number of issues remain to be addressed, and many major questions have yet to be answered. One significant caveat that remains to be dealt with relates to how accurately the recorded data represents the oxygen tension field in the brain tissue. The initial demonstration that P_{O_2}InterRBC reports the local tissue P_{O_2} was carried out in the olfactory bulb glomeruli of anaesthetised animals. The olfactory bulb glomeruli are well defined areas of neuropil with an extremely high density of capillaries (with the average distance from any given point to the nearest capillary being ~10.8μm (Lecoq et al., 2009). See Introduction, Section 2.1.2 for details). In the somatosensory cortex, in contrast the equivalent value is ~15-20 μm (Sakadžić et al., 2014) . This greater intercapillary distance, could potentially mean that there are tissue areas, distant from capillaries, in which the P_{O_2} is lower than what could be predicted from P_{O_2}InterRBC measurements.

If this is the case then the ability of our measurements to represent the full range of tissue P_{O_2} distribution would be compromised. This limitation might be most acute in layer I, where the relatively low capillary density would exacerbate inter-capillary distances, and where potentially oxygen diffusion from pial vessels could skew the tissue P_{O_2} distribution in a manner that would not necessarily be detectable from capillary-based measurements. Additionally, it is possible that in the awake brain, unforeseen alterations in the P_{O_2}InterRBC – tissue P_{O_2} relationship could exist. Thus, it for the future utility of this tissue P_{O_2} measurement technique and for correct appraisal and potential validation of my findings, it is important that the relationship of P_{O_2}InterRBC and tissue P_{O_2} be assayed in the awake cortex.

One solution to this issue is an experiment that I have not had time to do, but which is planned for the near future. This experiment takes advantage of the recently

characterised paravascular pathway by which solutes can enter the brain parenchyma from the cerebrospinal fluid (Iliff et al., 2012). The planned experiment would involve recording of P_{O_2}InterRBC in a population of capillaries in the cortex of an awake mouse, and then infusing PtP-C343 into the cerebrospinal fluid. The subsequent indirect loading of PtP-C343 into the interstitial fluid would allow for comparison of tissue P_{O_2} with the recorded P_{O_2}InterRBC in the awake animal. We will be able to assess whether, and to what extent (radial distance from the capillaries) P_{O_2}InterRBC is a reliable reported of tissue P_{O_2}. This experiment would also allow for the measurement of the magnitude and radial extent of P_{O_2} gradients around large arterioles and venules in the awake cortex.

A further limitation of the current results is that in spite of the simultaneously acquired RBC flow, haematocrit and P_{O_2} data, the description of blood flow and P_{O_2} interactions is incomplete due to the absence of RBC velocity measurements. This parameter could potentially be calculated for the current data set, by using images of the recorded capillaries to determine the diameter of each vessel and adopting a standard value for RBC volume, and thus working out the RBC linear density from the measured haematocrit. This could then be used to compute the RBC velocity from the RBC flow values. For future experiments, an approach that could profitably be employed would be to interleave each point measurement of P_{O_2} with a line-scan based measurement of the RBC flow, linear density and velocity. As discussed in the results section, it is likely that a strong correlation would exist between RBC velocity and P_{O_2}RBC, based on the finding that P_{O_2}RBC seems to be somewhat dependent on RBC flow but largely independent of haematocrit.

In this study, by employing the approach of using multiple, sequential, point measurements, we have gathered information on the relationship of blood flow parameters and vascular oxygenation to tissue P_{O_2}. However, this approach only gives us access to the supply side of the equation that determines tissue P_{O_2}. Without information on the consumption of oxygen in the local tissue volume, we will only

get a partial picture of the oxygen dynamics in the brain. An alternative, and complementary approach to measuring capillary and tissue P_{O2} is to employ an acquisition mode that has been developed in the lab to allow for detection of individual RBCs and the measurement of their associated P_{O2} values at two, possibly widely separated, points in a single capillary (Parpaleix et al., 2013). This 'kinetic' acquisition mode involves selecting two sites on a capillary segment that lie in the same XY-plane, for measurement of P_{O2}. The first point undergoes excitation during the 'On' phase of the AOM cycle, but rather than simply detecting the phosphorescence decay during the 'Off' phase and then exciting the same point, during this ~225μs delay the galvanometric scanning mirrors are used to move the illumination focus to the second point chosen for measurement, and the next cycle of excitation occurs at this position. This cycle is repeated 3,000-40,000 times. Due to the rapid movement of the mirrors, and frequent repetition rate (~2 kHz at each point) essentially the same population of RBCs are assessed at both positions (RBC velocity is on the order of 1 mm/s in brain capillaries). By comparing the P_{O2} values (and especially the P_{O2}RBC) at each point, it is possible to work out the extraction rate of P_{O2} from the RBCs, per unit capillary length in that tissue region (by measuring the RBC path length in the capillary the RBC velocity can be recorded). This measurement of the oxygen extraction rate from capillaries would provide an index of local oxygen consumption rate, and open up the possibility of approaching a complete description of the factors affecting P_{O2} and oxygen dynamics in specific brain subregions (and tissue volumes in general).

Part 5: Conclusion

The results of the research presented in this thesis describe a tissue oxygen tension field in the brain. This field is characterised by its heterogeneity, with regions of high P_{O2} (up to 60+ mmHg), in which the oxygen is supplied by capillaries with high RBC flow, generated by a high RBC velocity and high haematocrit; areas of low P_{O2} (down to nearly 0 mmHg) that are fed by capillaries with low haematocrit, and many intermediate regions with P_{O2} values between these extremes, typically around 10-30 mmHg. The form of this field differs from structure to structure and from subregion to subregion, and even in a given area it is constantly changing, reflecting the shifting gradients and the balance of supply and demand. The form of this oxygen tension field is influenced greatly by the vascular organisation, with the density of capillaries, the position of capillary segments in the microvascular network, the local RBC flow rate, RBC velocity and haematocrit, and the oxygenation of the passing RBCs moulding the local diffusion patterns in concert with the cellular and mitochondrial oxygen sinks. This dependence of P_{O2} on local vascular properties means that although constantly fluctuating, the local oxygen tension field will have a characteristic form, a dynamic equilibrium point around which the actual field at any given moment will oscillate. This property is represented in our data by the similarity of the frequency distribution plots based on the average P_{O2} associated with a capillary and one based on all the measurements from the population of capillaries.

At the end of the introduction, I stated that there were four questions that I would attempt to address over the course of this thesis. The answers, as succinctly as I can provide them, are as follows:

What range of P_{O2} values exist in the awake mouse brain under physiological conditions?

In the areas of the brain in which I made measurements, the P_{O2} spanned a wide range of values. Tissue P_{O2} was found to be as low as to be indistinguishable from zero in some cases, and as high as 70 mmHg in others. Vascular P_{O2} can also be as

low as less than 1 mmHg in capillary plasma that is distant from RBCs, or as high as over 90 mmHg in the vicinity of highly oxygenated red blood cells. These values are, however, the more extreme cases.

What are the typical levels of P_{O2} that exist in microvasculature and the neural tissue?

Typical levels of vascular P_{O2} are from around 50-80 mmHg at red blood cells, to 10-35 mmHg in the plasma of capillaries at points distant from red blood cells. This value, of 10-35 mmHg is also the typical range of P_{O2} in the neural tissue.

Do the typical P_{O2} values and the range of values vary between different subregions in the brain?

The typical P_{O2} values are different between different structures and subregions, but not by a large margin. Furthermore, each P_{O2} parameter can vary in a different manner in different regions, because of the number of factors that influence oxygen transport and consumption and the complexity of the interactions between these factors. For instance, in capillaries in layer I of the somatosensory cortex, the average P_{O2} at RBCs is similar to that in layer IV capillaries, whereas the average local tissue P_{O2} in layer IV is double that in the tissue of layer I.

How do the vascular perfusion characteristics affect the local tissue and vascular P_{O2}?

The blood flow affects local P_{O2} in a complex manner. However, generally speaking, local tissue and Inter-RBC plasma P_{O2} will change in line with the number of red blood cells that enter the volume, the level of oxygenation of these RBCs, and the surface area and time that is available for diffusion. The greatest level of tissue and Inter-RBC P_{O2} will likely be achieved by having a large number of highly oxygenated red blood cells flowing at high velocity and with a high haematocrit through a narrow capillary, for a long period of time.

In most situations however, not all of these criteria are met, but a subset thereof can be sufficient to markedly raise local tissue P_{O2}.

Part 6 : Bibliography & Appendices

Bibliography

Acker T, Acker H (2004) Cellular oxygen sensing need in CNS function: physiological and pathological implications. Journal of Experimental Biology 207:3171–3188.

Aken VH, Hemelrijck VJ (1990) Influence of anesthesia on cerebral blood flow and cerebral metabolism: an overview. … appliquees aux effets de l'agression Available at: http://europepmc.org/abstract/MED/1843831.

Altamura C, Dell'Acqua M, Moessner R, Murphy D, Lesch K, Persico A (2007) Altered neocortical cell density and layer thickness in serotonin transporter knockout mice: a quantitation study. Cerebral cortex (New York, NY©: 1991) 17:1394–1401.

Attwell D, Laughlin S (2001) An Energy Budget for Signaling in the Grey Matter of the Brain. Journal of Cerebral Blood Flow & Metabolism 21:1133–1145.

Baughman VL, Hoffman WE, Miletich DJ, Albrecht RF (1990) Cerebrovascular and cerebral metabolic effects of N2O in unrestrained rats. Anesthesiology 73:269–272.

Berg JM, Tymoczko JL, Streyr L (2002) Biochemistry, 5th ed. W.H.Freeman & Co Ltd.

Blinder P, Shih AY, Rafie C, Kleinfeld D (2010) Topological basis for the robust distribution of blood to rodent neocortex. Proc Natl Acad Sci USA 107:12670–12675.

Blinder P, Tsai PS, Kaufhold JP, Knutsen PM, Suhl H, Kleinfeld D (2013) The cortical angiome: an interconnected vascular network with noncolumnar patterns of blood flow. Nat Neurosci 16:889–897.

Borowsky IW, Collins RC (1989) Metabolic anatomy of brain: a comparison of regional capillary density, glucose metabolism, and enzyme activities. J Comp Neurol 288:401–413.

Chaigneau E, Oheim M, Audinat E, Charpak S (2003) Two-photon imaging of capillary blood flow in olfactory bulb glomeruli. Proc Natl Acad Sci USA 100:13081–13086.

Chaigneau E, Tiret P, Lecoq J, Ducros M, Knöpfel T, Charpak S (2007) The relationship between blood flow and neuronal activity in the rodent olfactory bulb. J Neurosci 27:6452–6460.

Chapin JK, Lin CS (1984) Mapping the body representation in the SI cortex of anesthetized and awake rats. Journal of Comparative Neurology Available at: http://onlinelibrary.wiley.com/doi/10.1002/cne.902290206/full.

Charbel FT, Hoffman WE, Misra M, Hannigan K, Ausman JI (1997) Cerebral interstitial tissue oxygen tension, pH, HCO3, CO2. Surg Neurol 48:414–417.

Clarke, Sokoloff (1999) Circulation and energy metabolism of the brain. In Basic Neurochemistry, 6th ed., (Siegel GJ, Agranoff BW, Albers RW, Fisher SK, Uhler MD, eds) pp 637–669. Lippincott-Raven.

Coyle P (1975) Arterial patterns of the rat rhinencephalon and related structures. Experimental neurology 49:671–690 Available at: http://www.sciencedirect.com/science/article/pii/0014488675900515.

Cross B, Silver I (1962) Some Facotrs Affecting Oxygen Tension in the Brain and other Organs. Proceedings of the Royal Society B: Biological Sciences 156.

Lübbers DW (1969) The meaning of the tissue oxygen distribution curve and its measurement by means of Pt electrodes. Progress in Respiratory Research 3:112–123.

Devor A, Sakadzic S, Saisan PA, Yaseen MA, Roussakis E, Srinivasan VJ, Vinogradov SA, Rosen BR, Buxton RB, Dale AM, Boas DA (2011) "Overshoot" of O_2 is required to maintain baseline tissue oxygenation at locations distal to blood vessels. J Neurosci 31:13676–13681.

Dirnagl U (2010) Oxygen maps in the brain. Nature methods 7:697–699.

Douglas RJ, Martin KA (2004) Neuronal circuits of the neocortex. Annu Rev Neurosci 27:419–451.

Duling B, Berne R (1970) Longitudinal Gradients in Periarteriolar Oxygen Tension A Possible Mechanism For the Participation of Oxygen in Local Regulation of Blood Flow.

Duling B, Kuschinsky W, Wahl M (1979) Measurements of the perivascular PO2 in the vicinity of the pial vessels of the cat. Pflügers Archiv.

Dunn J, Swartz H (2003) In vivo electron paramagnetic resonance oximetry with particulate materials.

Dunn JF, Khan MN, Hou HG, Merlis J, Abajian MA, Demidenko E, Grinberg OY, Swartz HM (2011) Cerebral oxygenation in awake rats during acclimation and

deacclimation to hypoxia: an in vivo electron paramagnetic resonance study. High Alt Med Biol 12:71–77.

Duvernoy H, Delon S, Vannson J (1981) Cortical blood vessels of the human brain. Brain research bulletin 7:519–579.

Erecińska M, Silver IA (2001) Tissue oxygen tension and brain sensitivity to hypoxia. Respir Physiol 128:263–276.

Finikova OS, Lebedev AY, Aprelev A, Troxler T, Gao F, Garnacho C, Muro S, Hochstrasser RM, Vinogradov SA (2008) Oxygen microscopy by two-photon-excited phosphorescence. Chemphyschem 9:1673–1679.

Fonta C, Imbert M (2002) Vascularization in the primate visual cortex during development. Cereb Cortex 12:199–211.

Golub AS, Pittman RN (2005) Erythrocyte-associated transients in PO2 revealed in capillaries of rat mesentery. Am J Physiol Heart Circ Physiol 288:H2735–43.

Golub AS, Pittman RN (2008) PO2 measurements in the microcirculation using phosphorescence quenching microscopy at high magnification. Am J Physiol Heart Circ Physiol 294:H2905–16.

Gray L, Steadman J (1964) Determination of the oxyhaemoglobin dissociation curves for mouse and rat blood.

Heiss WD, Pawlik G, Herholz K, Wagner R, Göldner H, Wienhard K (1984) Regional kinetic constants and cerebral metabolic rate for glucose in normal human volunteers determined by dynamic positron emission tomography of [18F]-2-fluoro-2-deoxy-D-glucose. J Cereb Blood Flow Metab 4:212–223.

Hellums JD (1977) The resistance to oxygen transport in the capillaries relative to that in the surrounding tissue. Microvasc Res 13:131–136.

Hightower MC, Vázquez BY, Park S, Sriram K, Martini J, Yalcin O, Tsai AG, Cabrales P, Tartakovsky DM, Johnson PC (2011) Integration of cardiovascular regulation by the blood/endothelium cell free layer. Wiley Interdisciplinary Reviews: Systems Biology and Medicine 3:458–470 Available at: http://onlinelibrary.wiley.com/doi/10.1002/wsbm.150/full.

Hirsch S, Reichold J, Schneider M, Székely G, Weber B (2012) Topology and hemodynamics of the cortical cerebrovascular system. J Cereb Blood Flow Metab 32:952–967.

Holtmaat A, Bonhoeffer T, Chow D, Chuckowree J, Paola V, Hofer S, Hübener M, Keck T, Knott G, Lee W-C, Mostany R, Mrsic-Flogel T, Nedivi E, Portera-Cailliau C, Svoboda K, Trachtenberg J, Wilbrecht L (2009) Long-term, high-resolution imaging in the mouse neocortex through a chronic cranial window. Nat Protoc 4:1128–1144.

Howarth C, Gleeson P, Attwell D (2012) Updated energy budgets for neural computation in the neocortex and cerebellum. J Cereb Blood Flow Metab 32:1222–1232.

Hu S, Maslov K, Tsytsarev V, Wang L (2009) Functional transcranial brain imaging by optical-resolution photoacoustic microscopy. Journal of biomedical optics 14:040503.

Hudetz AG (1997) Blood flow in the cerebral capillary network: a review emphasizing observations with intravital microscopy. Microcirculation 4:233–252.

Iliff J, Wang M, Liao Y, Plogg B, Peng W, Gundersen G, Benveniste H, Vates G, Deane R, Goldman S, Nagelhus E, Nedergaard M (2012) A Paravascular Pathway Facilitates CSF Flow Through the Brain Parenchyma and the Clearance of Interstitial Solutes, Including Amyloid β. Sci Transl Med 4:147ra111.

Bryan RM Jr. (1990) Cerebral blood flow and energy metabolism during stress. American Journal of Physiology-Heart and Circulatory Physiology 259:H269–H280 Available at: http://ajpheart.physiology.org/content/259/2/H269.short.

Jukovskaya N, Tiret P, Lecoq J, Charpak S (2011) What does local functional hyperemia tell about local neuronal activation? J Neurosci 31:1579–1582.

Kandel E, Schwartz J, Jessel T (2000) Principles of Neural Science, 4th ed. McGraw-Hill Medical Publishing Division.

Keller AL, Schüz A, Logothetis NK, Weber B (2011) Vascularization of cytochrome oxidase-rich blobs in the primary visual cortex of squirrel and macaque monkeys. J Neurosci 31:1246–1253.

Kim S, Kong RL, Popel AS, Intaglietta M, Johnson PC (2007) Temporal and spatial variations of cell-free layer width in arterioles. Am J Physiol Heart Circ Physiol 293:H1526–35.

Kleinfeld D, Mitra PP, Helmchen F, Denk W (1998) Fluctuations and stimulus-induced changes in blood flow observed in individual capillaries in layers 2 through 4 of rat neocortex. Proc Natl Acad Sci USA 95:15741–15746.

Kummitha CM, Kalhan SC, Saidel GM, Lai N (2014) Relating tissue/organ energy expenditure to metabolic fluxes in mouse and human: experimental data integrated with mathematical modeling. Physiol Rep 2.

Lauwers F, Cassot F, Lauwers-Cances V, Puwanarajah P, Duvernoy H (2008) Morphometry of the human cerebral cortex microcirculation: General characteristics and space-related profiles. NeuroImage 39:936–948.

Lecoq J, Parpaleix A, Roussakis E, Ducros M, Goulam Houssen Y, Vinogradov SA, Charpak S (2011) Simultaneous two-photon imaging of oxygen and blood flow in deep cerebral vessels. Nat Med 17:893–898.

Lecoq J, Tiret P, Najac M, Shepherd GM, Greer CA, Charpak S (2009) Odor-evoked oxygen consumption by action potential and synaptic transmission in the olfactory bulb. J Neurosci 29:1424–1433.

Lei H, Grinberg O, Nwaigwe C, Hou H, Williams H, Swartz H, Dunn J (2001) The effects of ketamine-xylazine anesthesia on cerebral blood flow and oxygenation observed using nuclear magnetic resonance perfusion imaging and electron paramagnetic resonance oximetry. Brain research.

Leniger-Follert E, Lübbers DW, Wrabetz W (1975) Regulation of local tissuePo 2of the brain cortex at different arterial O2 pressures. Pflügers Archiv Available at: http://link.springer.com/article/10.1007/BF00581279.

Linde R, Schmalbruch IK, Paulson OB, Madsen PL (1999) The Kety-Schmidt technique for repeated measurements of global cerebral blood flow and metabolism in the conscious rat. Acta Physiol Scand 165:395–401.

Liu KJ, Bacic G, Hoopes PJ, Jiang J, Du H, Ou LC, Dunn JF, Swartz HM (1995) Assessment of cerebral pO2 by EPR oximetry in rodents: effects of anesthesia, ischemia, and breathing gas. Brain Res 685:91–98.

Lochhead JJ, Wolak DJ, Pizzo ME, Thorne RG (2014) Rapid transport within cerebral perivascular spaces underlies widespread tracer distribution in the brain after intranasal administration. J Cereb Blood Flow Metab.

Lodish H, Berk A, Zipursky SL, Matsudaira P, Baltimore D, Darnell J (2000) Molecular Cell Biology, 4th ed. W.H. Freeman.

Lücker A, Weber B, Jenny P (2014) A dynamic model of oxygen transport from capillaries to tissue with moving red blood cells. Am J Physiol Heart Circ Physiol:ajpheart.00447.2014.

Madsen PL, Hasselbalch SG, Hagemann LP, Olsen KS, Bülow J, Holm S, Wildschiødtz G, Paulson OB, Lassen NA (1995) Persistent resetting of the cerebral oxygen/glucose uptake ratio by brain activation: evidence obtained with the Kety-Schmidt technique. J Cereb Blood Flow Metab 15:485–491.

Masamoto K, Takizawa N, Kobayashi H, Oka K, Tanishita K (2003) Dual responses of tissue partial pressure of oxygen after functional stimulation in rat somatosensory cortex. Brain Res 979:104–113.

Matta BF, Heath KJ, Tipping K, Summors AC (1999) Direct cerebral vasodilatory effects of sevoflurane and isoflurane. Anesthesiology Available at: http://journals.lww.com/anesthesiology/Abstract/1999/09000/Direct_Cerebral_Vasodilatory_Effects_of.19.aspx.

Metzger H, Erdmann W, Thews G (1971) Effect of short periods of hypoxia, hyperoxia, and hypercapnia on brain O 2 supply. J appl Physiol 31:751 Available at: http://jap.physiology.org/content/jap/31/5/751.full.pdf.

Milo R, Jorgensen P, Moran U, Weber G, Springer M (2010) BioNumbers--the database of key numbers in molecular and cell biology. Nucleic Acids Res 38:D750–3.

Mombaerts P (2006) Axonal wiring in the mouse olfactory system. Annual review of cell and developmental biology 22:713–737.

Myburgh JA, Upton RN, Grant C (2002) The cerebrovascular effects of adrenaline, noradrenaline and dopamine infusions under propofol and isoflurane anaesthesia in sheep. … and intensive care Available at: http://digital.library.adelaide.edu.au/dspace/handle/2440/5897.

Nair P, Whalen W, Buerk D (1975) PO2 of cat cerebral cortex: response to breathing N2 and 100 per cent O21. Microvascular research 9:158–165.

Nawroth JC, Greer CA, Chen WR, Laughlin SB, Shepherd GM (2007) An energy budget for the olfactory glomerulus. J Neurosci 27:9790–9800.

Ndubuizu O, LaManna J (2007) Brain tissue oxygen concentration measurements. Antioxidants & redox signaling 9:1207–1219.

Nilsson B, Siesjö BK (1976) A method for determining blood flow and oxygen consumption in the rat brain. Acta physiologica Scandinavica Available at: http://onlinelibrary.wiley.com/doi/10.1111/j.1748-1716.1976.tb10172.x/abstract.

Ortiz-Prado E, Natah S, Srinivasan S, Dunn JF (2010) A method for measuring brain partial pressure of oxygen in unanesthetized unrestrained subjects: the effect of acute and chronic hypoxia on brain tissue PO(2). J Neurosci Methods 193:217–225.

Parpaleix A, Goulam Houssen Y, Charpak S (2013) Imaging local neuronal activity by monitoring PO_2 transients in capillaries. Nat Med 19:241–246.

Paxinos G, Franklin K (2001) Mouse Brain in Stereotaxic Coordinates, 2nd ed. Academic Press.

Pierigè F, Serafini S, Rossi L, Magnani M (2008) Cell-based drug delivery. Adv Drug Deliv Rev 60:286–295.

Pittman RN (2011a) Oxygen gradients in the microcirculation. Acta physiologica (Oxford, England) 202:311–322.

Pittman RN (2011b) Regulation of Tissue Oxygenation. Morgan & Claypool Life Sciences.

Poole D, Copp S, Hirai D, Musch T (2011) Dynamics of muscle microcirculatory and blood–myocyte O2 flux during contractions. Acta Physiologica 202:293–310.

Purves D, Agustine GJ, Katz LC, LaMantia A-S, McNamara JO, Williams SM (2001) Neuroscience, 2nd ed. Sinauer Associates.

Quaranta M, Borisov SM, Klimant I (2012) Indicators for optical oxygen sensors. Bioanal Rev 4:115–157.

Raichle M, Mintun M (2006) Brain work and brain imaging.

Richard MB, Taylor SR (2010) Age-induced disruption of selective olfactory bulb synaptic circuits. Proceedings of the … Available at: http://www.pnas.org/content/107/35/15613.short.

Roberts M, Owens G (1972) Direct mass spectrographic measurement of regional intracerebral oxygen, carbon dioxide, and argon. J Neurosurg 37:706–710.

Rolett EL, Azzawi A, Liu KJ, Yongbi MN, Swartz HM, Dunn JF (2000) Critical oxygen tension in rat brain: a combined (31)P-NMR and EPR oximetry study. Am J Physiol Regul Integr Comp Physiol 279:R9–R16.

Rolfe DF, Brown GC (1997) Cellular energy utilization and molecular origin of standard metabolic rate in mammals. Physiol Rev 77:731–758.

Rosen (1967) Optimality principles in biology. Plenum press.

Sakadzić S, Roussakis E, Yaseen MA, Mandeville ET, Srinivasan VJ, Arai K, Ruvinskaya S, Devor A, Lo EH, Vinogradov SA, Boas DA (2010) Two-photon high-resolution measurement of partial pressure of oxygen in cerebral vasculature and tissue. Nat Methods 7:755–759.

Sakadžić S, Mandeville ET, Gagnon L, Musacchia JJ, Yaseen MA, Yucel MA, Lefebvre J, Lesage F, Dale AM, Eikermann-Haerter K, Ayata C, Srinivasan VJ, Lo EH, Devor A, Boas DA (2014) Large arteriolar component of oxygen delivery implies a safe margin of oxygen supply to cerebral tissue. Nat Commun 5:5734.

Seelke A, Dooley J, Krubitzer L (2012) The Emergence of Somatotopic Maps of the Body in S1 in Rats: The Correspondence Between Functional and Anatomical Organization. PLoS ONE.

Sharan M, Popel AS (2002) A compartmental model for oxygen transport in brain microcirculation in the presence of blood substitutes. J Theor Biol 216:479–500.

Sharan M, Vovenko EP, Vadapalli A, Popel AS, Pittman RN (2008) Experimental and theoretical studies of oxygen gradients in rat pial microvessels. J Cereb Blood Flow Metab 28:1597–1604.

Smith R, Guilbeau E, Reneau D (1977) The oxygen tension field within a discrete volume of cerebral cortex. Microvascular research 13:233–240.

Soucy ER, Albeanu DF, Fantana AL, Murthy VN (2009) Precision and diversity in an odor map on the olfactory bulb. Nature … Available at: http://www.nature.com/neuro/journal/v12/n2/abs/nn.2262.html.

Springett R, Swartz HM (2007) Measurements of oxygen in vivo: overview and perspectives on methods to measure oxygen within cells and tissues. Antioxid Redox Signal 9:1295–1301.

Takano T, Tian G-FF, Peng W, Lou N, Lovatt D, Hansen AJ, Kasischke KA, Nedergaard M (2007) Cortical spreading depression causes and coincides with tissue hypoxia. Nat Neurosci 10:754–762.

Thompson JK, Peterson MR, Freeman RD (2003) Single-neuron activity and tissue oxygenation in the cerebral cortex. Science Available at: http://www.sciencemag.org/content/299/5609/1070.short.

Tsai A, Johnson P, Intaglietta M (2003) Oxygen Gradients in the Microcirculation. Physiological Reviews 83:933–963.

Tsai AG, Cabrales P, Johnson PC, Intaglietta M, Golub AS, Pittman RN (2005) Effect of oxygen consumption by measuring method on PO2 transients associated with the passage of erythrocytes in capillaries of rat mesentery. Am J Physiol Heart Circ Physiol 289:H1777; author reply H1778–9.

Tsai AG, Friesenecker B, Mazzoni MC, Kerger H, Buerk DG, Johnson PC, Intaglietta M (1998) Microvascular and tissue oxygen gradients in the rat mesentery. Proc Natl Acad Sci USA 95:6590–6595.

Tsai PS, Kaufhold JP, Blinder P, Friedman B, Drew PJ, Karten HJ, Lyden PD, Kleinfeld D (2009) Correlations of neuronal and microvascular densities in murine cortex revealed by direct counting and colocalization of nuclei and vessels. J Neurosci 29:14553–14570.

Vadapalli A, Pittman RN, Popel AS (2000) Estimating oxygen transport resistance of the microvascular wall. Am J Physiol Heart Circ Physiol 279:H657–71.

Vazquez AL, Fukuda M, Tasker ML, Masamoto K, Kim S-GG (2010a) Changes in cerebral arterial, tissue and venous oxygenation with evoked neural stimulation: implications for hemoglobin-based functional neuroimaging. J Cereb Blood Flow Metab 30:428–439.

Vazquez AL, Masamoto K, Fukuda M, Kim S-GG (2010b) Cerebral oxygen delivery and consumption during evoked neural activity. Front Neuroenergetics 2:11.

Villringer A, Them A, Lindauer U, Einhäupl K, Dirnagl U (1994) Capillary perfusion of the rat brain cortex. An in vivo confocal microscopy study. Circ Res 75:55–62.

Vovenko E (1999) Distribution of oxygen tension on the surface of arterioles, capillaries and venules of brain cortex and in tissue in normoxia: an experimental study on rats. Pflugers Arch 437:617–623.

Weber B, Keller AL, Reichold J, Logothetis NK (2008) The microvascular system of the striate and extrastriate visual cortex of the macaque. Cereb Cortex 18:2318–2330.

Wu J, Guo C, Chen S, Jiang T, He Y, Ding W, Yang Z, Luo Q, Gong H (2014) Direct 3D Analyses Reveal Barrel-Specific Vascular Distribution and Cross-Barrel Branching in the Mouse Barrel Cortex. Cerebral Cortex.

Yaseen MA, Srinivasan VJ, Sakadžić S, Radhakrishnan H, Gorczynska I, Wu W, Fujimoto JG, Boas DA (2011) Microvascular oxygen tension and flow measurements in rodent cerebral cortex during baseline conditions and functional activation. J Cereb Blood Flow Metab 31:1051–1063.

List of Figures

PART 1: INTRODUCTION

Introduction Figure 1. Schematic diagram of glycolysis. 6

Introduction Figure 2. Schematic of the citric acid cycle and oxidative phosphorlyation 7

Introduction Figure 3. Oxygen-Haemoglobin binding-curves of human, rat and mouse blood. 13

Introduction Table 1. Values of oxygen in vascular compartments and interstitial fluid 14

Introduction Figure 4. Diagrams of some major features of the cerebrovasculature 20

Introduction Figure 5. Somatotopic representation of the body in the somatosensory cortex 29

Introduction Table 2. Depths of layers in the cortex. 31

Introduction Figure 6. Microvascular density in the Cortex 31

Introduction Figure 7. Perrin Jablonski diagram of excitation and de-excitation in luminophores. 41

Introduction Figure 8. Structure and properties of PtP-C343 46

Introduction Table 3. Quantitative Estimates of Brain Tissue pO2 Partial Pressure. 55

PART 2: METHODS & PROCEDURES

Methods Figure 1. 2PLM system 62

Methods Figure 2. RBCs detected as transient dips in fluorescence 62

Methods Figure 3. EAT schematic and evidence that P_{O_2}InterRBC reports tissue P_{O_2} 64

Methods Figure 4. Procedure for mouse restraint and training. Image of cranial window. 70

PART 3: RESULTS

Figure 1. Capillary and tissue P_{O_2} in the olfactory bulb GL. 76

Figure 2. Diagrams of some major features of the cerebrovasculature 78

Figure 3. Capillary RBC flow and haematocrit in the olfactory blub GL. 79

Figure 4. The correlation of haematocrit on capillary and tissue P_{O_2} in the olfactory bulb GL. 80

Figure 5. Correlation of blood flow with capillary P_{O2} in low- P_{O2}InterRBC capillaries in the GL. ... 81

Figure 6. Capillary and tissue P_{O2} in the somatosensory cortex.. ... 83

Figure 7. Capillary RBC Flow and haematocrit in the somatosensory cortex ... 85

Figure 8. The effect of RBC Flow on capillary and tissue P_{O2} in the somatosensory cortex... 86

Figure 9. The effect of haematocrit on capillary and tissue P_{O2} in the somatosensory cortex ... 87

Figure 10. Influence of blood flow on capillary P_{O2} in low-P_{O2}InterRBC capillaries in the cortex.. ... 88

Figure 11. Capillary and tissue P_{O2} in layers I-IV of the somatosensory cortex... 90

Figure 12. Capillary RBC flow and haematocrit in layers I-IV of the somatosensory cortex. ... 91

Figure 13. P_{O2}RBC and P_{O2}InterRBC as a function of RBC Flow, in layers I-IV of the cortex.. ... 94

Figure 14. P_{O2}RBC and P_{O2}InterRBC as a function of haematocrit, in layers I-IV of the cortex.. ... 95

Figure 15. Capillary P_{O2}Mean as a function of RBC Flow, in layers I-IV of the cortex.. ... 96

Figure 16. Capillary P_{O2}Mean as a function of haematocrit, in layers I-IV of the cortex.. ... 96

Figure 17. Penetrating vessel P_{O2} as a function of depth below cortical surface ... 98

Figure 18. Capillary P_{O2} and RBC Flow in the awake state and under isoflurane anaesthesia.. ... 100